School of Chemistry

Department of Inorganic and Materials Chemistry

Development of novel degradable pH-responsiveness polymers for potential applications in 3D printing

Yu Lu

Student ID: 20243903

Supervisor: Prof. Steve Howdle

Nottingham 2021

Table of Contents

Abstract

Stimuli-responsive materials have been researched for decades, there are many forms of stimuli-responsiveness, such as pH-, light- and thermal-responsiveness among others. In addition, the use of degradable materials can expand the range of possible final applications, e.g., coating and drug delivery. 3D printing is a subset of rapid prototyping technologies, which is based on computer model files and bondable material (such as powder-like polymer) to fabricate objects via a layer-by-layer process, there are many related technologies, such as, inkjet printing and selective laser sintering (SLS). However, they suffer of key shortcomings based on the lack of functionalised available materials. For example, for SLS, limited polymers nature and restricted range of colours are reported for the production of the final printed objects. In this project, we designed and synthesized a series of coloured copolymers endowed with a further pH-responsiveness, foreseeing pH and "sweat" sensors as possible final applications. Dispersed Red I and 4-phenylazophenol (yellow dye) have been selected as two of the three-primary colours. 2-hydroxyethyl methacrylate (HEMA), 2-hydroxyethyl acrylate (HEA), lactide and succinic anhydride were used as building blocks to synthesize macroinitiators with degradable features. The degradable moiety and colour groups were linked through a labile ester functionality. ^{1}H NMR, FT-IR and GPC analysis were used to confirm the success of the reactions and the final molecular structures. Degradation test was set up in 1M H_2SO_4 and 1M NaOH aqueous environments. The colour change of the aqueous media can be observed when the colour moiety was cleaved and the decreasing in Mn was monitored by GPC.

Key words: 3D printing; colour copolymer; degradable material; pH-responsiveness

Acknowledge

Time flies, and my master's career is coming to an end unconsciously. I am writing this acknowledgment to express my most sincere gratitude.

Firstly, I would like to thank my supervisor, Prof Steve Howdle, for giving me this opportunity to work within his group, which is the most memorable time in my study life.

Secondly, I would like to express my most sincere acknowledge toward some of people in B10 lab. First of all, Vincenzo Taresco, for introducing me to the lab, and he was the first person I met in the B10 lab. Besides, during the whole time of my experience in B10 lab, I am very grateful to him for his guidance in my experiment. Secondly, Eduards Krumins, for his guidance and help in my experiment.

I am very grateful that Vincenzo and Eduards can take the precious time to help me review my thesis.

Thanks to other people who helped me in the experiment, let me get the best scientific research training during my master’s time.

My experience in B10 lab is my most pleasure time during my scientific career so far.

Yu Lu

01/09/2021

Declaration

I declare that the thesis is the result of my own work which has been mainly undertaken during my period of registration for this degree at The University of Nottingham. I have complied with the word limit for my degree.

Yu Lu

01/09/2021

List of symbols

Abbreviation	Full name
SLS	Selective laser sintering
AM	Additive manufacturing
3DP	3D printing
FRP	Free radical polymerization
M_n	Number average molecular weight
Đ	Dispersity
T_g	Glass transition temperature
MMA	Methyl methacrylate
AIBN	2,2’ - Azobis (2 - methylpropionitrile)
HEMA	2-hydroxyethyl methacrylate
HEA	2-hydroxyethyl acrylate
ROP	Ring opening polymerization
DBU	1,8-Diazabicyclo[5.4.0]undec-7-ene
LA	Lactide
DCM	Dichloromethane
THF	Tetrahydrofuran
4-DMAP	4-Dimethylaminopyridine
DCC	N,N'-Dicyclohexylcarbodiimide
TEGMA	Triethylene glycol methyl ether methacrylate
PEGMA	Poly(ethylene glycol) methacrylate
$CDCl_3$	Chloroform-d
^{1}H-NMR	Proton Nuclear Magnetic Resonance
GPC	Gel Permeation Chromatography

1. Introduction

1.1 3D printing

3D printing is a subset of additive manufacturing (AM), it provides a new method to fabricate different kinds of objects. This technology was developed and commercialised by Charles Hull in 1980 [1]. Previously, the main method of creating objects called subtractive manufacturing (SM). SM is to manufacture a target object by continuous reduction of a complete model, AM is the opposite technology of SM. Layer and layer fabrication and computer aided design (CAD) are characteristics of AM [2]. From the emergence of AM to the present, more and more people are using this technology and benefiting from it, therefore, AM has the potential to become a disruptive technology. Thanks to the rapid development of materials science and computer science, 3D printing has been utilised in a wide range of industries. AM can increase the speed of creating objects and reduce cost through saving material. Simultaneously, AM can customize the size of materials according to the needs of different types of customers [3,4].

Many 3D printing methods have been developed, currently, the most common are fused deposition modelling (FDM), inkjet printing, contour crafting, stereolithography, selective laser melting (SLM), liquid binding in 3D printing and selective laser sintering (SLS) [5].

AM has been used in many fields due to not only to its customization, but also because many sorts of materials can be applied in AM. Ceramics, metallics, polymers and their combinations can all be used in AM [2].

Since 3D printing can freely customize the shape of the material and apply to a variety of materials, it can be applied in many fields. In the aerospace industry, 3D printing can reduce energy usage and resources, including reduced cycle time, resources, and lower component weight. [6,7]. In the automotive industry, 3D printing allows for the use of lighter and more complex structural materials and builds in faster times, this is thanks

to the rapid production capabilities of 3D printing technology and can maintain the stability and continuity of the work process, and avoid the losses caused by the shutdown of the production line. [8]. In addition, 3D printing can be used to print 3D skin [9] and is used in drug and pharmaceutical research [10] and many other industries. For example, in the field of automobile manufacturing, 3D printing technology can design and produce car models faster; In the aerospace field, compared with traditional processing methods, high-performance materials can be prepared more conveniently through 3D printing technology while saving costs. Besides, through 3D printing technology, bones and organs can be made faster and more accurately.

1.1.1 Selective laser sintering (SLS)

Selective laser sintering (SLS) is a subset of powder bed fusion 3D printing. Its principle is to use a laser beam to heat powder particles, fusing them together to create an object [11]. SLS was developed by Carl Deckard in 1987 at the University of Texas, and utilised a neodymium-doped yttrium aluminium garnet (Nd:YAG) laser [12].

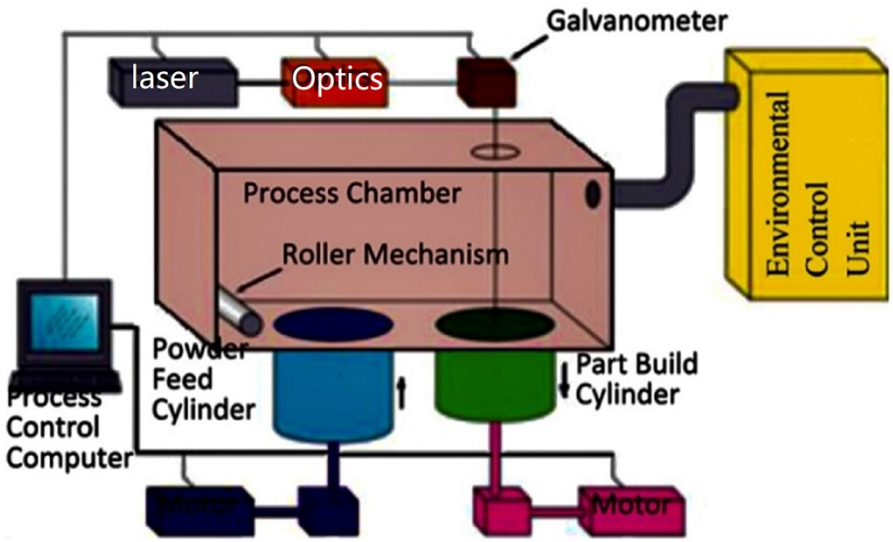

Figure 1.1.1-1 SLS machine (EOSINT P-395) [13]

Based on the figure 1.1.1-1, the SLS machine consists of 6 parts. (1) build platform on which the 3D object is fabricated. (2) Laser, which allow for particle sintering. (3) Galvano mirrors, which are used to adjust the laser beam to the specific location. (4) a powder reservoir or hopper, which can lift fresh powder up and down to the building

platform. (5) a spreading apparatus, which can be used to spread and flat fresh powder on the platform. (6) a material vat, which can be used to collect unsintered powder [22,23,24].

The object can be designed by CAD. The layering roller mechanism spreads the powder on the upper surface with a specific layer thickness. A high intensity laser is used to scan the part to fuse the powder at specific locations for each layer. Once the layer is completed the build platform drops and the powder is spread by roller again. The laser repeats the previous process according to the designed object until the build is finished [13].

Carbon dioxide (CO_2) laser is currently the most commonly used laser in commercial SLS. CO_2 lasers provide higher power at low cost. It means that many sorts of thermoplastic material can be processed by SLS, so that SLS can be applied in many fields, include the aerospace, automotive, medical, engineering and so on [14,15, 16,17,18,19].

Objects are built layer by layer, and all powders will be used as feedstock material. Thus, one of advantages of SLS is that the unused powder is recycled, and maintains the integrity of the object during the building process, hence this technique does not need scaffolds [20]. Thermoplastic polymers are the main feedstock materials for SLS, the laser beam melts the surface of the powder particles and fuses them together, this process is called sintering [21].

As a new technology for manufacturing and processing objects, SLS has received much attention. But its application is still limited, the most critical limitation resides on the that can currently be used for SLS. Most of polymers used in SLS process are thermoplastics, such as polyester, nylon, polyvinylchloride (PVC), etc. Amorphous plastics include ABS, acrylonitrile copolymer (SAN), PVC, polycarbonate (PC) and polystyrene (PS). Crystalline plastics include nylon (PA), polyethylene (PE), polypropylene (PP). When the laser heats the crystalline powder to the melting temperature T_m, the molten powder flows and overlaps to the previous layer. As the temperature decreases, the powder solidifies. Compared with amorphous materials,

crystalline materials have a lower viscosity at T_m [25,26,27]. Polymethyl methacrylate (PMMA) and polyamide (PA-11 or PA-12) are the two most commonly used polymers in SLS. PMMA is hard, brittle, scratch resistant, transparent, low cost, while PA-11 or PA-12 has a high strength, chemical resistant [28]. When the powder material absorbs the laser energy, the temperature rises above Tg and sinters, and the powder particles begin to agglomerate due to mutual adhesion. In addition to the materials available for SLS, there are other aspects that inhibit SLS technology. For example, the surface of the object printed by SLS technology is rough, and it is prone to warpage and deformation when forming large-size parts, and the processing time is long, with respect to some AM techniques, because before processing, it should have a preheat time, after printing, it should take 5 to 10 hours to cool down before it can be taken out of the powder tank.

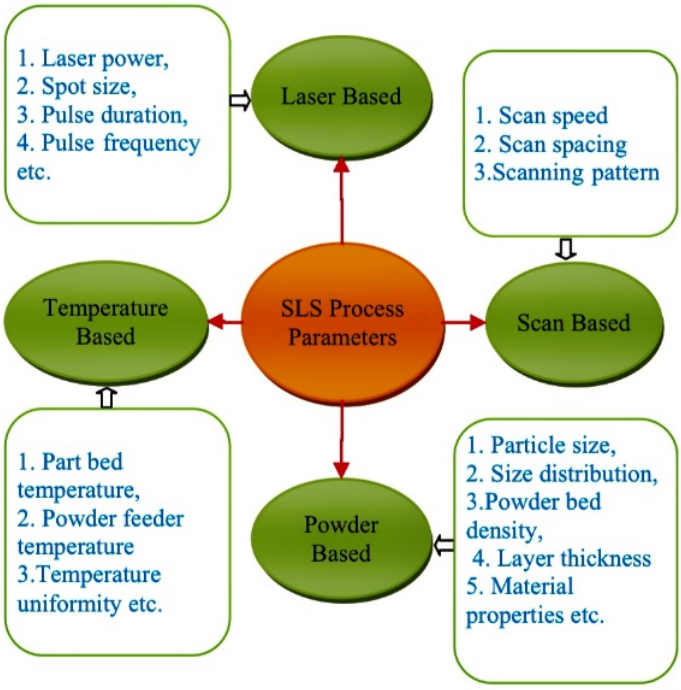

Figure 1.1.1-2 SLS process parameter [29,30]

From figure 1.1.1-2, SLS process parameters can be divided into four main parts: laser, temperature, scan and powder. The use and development of SLS can be impacted by each parameter.

Currently, PA-12 is the most common commercial powder for SLS [31]. Other polymers, such as PE(E)K, TPE, TPU, PEBA and PA-6 are gradually becoming commercially available substituted, but there are still shortcomings.

In order to figure out why some materials are suitable to SLS, but some not, several considerations need to be taken into account. The parameters of material and SLS apparatus are important clues to answer this question. Some properties, such as thermal, optical and rheological belong to intrinsic properties of the molecular structure, which are difficult to change. Other properties, include particle and powder are belong to extrinsic properties, which are easier to control [33].

CO_2 laser beams are used to fuse or melt the powder material in specific locations, resulting in the upper powder being bonded with the previous sintered layers. For crystalline polymers, crystallization should be inhibited during processing so the processing temperature must be between the T_m and T_c, which narrows the field of possible materials, as the gap between T_m and T_c should be at least of 10 °C[34]. Optical properties are also important, but generally less restrictive because as long as the powder absorbs the wavelength of the laser, the power of laser can be optimized for the material in question. [35,36]. The slower the laser scanning speed, the higher the energy density and processing time, which means that more energy needs to be consumed, and the density of the material is higher. On the contrary, the faster the scanning speed, the more conducive to the manufacture of porous materials [37]. Besides, laser beam spot size is also an important parameter. Process rate well be limited if a small laser is used. large laser size can be used with small one to reduce thermal gradient and residual stress. Particle size and shape play a key role in the sintering process [38]. If the particles are too big, it will need more energy and decrease the resolution of printing. However, small particles will result in high electrostatic force which hinder flow and result agglomeration [39]. Normally, it is better if the shape of particle is spherical and the size between 58 and 180μm [40]. Thickness is another key factor, typically, the thickness ranges from 0.07 to 0.5mm [41]. The greater the thickness, the lower the resolution, and vice versa [30].

1.1.1.1 PMMA powders for SLS

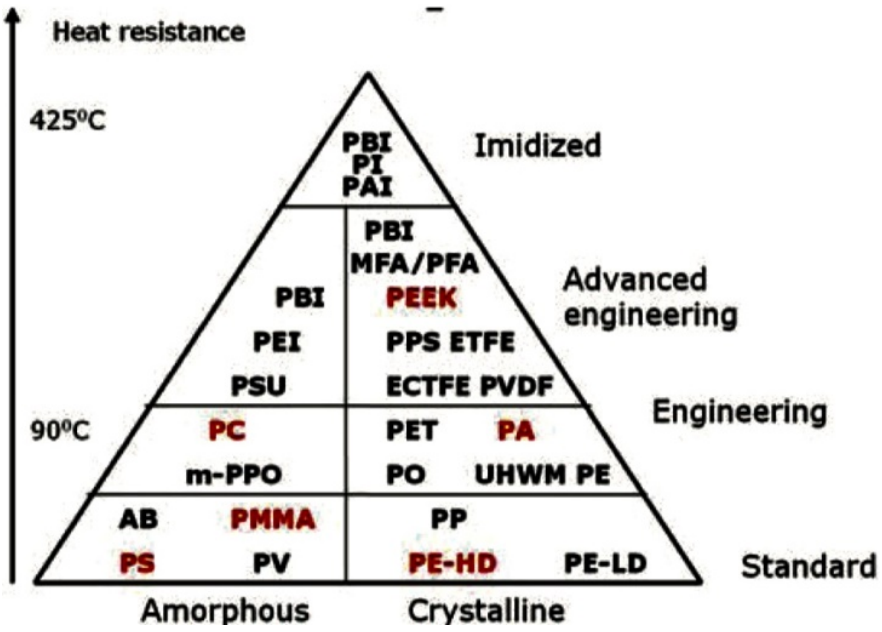

Figure 1.2.1.1-1 Thermoplastic polymer (Materials in red are used in SLS)) [42]

Current thermoplastic polymers which can be used in SLS are listed in the figure 1.2.1.1-1.

The most common method to obtain PMMA is free radical polymerization (FRP). PMMA has excellent physical and chemical properties, such as high colourability, good chemical resistance and excellent compatibility with human tissue [43,44]. Complex shapes, such as most biomedical applications have been difficult to fabricate through conventional process method [45,46]. Also, SM methods offer several drawbacks, for example, when fabricating PMMA objects, more processing steps are required, lack of automation, more raw materials are consumed, and customized tools are required [47]. Thanks to the development of additive manufacturing, it is feasible to process PMMA through 3D printing. Fused Deposition Modeling (FDM) has been exploited to fabricate customized porous materials of PMMA [48]. However, SLS has some inherent advantage comparing to FDM. SLS can be allowed to create complex shapes of parts and there is a low compaction force among powders, so that the objects are porous consistently [49]. Although the use of SLS to process PMMA materials has obvious advantages, there are not many related reports [50].

1.1.2 Inkjet printing and digital light processing

Inkjet printing uses droplets as the basic forming unit. There are two types of inkjet printing methodologies: continuous inkjet printing and drop-on-demand (DOD) inkjet printing.

In the process of continuous inkjet printing, the liquid-like material is reserved in a chamber, liquid is broken up into droplets through a piezoelectric action. Then droplets fall out via a contraction of voltage and fall on the platform by gravity. The dropped droplets will spread according to the difference in viscosity. The object will be shaped after the solvent evaporates [51,52,53].

The advantage of DOD inkjet printing is that it has good regional accuracy and time control, and the droplet size is also smaller. In thermal DOD inkjet printing (or bubble jet), liquid is heated via a heating resister to evaporate solvent and form a bubble. An ink drop is extruded with the expansion of the bubble [54]. Piezoelectric DOD inkjet printing is another type of DOD inkjet printing, in which there is a piezoelectric material in the nozzle. The piezoelectric material is deformed when the electric current passes through, then ink drop can fall out [55].

Photopolymerization plays a crucial role in the synthesise of novel polymers. The strategy of using photopolymerization-based 3D printing has also attracted a significant amount of attention [56]. The main two techniques of using photopolymerization-based 3D printing are stereolithography (SLA) and digital light processing (DLP) [57]. The advantage of DLP is that it can reduce the printing time whilst maintaining high precision fabrication [58]. Due to the 3D network structure of hydrogel, and other properties, such as high elasticity and softness, several technologies of 3D printing have been applied in hydrogel, such as DLP. Hydrogels play an essential role in many fields, such as drug delivery [59]. 3D printing of hydrogels has been expected to be applied in bio-relevant fields, such as model tissues [60], biosensors [61]. Drop-on-demand inkjet printing of hydrogels can achieve high resolution, the range of suitable viscosity for inkjet printing is 3.5-12 mPa s^{-1} [62]. Currently, different methods of polymerization, such as ATRP or RAFT have been used to synthesis gel-like materials for inkjet printing. 2-Hydroxyethyl methacrylate (HEMA), triethylene glycol methyl ether

methacrylate (TEGMA) and poly(ethylene glycol) methacrylate (PEGMA), have been used as co-monomers to synthesize gel-like materials for inkjet printing [63], [64], [65].

1.2 Polymers

The word “polymer”, is derived from the Greek word “poly”, meaning “many” and “meros”, meaning “part”, refers to large molecules whose structure is composed of multiple repeating units. Small molecule compounds that can form repeating structural units are called monomers. Degree of polymerization (DP), number average molecular weight (Mn), weight average molecular weight (Mw) and dispersity (Đ) are important parameters for characterise a polymeric molecule. The degree of polymerization refers to the number of repeating units consecutively appearing in the polymer molecular chain, and is represented by n. The number average molecular weight is a statistical average representing the molecular weight of all polymers. Polydispersity is used to measure the polymer molecular weight distribution [66].

1.2.1 Classification of polymers

When classified by source, polymers can be divided into two categories: natural polymers and synthetic polymers. According to performance classification, polymers can be divided into three categories: plastic, rubber and fibre.

If classified by purpose, it can be divided into general polymer, engineering material polymer, functional polymer, biomimetic polymer, medical polymer, polymer medicine, polymer reagent, polymer catalyst and biopolymer.

According to the main chain structure, it can be divided into four categories: carbon chain polymer, hetero chain polymer, element organic polymer and inorganic polymer [67].

Besides, according to the types of monomers in the polymer, it can be classified into homopolymers and copolymers. Copolymers can also be divided into block copolymers and random copolymers.

1.2.1.1 Homopolymers

Homopolymer is a polymer formed by polymerization of only one monomer, such as polyvinyl chloride and polystyrene, and their repeating units are their respective structural units, such as -A-A-A-A- or -$(A)_n$-, that is, repeating units can be used to represent the polymer structure (fig. 1.2.1.1-1).

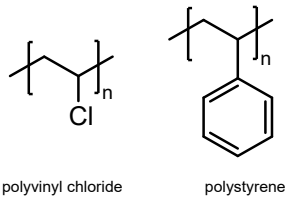

Figure 1.2.1.1-1 examples of homopolymer

1.2.1.2 Copolymers

Copolymer is produced from a polymerization involving two or more monomers. According to the sequence of structural units, copolymers can be divided into alternating copolymers, random copolymers, block copolymers, and graft copolymers (figure 1.2.1.2-1). In alternating copolymer the two structural units A and B in the copolymer are strictly alternating. In random copolymer the random distribution of two structural units A and B in the copolymer. The combination through a single link of polymer A and polymer B in the form of a chain is called a block copolymer. A graft copolymer is composed of a main chain and a branch, and the main chain and the branch are composed of two monomers respectively.

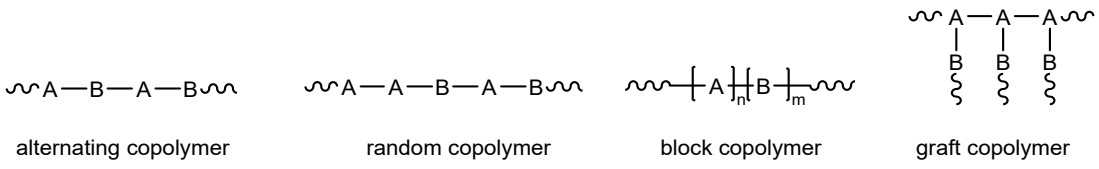

Figure 1.2.1.2-1 illustration of different types of polymers

1.3 Polymerization

Polymerization is the process of converting monomers into polymers. The polymerization reaction can be divided into step-growth polymerization and chain-growth polymerization. Step-growth polymerization refer to a polymerization reaction in which monomers with two or more functional groups condense with each other and produce small molecular by-products (water, alcohol, ammonia, hydrogen halide, etc.) to generate polymer compounds. Chain-growth polymerization refers to the synthesis of polymers from one or more monomers. During the reaction, no low-molecular by-products are formed. The resulting polymer has the same base chemical composition as the raw material, while its relative molecular mass is a multiple of the relative molecular mass of the raw material. [68]

1.3.1 Free radical polymerization (FRP)

Free radical polymerization (FRP) is a chain growth polymerization reaction initiated by free radicals. In this reaction the free radicals continue to grow as the propagation of the polymer chain continues. Once the monomer is depleted the reaction is finished. By opening the double bonds in the monomer, repeated addition reactions occur between the molecules to connect many monomers to form the final polymer. [69].

The FRP reaction can be divided into five polymerization methods: bulk polymerization [70], solution polymerization [71], suspension polymerization [72], emulsion polymerization [73] and dispersion polymerization [74]. Besides, photo radical polymerization is also a strategy to prepare polymer [75].

1.3.1.1 Initiators for free radical polymerization

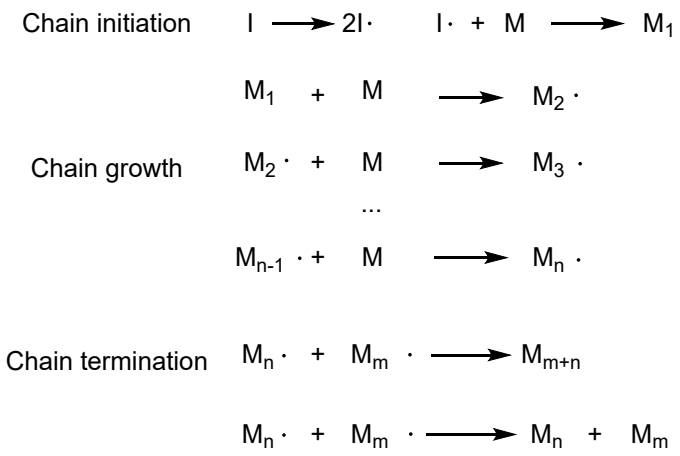

Figure 1.3.1-1 The mechanism of free radical polymerization

As the mechanism shows (fig. 1.3.1-1), at the beginning of the FRP, the initiator plays an essential role to start the chain initiation. If there is no initiator, FRP cannot take place. According to molecular structure classification, initiators can be divided into three groups azo-based, peroxy-based and redox. Besides, according to the solubility properties, they are then subdivided into water-soluble initiators and organic initiators. According to the decomposition method of the initiator, there are thermal-, chemical- and photo-decomposition [69].

Azo initiators are a particular group of initiators that generate free radicals triggered by thermal or photo degradation. Almost all the decomposition of azo initiators are first-order reactions, with no side reactions. There are two sorts of azo-initiators, one is oil soluble, such as Azobisisobutyronitrile (AIBN). Another is water soluble, such as 2,2'-azobis[2-methylpropionamidine] dihydrochloride (AIBA) (fig. 1.3.1.1-1).

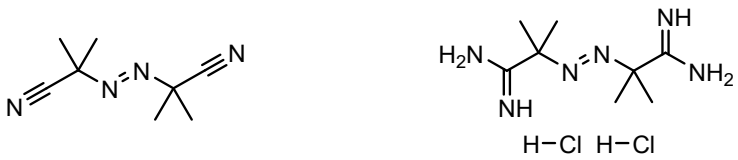

AIBN AIBA

Figure 1.3.1.1-1 initiator for FRP

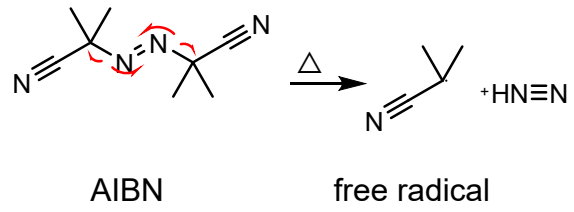

Figure 1.3.1.1-2 the mechanism of decomposition of AIBN under heating.

AIBN is a common initiator for FRP. There are several advantages of AIBN as a radical initiator: 1) only one kind of free radical can be created; 2) fewer side reactions; 3) high reactivity for the polymerization of vinyl, acrylate, methacrylate-based, etc. monomers [76]. Under heat (fig. 1.3.1.1-2) or light-based decomposition, AIBN can be degraded to cyano isopropyl (CI) radicals, which can initiate the propagation of the polymer chain. Organic peroxide initiators, such as benzoyl peroxide (BPO), are another kind of initiator used to initiate polymerization of monomers (fig. 1.3.1.1-3).

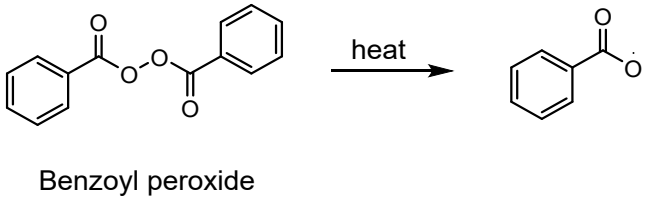

Figure 1.3.1.1-3 the mechanism of decomposition of BPO under heating

Photo-initiators are also an effective method to initiate polymerization. According to the mechanism of polymerization, photo-initiators can be divided into three classes: radical, cationic, and anionic. These photo-initiators can be triggered under UV-vis light and create free radicals, cations and anions [77]. Photo-initiator radical polymerization can be categorized two kinds, one is type I (radical formation after α-cleavage of the excited molecule), such as acetophenones [78], hydroxyalkyl phenones [79] and their derivatives (fig. 1.3.1.1-4).

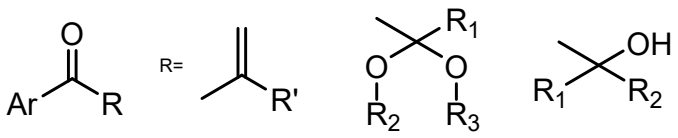

Figure 1.3.1.1-4 some kinds of type I photo-initiator

After absorbing the photon energy, they transition from the ground state to the excited singlet state and reach the excited triplet state through intersystem crossing (ISC). The molecules in the excited state form active radicals with initiating ability through the

homolysis of chemical bonds [80]. Another one is type II (radical formation after H-abstraction from a second molecule), such as aromatic ketone compound [81] (fig. 1.3.1.1-5).

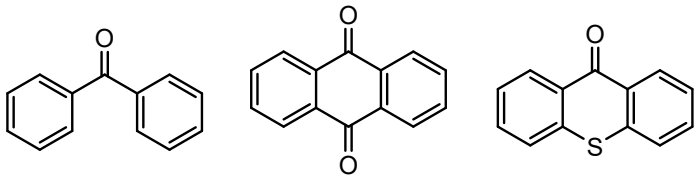

Figure 1.3.1.1-5 some kinds of type II photo-initiator

1.3.1.2 Solution polymerization

Solution polymerization is a process in which monomers and initiators are dissolved in a suitable solvent for polymerization. If the polymer can be dissolved in the solvent, it is a typical solution polymerization. The advantages of solution polymerization are different, among others, the heat generated during the polymerization process is easily to remove, the temperature of the polymerization reaction is easy to control, the low molecular weight products are easy to remove, and the automatic acceleration phenomenon can be eliminated [71]. If the product can be dissolved in the solvent, it can be called homogeneous solution polymerization. It means that the product can be taken out through precipitating in another organic solvent in which it is not soluble or evaporating the solvent [82]. On the other hand, if the product can be separated out during the reaction time, it can be called the precipitation polymerization [83].

1.3.1.3 Radical photo polymerization

Free radical photopolymerization refers to a reaction that generates free radicals and initiates polymerization after exposure to UV-vis light [84]. One of advantages of this photoinitiated polymerization is that it can be conducted under mild condition [85]. It means that an environmentally friendly and high effective process can be provided to prepare materials [86]. Unlike thermal initiators, photopolymerization can be carried out at room temperature, and the reaction time is shorter than thermal polymerization

[87]. After a long period of development, photopolymerization has been combined with a variety of polymerization techniques to prepare novel materials, such as photo-ATRP [88], photo-RAFT [89], and so on. based on this, photo radical polymerization has numerous applications in electrochemistry [90], biological [91], pharmacology [92], 3D printing [93].

1.4 Ring-Opening Polymerization (ROP) of lactones and relevant functional polyester applications

Ring-opening polymerization is a reaction that converts cyclic compounds to linear compounds. Comparing with the polycondensation reaction, there is no formation of small molecules during the ring-opening polymerization process. Comparing with the addition polymerization of olefins, there is no cleavage of double bonds during the polymerization process. The driving force that initiates ring-opening polymerization is the release of ring tension. Cyclic ethers, cyclic acetals, cyclic esters, cyclic amides, and cyclic silanes can all undergo ring-opening polymerization [94] (fig. 1.4-1).

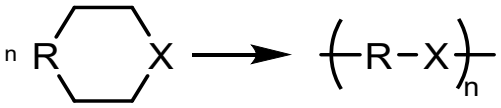

Figure 1.4-1 a demonstration of ring-opening polymerization

Aliphatic polyesters have attracted more and more interest, owing to their properties.(ref) Ring-opening polymerization is the most common method used to prepare polyesters and aliphatic polycarbonates. Polyesters are biocompatible and degradable in some specific circumstances [95,96]. For example, in the medical field, polyester based materials can be degraded in the human body, therefore, polyester can be used in drug delivery systems [97] or implantation [98].

Degradation is an important feature for aliphatic polyesters. However, during the degradation process of polyesters, acidic compounds can be created, which can be harmful to the human body [99]. In comparison, there is no such acidic compound created during the degradation process of aliphatic polycarbonates according to in vivo

and in vitro test [100,101]. Degradation rates of polyesters are faster than aliphatic polycarbonates, meaning that they have different applications according to the different degradation rates [102,103].

Polyesters, such as poly(lactide) or poly(caprolactone), polycarbonates, such as poly(trimethylene carbonate), are widely used and are of low cost to produce[104].

1.4.1 Catalysts for ROP

Traditional catalysts are mainly organometallic catalysts. D-orbital metals, such as Sn, Zn, Ti, Al, etc. The mechanism of such catalysts is an insertion-coordination mechanism [105,106] (fig. 1.4.1-1).

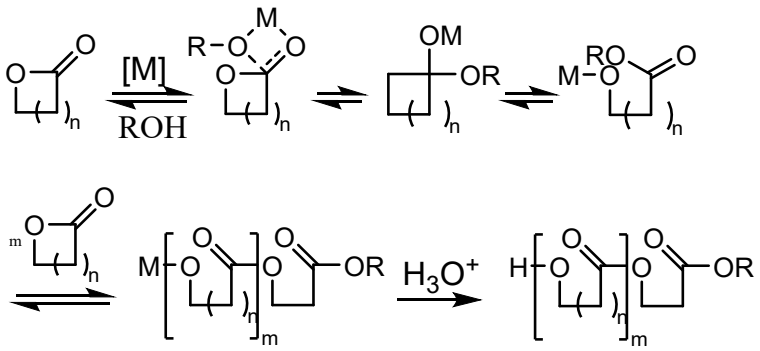

Figure 1.4.1-1 the mechanism of organometallic catalysts to initiate ROP

Sn-based catalysts, such as $Sn(Oct)_2$ is a common organometallic catalyst. However, there are shortcomings of using organometallic catalysts. One of which, is metal residue is difficult to remove after purification, which can hinder the application of product in biomedical and microelectronic fields [107]. Because of this shortcoming, metal-free catalysts are becoming an alternative technique to realize ring-opening polymerization. Enzymes are one of them [108,109]. There are several advantages of using enzymes as catalysts. 1) reaction process can be carried out in milder conditions; 2) Enzymes are derived from renewable resources, and they can be recycled after reaction and purification; 3) various reaction media can be selected, such as bulk, organic solvent, etc; 4) well-defined structures can be created via enzymes catalysis; 5) in comparison with organometallic catalysts, enzymes-catalysts do not need any extra air or water during the reaction time [110,111,112].

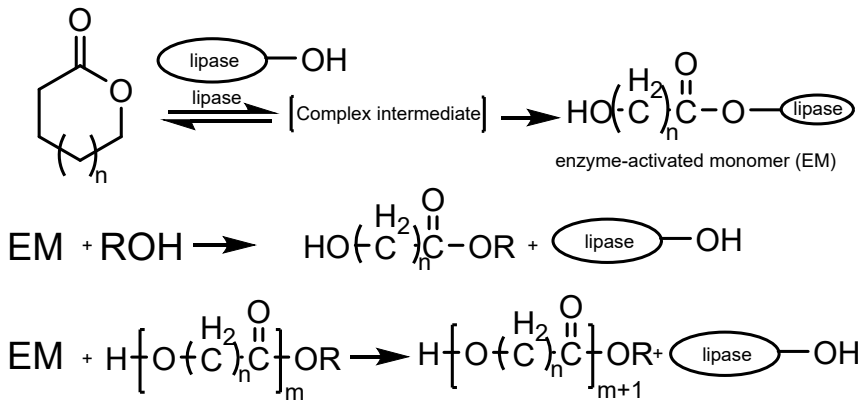

Figure 1.4.1-2 the mechanism of using enzymes as catalysts

Unfortunately, there are some drawbacks of using enzymes as catalysts. 1) it could take a long time to react; 2) difficult control over final polymer architecture [113]. Also, for the specific aim of this thesis work, enzymes-catalyzed ring-opening polymerization (eROP) has lower sensitivity to HEMA-initiator and can cause side reactions, such as transesterification processes [114]. Triazabicyclodecene (TBD), has been shown to be a highly effective basic catalyst for many reactions, such as Michael additions [115], Wittig reactions [115], Henry reactions [117], and transesterification reactions [118]. TBD is also an effective catalyst for ring-opening polymerizations of lactide [119] (fig. 1.4.1-3).

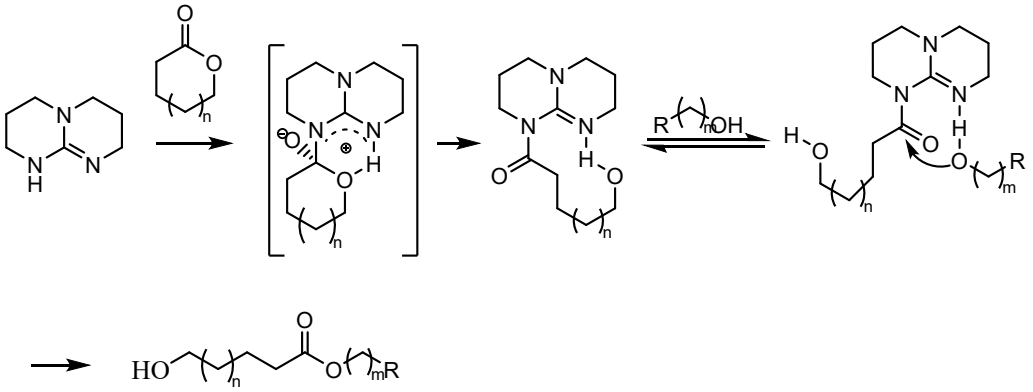

Figure 1.4.1-3 the mechanism of dual activation of monomer and initiator via TBD

Generally, there are some advantages of using TBD as the catalyst. 1) high reactivity for ROP of LA, CL; 2) good control of molecular weight and polydispersity; 3) commercially available and relatively easy of use [119,120].

4-DMAP has been reported that as a Lewis basic amines catalyst to initiate the ROP of lactide in 2001 [121].

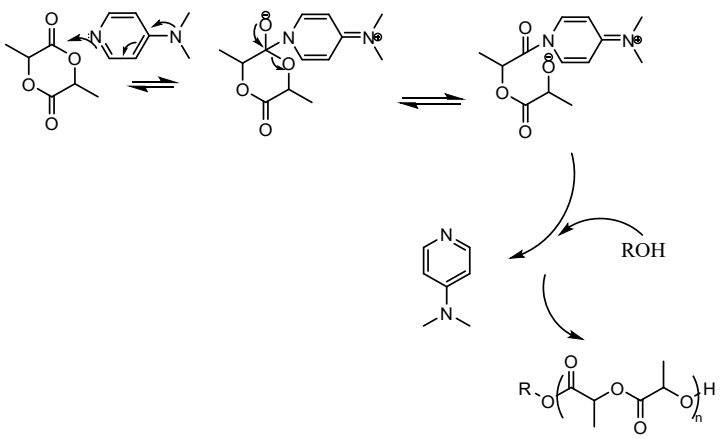

Figure 1.4.1-4 the mechanism of using 4-DMAP as catalyst to catalyze ROP of LA

1,8-Diazabicyclo[5.4.0]undec-7-ene (DBU) is an effective catalyst for ROP [122].

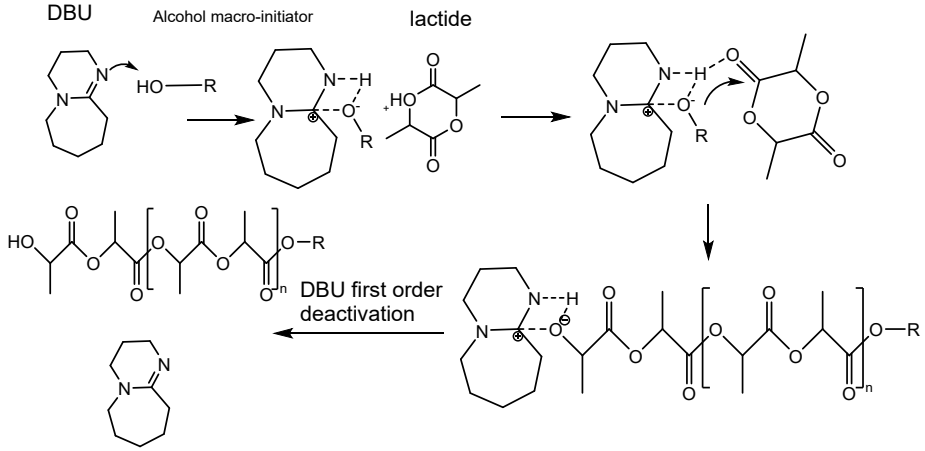

Figure 1.4.1-5 a brief explanation of mechanism of the ROP of DBU catalysed

1.4.2 Functional initiators for ROP

Polyesters and polycarbonates are excellent materials for medical applications, such as drug delivery system (DDS) [123]. Generally, there are three routes to modify and functionalize a polyester from ROP, one is to modify the lactones to obtain functional lactones [124] (fig. 1.4.2-1). Another is to post-polymerization functionalization of the end group. (ref)

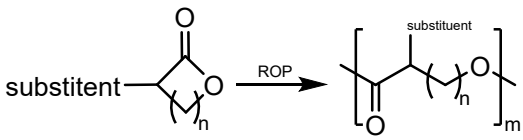

Figure 1.4.2-1 the strategy for synthesis of functional polycarbonates

While a more straightforward and high yield strategy is to use a functional molecule as ROP initiator, such as 2-Hydroxyethyl methacrylate (HEMA) or 2-Hydroxyethyl acrylate (HEA). According to this, the introduction of ROP and FRP at the same time is a promising strategy to create novel materials for different applications.

1.4.2.1 2-Hydroxyethyl methacrylate (HEMA) and 2-Hydroxyethyl acrylate (HEA) and relevant ring-opening polymerization

2-hydroxyethyl methacrylate (HEMA) is a bifunctional group molecule, there is an end-group carbon-carbon double bond and a hydroxyl moiety in the HEMA. HEMA-based polymers can be used in many biological fields, such as contact lenses, drug delivery system, etc. [125]. There are some special features for the homopolymer of HEMA, poly(HEMA), such as if the degree of polymerization (DP) of poly(HEMA) is less than 20, the polymer is completely soluble in water [126]. HEA is similar in structure to HEMA, poly(HEA) can be completely dissolved in water, regardless of the molecular weight [127]. Other differences between poly(HEMA) and poly(HEA) are that poly(HEMA) has exhibited the trait of temperature-responsive, but poly(HEA) has not [128]. HEMA and HEA have been used as initiators to initiate ring-opening polymerization [129,130,131]. There are some advantages of using HE(M)A as an initiator: 1) the molecular weight can be tailored through calculating different ratios of initiator and monomer; 2) many kinds of catalysts can be used, such as DBU, TBD; 3) polymerizable macromonomers can be obtained through ROP, then, ATRP, RAFT can be used to synthesize the final polymers, according to the actual application, such as nanoparticles (NPs).

1.5 Degradation of polyesters and polycarbonates

Traditional polymeric materials, such as polyethylene, are not fully degradable, and can cause huge environmental problems and can be harmful to people. Because of such problems, environmentally friendly and sustainable polymeric materials should be synthesized. According to the mechanism of degradation, degradable polymers can be

split into two types, biodegradable polymers [132] and stimuli-responsiveness polymers [133,134]. Degradable polymers, normally contain degradable groups, such as: an ester [135], azo [136], ketal [137], disulfide [138], diselenum [139]. These kinds of polymers can be cleaved under specific circumstances, such as heat [140], light [141], force [142], acid or base [143], redox [144]. Figure 1.5-1 is an example of how ester structure degrades under base and acid circumstance respectively.

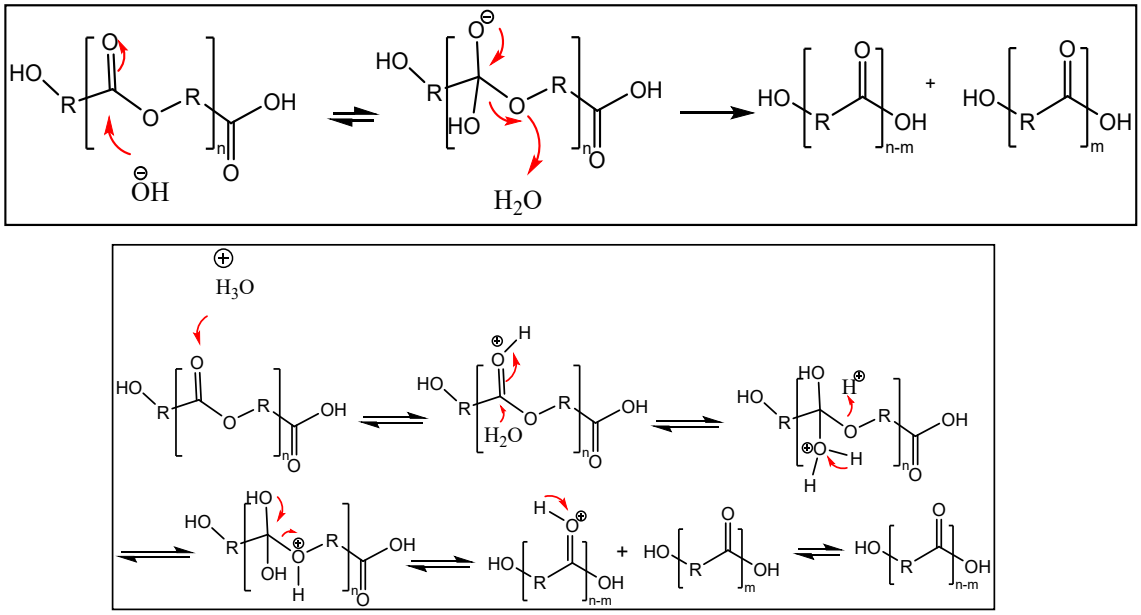

1.5-1 the mechanism of degradation processes of polyesters under base (above) and acid (below) aqueous

Currently, degradable polymers are used in many fields, such as drug delivery [145], biomedical implants [146], etc..

Many synthesized methods have been used to obtain degradable polymers. For example, a combination of ROP and ATRP or RAFT has been used to synthesize stimuli-responsiveness polymers [147,148].

1.6 Dye monomer

Dispersion dyes are a class of dyes with relatively small molecular weight and with low water-solubility. Disperse dyes are polar molecules containing anthraquinone or azo groups Dispersion dyes can dye polyester and other fibers. [149].

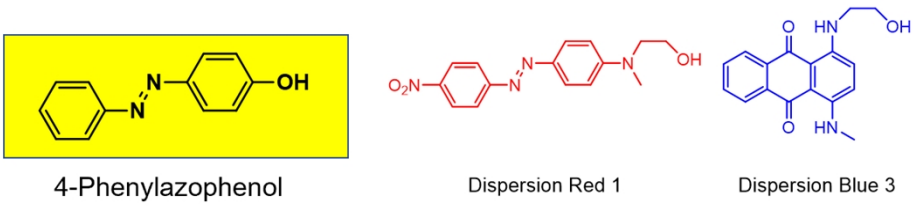

Figure 1.6-1 three types of dispersion dyes

Figure 1.6-1 shows three-primary color of dye: yellow, red and blue. Other colors can be obtained via a mixture of different ratios of these three-primary colors.

There are three performance defects in dyeing with disperse dyes: 1. Thermal cohesion; 2. Poor alkali resistance and stability; 3. Thermal migration and 4. Low color fastness [150].

Covalent combination of chromophores and monomer is a new method to improve these drawbacks, such as the promotion of dye fastness [151]. The change of ratios of colored monomer and monomer can lead to different colors of the obtained copolymer. In copolymerization, the copolymerization of different color monomers can create new chromophoric polymers.

In SLS, a mixture of differently colored polymer powders can fabricate colored objects [152].

1.8 The main research ideas of this thesis

Currently, most of the materials used for SLS are white or grey. If the final printed system needs to be coloured, post printing painting is usually used. However, there are shortcoming for traditional painting: 1. most paints are prepared with volatile organic solvents, which are not good for the human body. 2. the already coloured paint can be scraped off. 3. it will increase costs and time. 4. for objects with complex shapes, the difficulty of colouring will increase and 5. it is difficult to have different colours on the same part of an object.

Besides, most objects lack of function after printing, post-functionalization can be seen as indispensable for particular applications. Therefore, development of functional materials, such as stimuli-responsive inks for 3D printing is an emergent topic.

Based on the above, this thesis aimed to develop novel-coloured materials with pH-responsiveness for 3D printing. 1) synthesis of degradable monomer with cleavable colour moiety. In this section, synthesis of red and yellow monomers with pH-responsiveness was be arranged. First of all, HEMA and HEA as initiator, DBU as a catalyst to start the ROP of LA to obtain a liner structure of ester with an end-group hydroxyl, HE(M)A-p(LA)$_n$-OH; synthesis of HE(M)A-p(LA)$_n$-OH and succinic anhydride was the second step to obtain a liner structure with an end-group carboxylic acid, HE(M)A-p(LA)$_n$-COOH; esterification of HE(M)A-p(LA)$_n$-COOH and Dispersion Red 1 or 4-Phenylazophenol to obtain HE(M)A-p(LA)$_n$-COO-Red (or Yellow) was the final step. These kinds of compounds are composed through a linear structure of many ester groups and a cleavable moiety of colour. These materials can be hydrolysed in acidic and basic aqueous. The degradation process can be observed via the change of colour of aqueous; 2) in this section, as a co-monomer, MMA was used to obtain pH responsive copolymers with different color shades through different ratios with color monomers. The polymerization was undertaken by FRP. PMMA has been proved that is suitable for SLS. DSC will be used to check whether the Tg of copolymers are suitable for SLS; 3) in this section, photopolymerization of HEMA (and TEGMA, PEGMA) and color monomers to synthesize a series of amphiphilic materials for inkjet printing. Several literatures have reported to use HEMA, TEGMA and PEGMA as co-monomers to synthesize materials for inkjet printing. Materials of using photopolymerization can also be applied in DLP. Copolymers composed of hydrophilic and hydrophobic side chains have special properties, such as self-assembly or prepared to NPs.

2. Experimental section

2.1 Materials

Methyl methacrylate (MMA), 2,2'-Azobis(2-methylpropionitrile) (AIBN), 2-hydroxyethyl methacrylate (HEMA), 2-Hydroxyethyl acrylate (HEA), 1,8-Diazabicyclo(5.4.0)undec-7-ene (DBU), Dispersed Red 1, Dispersed yellow, 4-Dimethylaminopyridine (4-DMAP), N,N'-Dicyclohexylcarbodiimide (DCC), Lactide (97%), Succinic anhydride (99%), Triethylene glycol methyl ether methacrylate (TEGMA), Poly(ethylene glycol) methacrylate (PEGMA) were purchased from Sigma-Aldrich UK. All chemicals were used without purification. Solvents (DCM, THF, toluene) were purchased from Fischer Scientific UK and used without further purification. Deionized water was used.

2.2 Characterization Methodologies

2.2.1 Proton Nuclear Magnetic Resonance (^{1}H-NMR)

^{1}H-NMR spectra were recorded by Bruker (400MHz): Bruker AV(III)400HD, Bruker AV400 and Bruker AV(III)400. 5mg of sample was weighted and dissolved in 600 µL of $CDCl_3$. $CDCl_3$ solvent peak reference was taken at 7.26 ppm.. Chemical shifts were expressed through parts per million (ppm) relative to the internal standard tetramethylsilane (TMS). Mnova 14.2.0 was used to analyze the ^{1}H-NMR data.

2.2.2 Gel Permeating Chromatography (GPC)

An Agilent 1260 infinity HPLC was adopted. provided with 4 detectors: a differential refractive index, a viscometer, a UV-vis detector and a multi-angle light scattering detector. Two Agilent mixed D columns kept at 40 °C were used. THF was used as the mobile phase with a flow rate of 1 ml/min. The system was calibrated with poly(methyl

methacrylate) standards with average Mn in a range from 540 to 1.02×10^6 g/mol^{-1} with narrow dispersities (Đ). Astra 6.1 was used to analyze the GPC data.

2.2.3 Differential scanning calorimetry (DSC)

TA-Q2000 DSC system (TA instruments) was used to test the thermal properties (such as Tg) of the produced polymers. The system was calibrated by indium and sapphire standards under a N_2 flow (50 ml/min^{-1}). The sample (5mg) was weighed in a T-zero sample pan. The sample was heated at a rate of 10^{o}C/min^{-1} from 10^{o}C to 200^{o}C.

2.3 Synthesis procedures

2.3.1 Synthesis of HE(M)A-p(LA)$_n$-OH (n=10, 20)

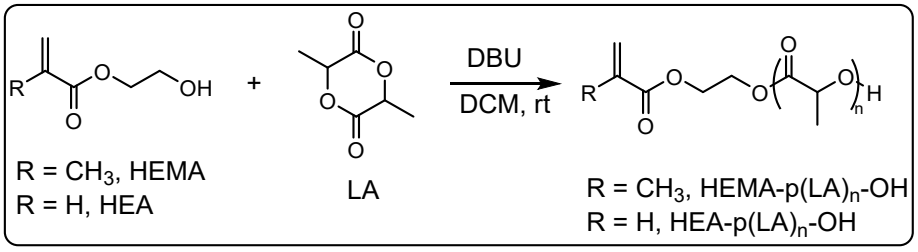

Scheme 2.3.1-1 the synthesis of HR(M)A-p(LA)$_n$-OH, n=10, 20

The degree of polymerization (DP) can be targeted by changing the molar monomer/initiator [M/I] ratio. DP=20 means that the ratio between monomer and initiator is 20:1 [M/I=20:1].

The synthesis of HEMA-p(LA)$_{20}$-OH is reported as an example. A mixture of HEMA (45mg, 0.347mmol) and DL-lactide (1g, 6.94mmol) was placed in a vial (predried at 100^{o}C overnight) and anhydrous DCM (7ml) was added and the mixture was stirred until complete dissolution. DBU (2% w/w to [M]), as a catalyst, was added to the vial to initiate ring opening polymerization at room temperature for 20min.

To terminate the reaction, the mixture was poured in a centrifuge tube containing a cold mixture of hexane (20ml) and Et_2O (10ml) in order to precipitate the polymer. The solid

was collected and washed with hexane (20ml) twice. The product was put in freezer for later use.

The synthesis of HEMA-p(LA)$_{10}$-OH and HEA-p(LA)$_{10/20}$-OH used the same method, with the only difference being that hexane (30ml) was used to precipitate and wash.

. ^{1}H-NMR (400MHz, $CDCl_3$), **HEMA-p(LA)$_{20}$-OH**: δ 6.12 (s, 1H, CH), 5.6 (s, 1H, CH), 5.18 (m, 1H, CH), 4.37 (m, 4H, CH_2CH_2), 2.76 (s, 1H, OH), 1.94 (s, 3H, CH_3), 1.59 (m, 3H, CH_3). **HEA-p(LA)$_{20}$-OH**: δ 6.44 (d, 1H, CH), 6.12 (m, 1H, CH), 5.9 (d, 1H, CH), 5,18 (m, 1H, CH), 4,37 (m, 4H, CH_2CH_2), 1.59 (m, 3H, CH_3).

2.3.2 Synthesis of HE(M)A-p(LA)$_n$-COOH (n=10, 20)

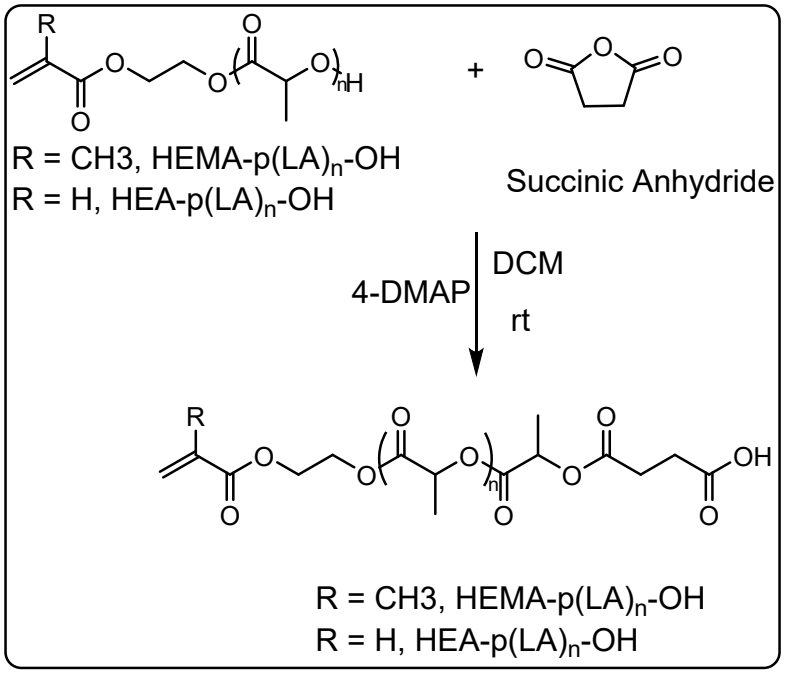

Scheme 2.3.2-1 the synthesis of HE(M)A-p(LA)$_n$-COOH, n=10, 20

DCM (10ml) was added in a vial with HEMA-p(LA)$_{20}$-OH (1g, 0.33mmol) till dissolution.

THF (2ml) was added in a vial with Succinic Anhydride (66mg, 0.66mmol) till dissolution. Two vials of solution were mixed. 4-DMAP (44mg, 0.36mmol) was added to catalyse the reaction. The reaction mixture was stirred at room temperature for 1-4 hrs. After termination, the reaction mixture was poured into a centrifuge tube which

contained a cold solvent mixture of cold hexane (20ml) and Et_2O (10ml) in order to precipitate the product. The solid was washed by Et_2O (20ml) twice. The product was put in freezer for later use. The synthesis of HEMA-p$(LA)_{10}$-COOH and HEA-p$(LA)_{10/20}$-COOH used the same method, with the only difference being that hexane (30ml) was used to precipitate.

The ^{1}H-NMR data was recorded by Bruker (400MHz, $CDCl_3$). **HEMA-p$(LA)_n$-COOH**: δ 6.12(s, 1H, CH), 5.6(s, 1H, CH), 5.18(m, 1H, CH), 4.37(m, 4H, CH_2CH_2), 2.73(m, 4H, CH_2CH_2), 1.92(s, 3H, CH_3), 1.56(m, 3H, CH_3). **HEA-p$(LA)_n$-COOH**: δ 6.44 (d, 1H, CH), 6.12 (m, 1H, CH), 5.9 (d, 1H, CH), 5,18 (m, 1H, CH), 4,37 (m, 4H, CH_2CH_2), 2.65(m, 4H, CH_2CH_2), 1.59 (m, 3H, CH_3).

2.3.3 Synthesis of HE(M)A-p$(LA)_n$-COO-Red (n=10, 20)

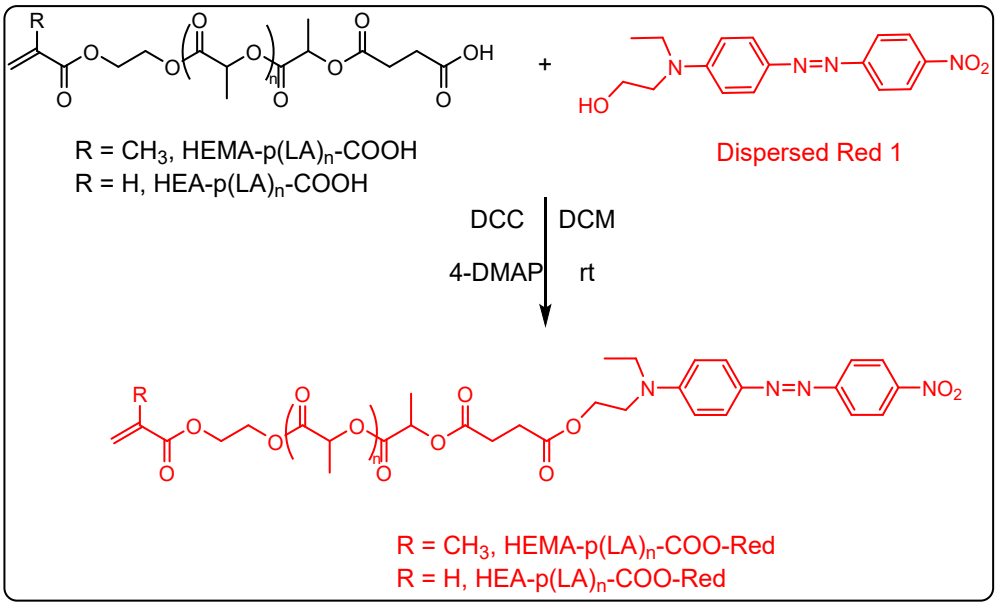

Scheme 2.3.3-1 the synthesis of HE(M)A-p$(LA)_n$-COO-Red, n=10, 20

HEMA-p$(LA)_{20}$-COOH (1.2g, 0.38mmol) was added to a vial and dissolved in DCM (10ml). Hydroquinone (1mg) was dissolved by THF (2ml) and added to the vial. Dispersed Red 1 (143mg, 0.45mmol) and DCC (93mg, 0.45mmol) were added and dissolved completely. 4-DMAP (9.27mg ,0.076mmol) was solubilised in DCM (2ml) and added to the vial. The mixture solvent was kept stirring at room temperature for 24h. The reaction mixture was filtered via a Buchner Funnel, the filtrate was collected

and poured in a centrifuge tube which contained a solvent mixture of cold hexane(20ml) and Et_2O(10ml) in order to precipitate the product, the solid was washed by Et_2O (20ml) twice. The product was stored in freezer for later use.

The synthesis of HEMA-p$(LA)_{10}$-COO-Red and HEA-p$(LA)_{10/20}$-COO-Red used the same method, with the only difference being that hexane (30ml) was used to precipitate. The ^{1}H-NMR data was recorded by Bruker (400MHz, $CDCl_3$). **HEMA-p$(LA)_n$-COO-Red**: δ 8.47 (m, 2H, CH×2), 8.0 (m, 4H, CH×4), 6.9 (m, 2H, CH×2), 6.12(s, 1H, CH), 5.6(s, 1H, CH), 5.18(m, 1H, CH), 4.37(m, 8H, CH_2CH_2×2), 3.7 (m, 4H, CH_2CH_2), 2.65(m, 4H, CH_2CH_2), 1.92(s, 3H, CH_3), 1.56(m, 3H, CH_3). **HEA-p$(LA)_n$-COO-Red**: δ 8.47 (m, 2H, CH×2), 8.0 (m, 4H, CH×4), 6.9 (m, 2H, CH×2), 6.44 (d, 1H, CH), 6.12 (m, 1H, CH), 5.9 (d, 1H, CH), 5,18 (m, 1H, CH), 4,37 (m, 8H, CH_2CH_2×2), 3.7 (m, 4H, CH_2CH_2), 2.65(m, 4H, CH_2CH_2), 1.59 (m, 3H, CH_3).

FT-IR spectrum: the absorption of N-H stretching was at 3300 cm^{-1}; the absorption of =C-H stretching (arene, alkene) was in 3080-3010 cm^{-1}; the absorption of C=O stretching was 1770 cm^{-1}; C=C stretching was at 1650 cm^{-1}; C=C (arene) stretching was in 1600-1450 cm^{-1}; N=N stretching was in 1410-1400 cm^{-1}; C-O stretching was in 1270-1200 cm^{-1}; C-H (arene) bending was in 880-860 cm^{-1}.

2.3.4 Synthesis of HE(M)A-p$(LA)_n$-COO-Yellow (n=10, 20)

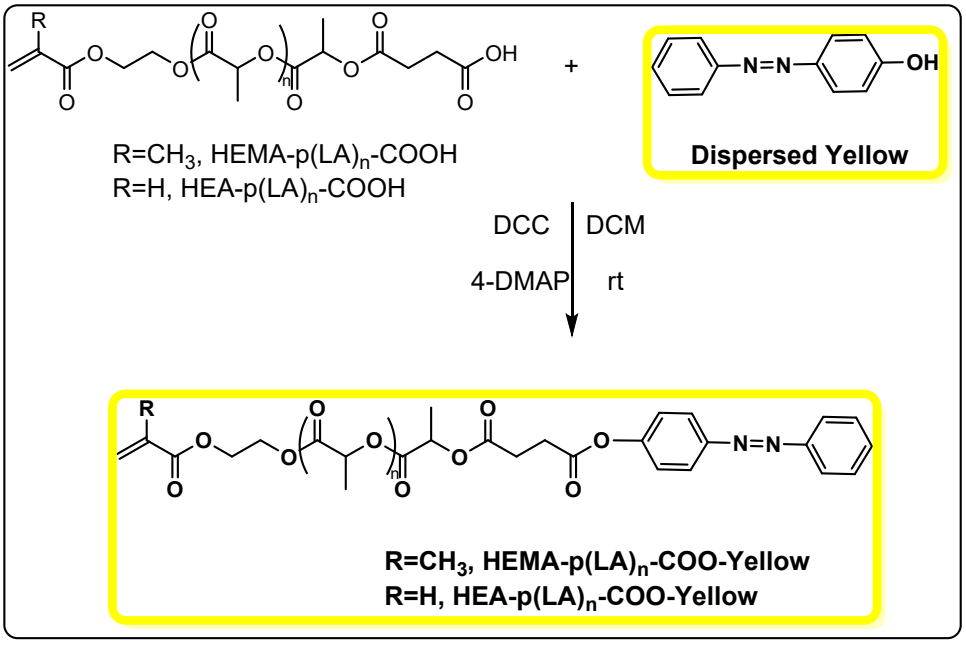

Scheme 2.3.4-1 the synthesis of HE(M)A-p(LA)n-COO-Yellow, n = 10, 20

HEMA-p(LA)$_{20}$-COOH (1.2g, 0.38mmol) was added to a vial and dissolved by DCM (10ml) completely. Hydroquinone (1mg) was dissolved by THF (2ml) and added to the vial. Dispersed yellow (89mg, 0.45mmol) and DCC (93mg, 0.45mmol) were added to the vial and dissolved completely. 4-DMAP (9.27mg ,0.076mmol) was dissolved by DCM (2ml) and added to the vial. The mixture solvent was kept stirring at room temperature for 24h. After termination of the reaction, the reaction mixture was filtered via Buchner filtration, the filtrate was collected and poured in a centrifuge tube which contained a solvent mixture of cold hexane(20ml) and Et_2O(10ml) to precipitate the product, the solid was washed by Et_2O (20ml) twice. The product was put in freezer for later use.

The synthesis of HEMA-p(LA)$_{10}$-COO-Yellow and HEA-p(LA)$_{10/20}$-COO-Yellow used the same method, with the only difference being that hexane (30ml) was used to precipitate.

The ^{1}H-NMR data was recorded by Bruker (400MHz, $CDCl_3$). **HEMA-p(LA)$_n$-COO-Yellow**: δ 7.9 (m, 4H, CH×4), 7.5 (m, 2H, CH×2), 7.05 (m, H, CH), 6.9 (m, 2H, CH×2), 6.12(s, 1H, CH), 5.6(s, 1H, CH), 5.18(m, 1H, CH), 4.37(m, 4H, CH_2CH_2), 3.5 (m, 4H, CH_2CH_2), 1.92(s, 3H, CH_3), 1.56(m, 3H, CH_3). **HEA-p(LA)$_n$-COO-Yellow**: δ 7.88 (m, 4H, CH×4), 8.06 (m, 2H, CH×2), 7.9 (m, H, CH), 6.92 (m, 2H, CH×2), 6.48 (d, 1H, CH), 6.23 (m, 1H, CH), 5.92 (d, 1H, CH), 5.25 (m, 1H, CH), 4.48 (m, 4H, CH_2CH_2), 3.5 (m, 4H, CH_2CH_2).

FT-IR spectrum: the absorption of =C-H stretching (arene, alkene) was in 3080-3010 cm^{-1}; the absorption of C=O stretching was 1770 cm^{-1}; C=C stretching was at 1650 cm^{-1}; C=C (arene) stretching was in 1600-1450 cm^{-1}; N=N stretching was in 1410-1400 cm^{-1}; C-O stretching was in 1270-1200 cm^{-1}; C-H (arene) bending was in 880-860 cm^{-1}.

2.3.5 Free radical copolymerization of HEMA-p(LA)$_n$-COO-Red and MMA in toluene (n=10, 20)

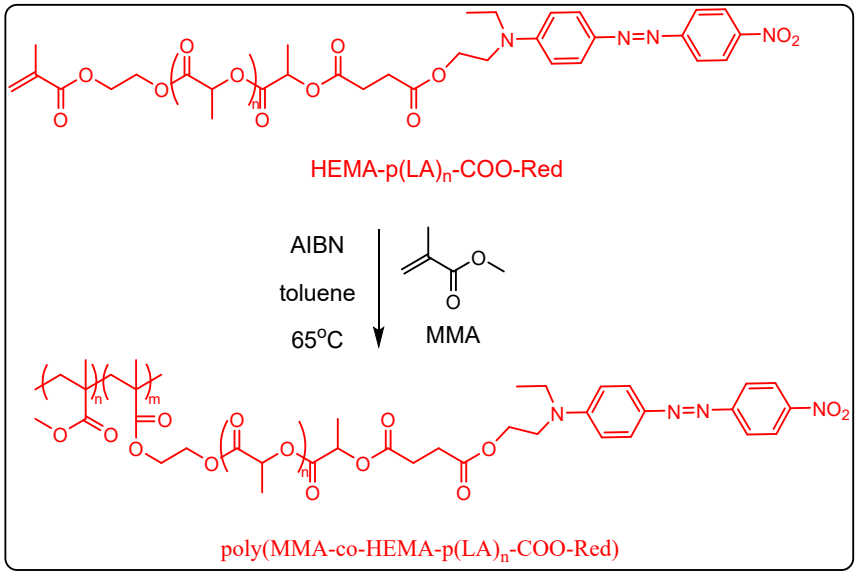

Scheme 2.3.5-1 the free radical copolymerization of HEMA-p(LA)$_{10/20}$-COO-Red and MMA in toluene

HEMA-p(LA)$_{20}$-COO-Red (0.6g, 10% w/w% to MMA) and MMA (6g) were added to a round-bottomed flask, AIBN (66mg, 1% w/w% to [M]) was dissolved in 2ml toluene and added to the flask. Toluene (28 mL) (the mass ratio of [M] and toluene is 30% to 70%) was added to the flask to dissolve the mixture completely. The reaction system was heated at 65°C for 24h. After termination of the reaction, the reaction solvent was added dropwise into cold methanol to precipitate the product. The solid was washed by methanol twice until there was no red colour in the filtrate. The product was dried in a vacuum oven at 25°C for 24h.The synthesis of HEMA-p(LA)$_{10}$-COO-Red used the same method.

2.3.6 Free radical copolymerization of HEMA-p(LA)$_n$-COO-Yellow and MMA in toluene (n=10, 20)

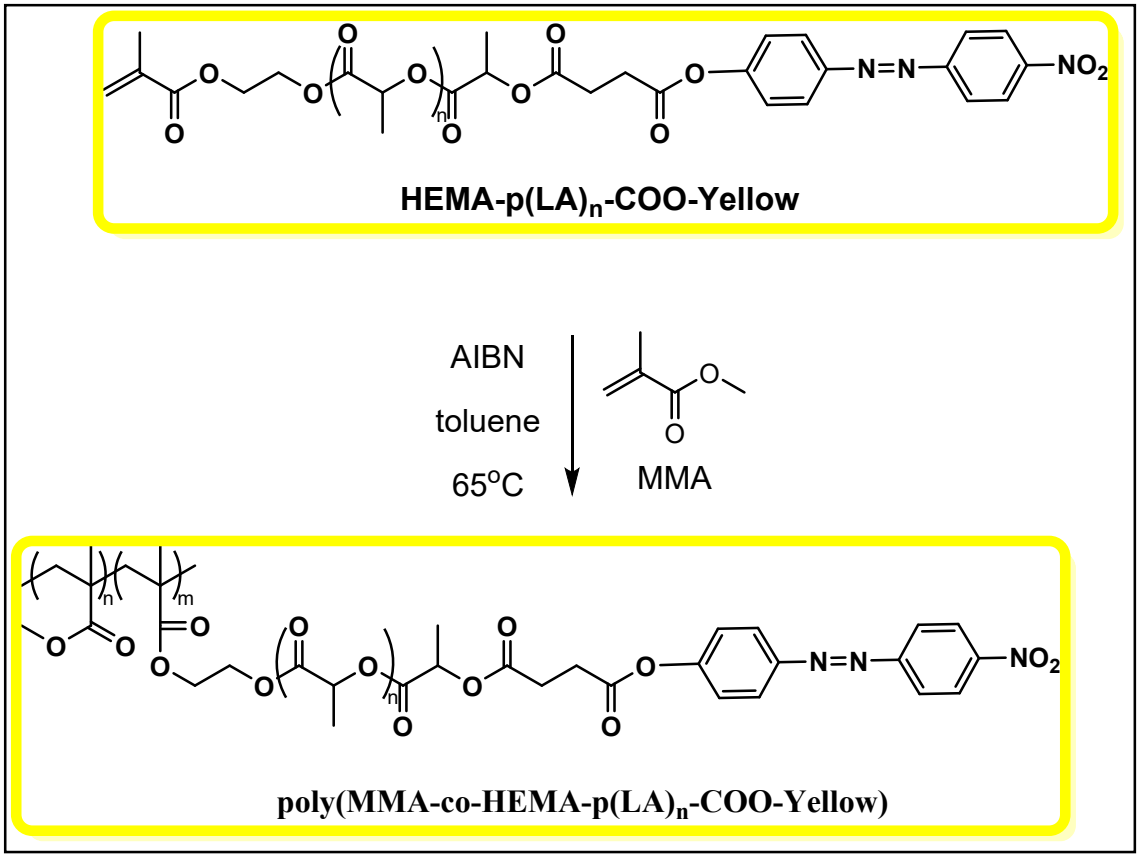

Scheme 2.3.6-1 the free radical copolymerization of HEMA-p(LA)$_{10/20}$-COO-Yellow and MMA in toluene

HEMA-p(LA)$_{20}$-COO-Yellow (0.6g, 10% w/w% to MMA) and MMA (6g, 60mmol) were added to a round-bottomed flask, AIBN (66mg, 1% w/w% to [M]) was dissolved in 2ml toluene and added to the flask. Toluene (28 mL) (the mass ratio of [M] and toluene is 30% to 70%) was added to the flask to dissolve the mixture completely. The reaction system was heated at 65 °C for 24h. After termination of the reaction, the reaction solvent was added dropwise into cold methanol to precipitate the product. The solid was washed by methanol twice until there was no yellow colour in the filtrate. The product was dried via vacuum oven at 25 °C for 24h.The synthesis of HEA-p(LA)$_{10}$-COO-Yellow used the same method.

2.3.7 Free radical copolymerization of TEGMA with red or yellow monomer

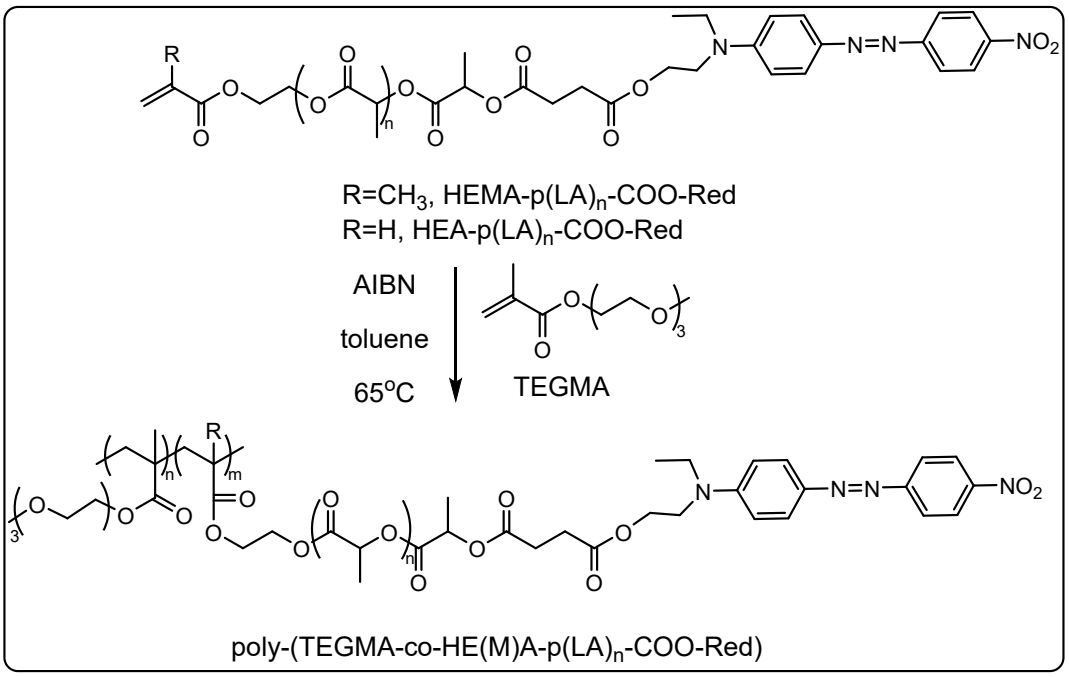

Scheme 2.3.7-1 the free radical copolymerization of HE(M)A-p$(LA)_{10/20}$-COO-Red and TEGMA in toluene

HEMA-p$(LA)_{10}$-COO-Red (1g, 20% wt% to TEGMA) and TEGMA (4g) were added to a round-bottomed flask and 10ml toluene was added to dissolve the monomer. AIBN (50mg 10wt% to [M]) was dissolved in 2ml toluene and added in the flask. Toluene (15 mL) was added to the flask. The reaction system was degassed for 30 min by argon and heated to 65°C for 24h. After termination of the reaction, the reaction solvent was added dropwise to a flask with 60ml of cold hexane to precipitate the product. The solid was washed by 30ml hexane twice. The product was dried via vacuum oven at 25°C for 24h. The ^{1}H-NMR data was recorded by Bruker (400MHz, $CDCl_3$). δ 8.32 (m, 2H, CH×2), 8.02 (m, 2H, CH×2), 5.18 (m, 1H, CH), 4.11 (s, 3H, CH_2), 3.66 (s, 6H, CH_2), 3.48 (s, 3H, CH_3), 2,18 (s, 3H, CH_3), 1.04 (s, 3H, CH_3), 0.88 (s, 3H, CH_3).

2.1.8 Photopolymerization of HEMA, TEGMA, mPEGMA and red or yellow monomer

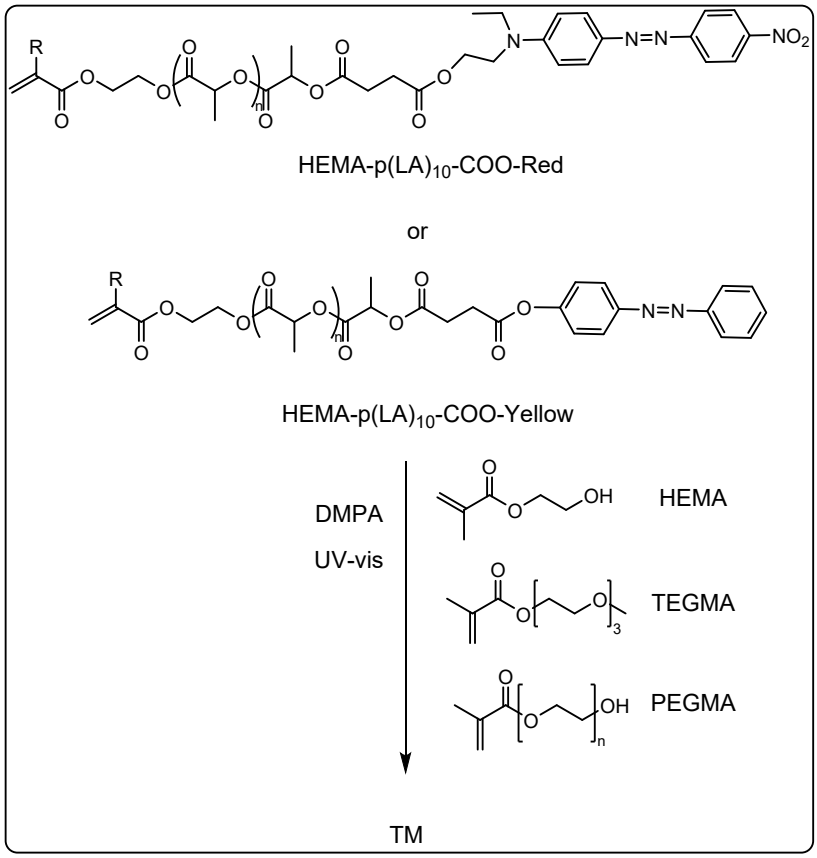

Scheme 2.3.8-1 photopolymerization of HEMA, TEGMA, mPEGMA and red or yellow monomer

HEMA-p(LA)$_{10}$-COO-Red (Yellow) (10-20% wt%) was dissolved in HEMA (or TEGMA, mPEGMA) (1g) in a vial, DMPA (1-2% wt% to [M]) was added and dissolved. The reaction mixture was placed in a well plate. The UV reaction set up was degassed for 30min before reaction. After 30min, the well plate was put in the UV reactor and the light was turned on to start the reaction. After 4h, the light was turned off to stop the reaction.

2.3.9 Degradation test of colored monomers and copolymers

2.3.9.1 Degradation test of colored macromonomers.

A specific mass of macromonomer was weighed and put in a vial of 1M NaOH or 1M H_2SO_4 aqueous under ambient temperature. A piece of the material was taken and tested by ^{1}H-NMR and GPC every 24h to check the change of molecular weight.

2.3.9.2 Degradation test of copolymers produced via FRP.

1) Solvent casted films were produced. A specific mass of copolymer was weighed and dissolved in THF (5wt%), the mixture was then poured in a petri dish. After the evaporation of THF, a film was obtained (fig. 2.3.9.2-1). A piece of film was cut and put in a vial containing 1M NaOH or 1M H_2SO_4 aqueous. The film was taken out and weighed every day for 5 months.

2) a specific mass of copolymer as sample was weighed and put in a vial containing 1M NaOH or 1M H_2SO_4 (fig. 2.3.9.2-1). Sample was taken to test via GPC and ^{1}H NMR in order to observe the degradation process.

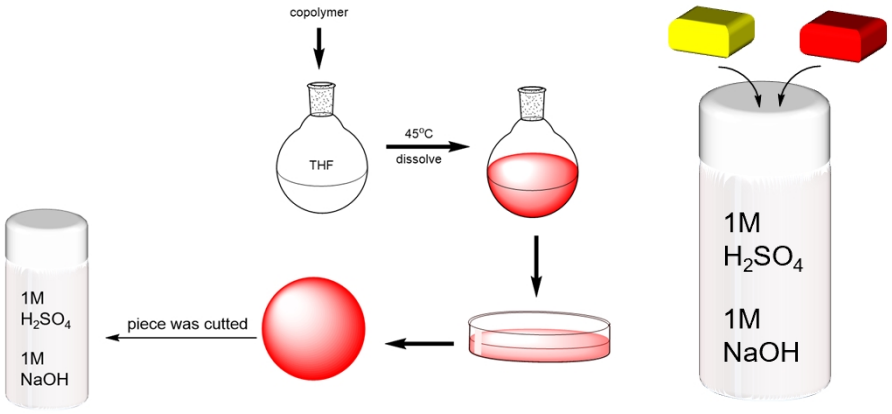

Figure 2.3.9.2-1 a demonstration of solvent casted film (left) and test by copolymers (right)

2.3.9.3 Degradation test of copolymers produced via photopolymerization

A piece of copolymer as sample was taken and put in a vial with 1M NaOH or 1M H_2SO_4. Sample was taken to test via GPC and ^1H NMR to observe the degradation test.

3. Result and discussion

3.1 Synthesis of HE(M)A-p(LA)$_n$-OH (n=10, 20) and characterization

In this section, a linear structure of ester moieties with an end-group carbon-carbon double bond and an end-group hydroxyl was aimed to obtain. End-group double bond can be used to FRP, while end-group hydroxyl can be used to next ring opening reaction. The terminal hydroxyl group of HEMA or HEA can initiate the ROP of lactide (LA) as a nucleophilic initiator with DBU as catalyst. DBU can activate the free hydroxyl group to initiate the nucleophilic reaction.

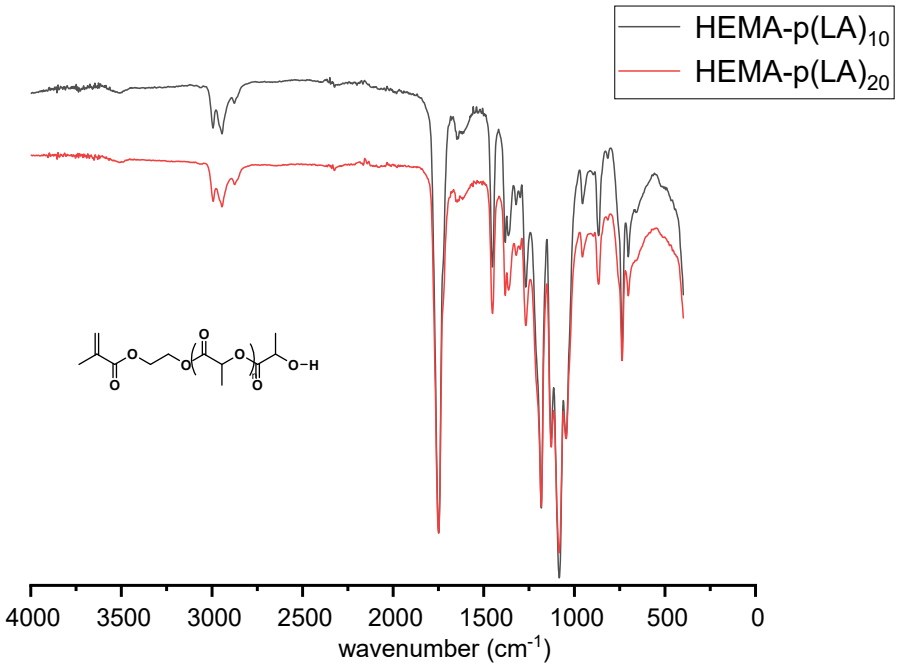

Figure 3.1-1 The FT-IR spectrum of HEMA-p(LA)$_n$-OH (n=10, 20)

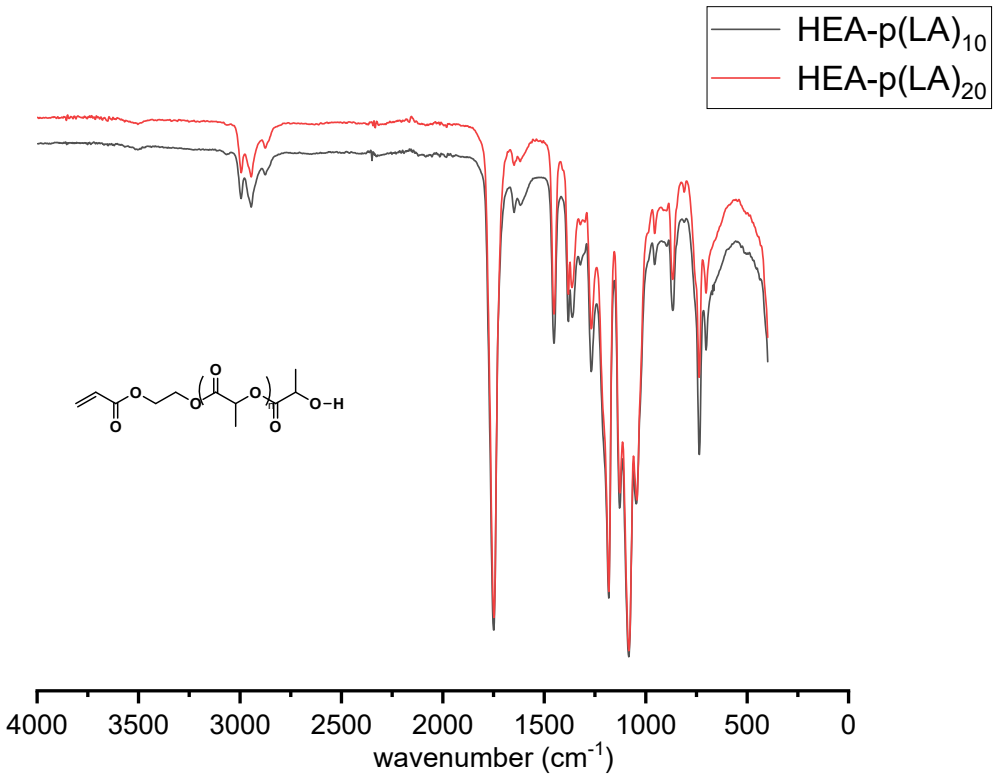

Figure 3.1-2 The FT-IR spectrum of HEA-p(LA)$_n$-OH (n=10, 20)

From Figure 3.1-1 and 3.1-2, O-H stretching was observed at 3490 cm^{-1}; C=O stretching was at 1760 cm^{-1}; C=C stretching was at 1650 cm^{-1}; C-O stretching was at 1275-1200 cm^{-1}. They were the main group of HE(M)A-p(LA)$_n$-OH.

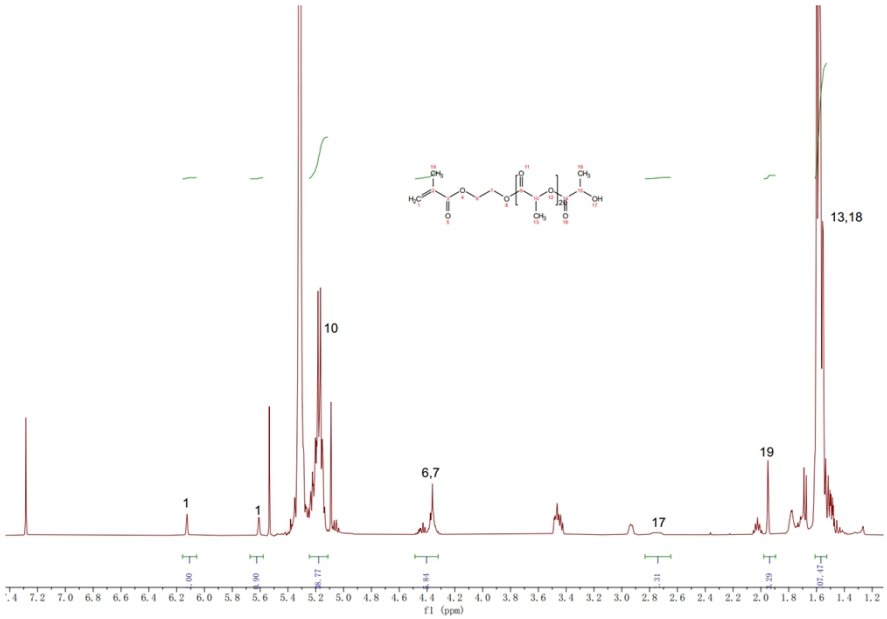

Figure 3.1-3 the ^{1}H-NMR spectrum of HEMA-(LA)$_{20}$-OH

ROP of LA, HEMA as an initiator, DBU as an catalyst

In Figure 3.1-3, the end-group double bond were at around 6.12ppm and 5.60ppm, and the integration was 1:1; the repeating unit of poly(lactide) was at 5.23ppm; two methylene of HEMA and methyne of lactide were at around 4.4ppm; hydroxyl end-group was in spectra range of 2.78ppm, methyl of HEMA was in 1.98ppm; methyl of lactide were in 1.58ppm.

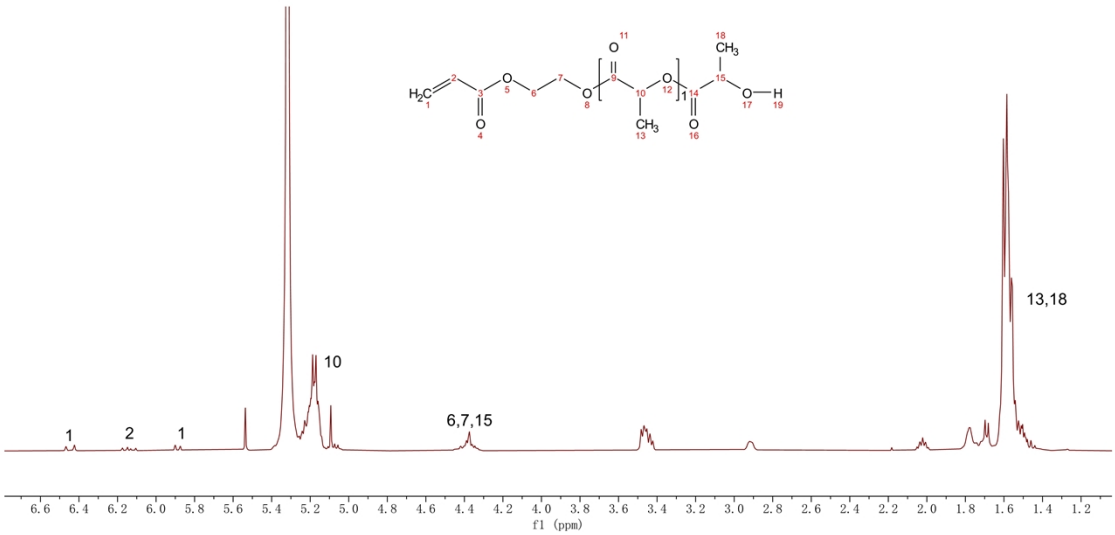

Figure 3.1-4 the ^{1}H-NMR spectrum of HEA-$(LA)_{20}$-OH

ROP of LA, HEA as an initiator, DBU as a catalyst

In the Figure 3.1-4, end-group double bond was in 6.44ppm and 5.87ppm; α-H of vinyl was at 6.18ppm; the repeating unit of lactide was at 5.2ppm, two methylene of HEMA and methyne of lactide were at 4.4ppm, end-group hydroxyl was at 2,83ppm; methyl of lactide were at 1.58ppm.

In summary, FT-IR spectrum shows the main groups of HE(M)-$(LA)_{10/20}$-OH, such as vinyl, carbonyl, hydroxyl. Each hydrogen can be assigned via ^{1}H NMR spectrum. The success of the reaction can be proven by the analysis of FT-IR and ^{1}H NMR.

The actual degree of polymerization (DP) can be calculated by ^{1}H-NMR data. For example, for HEMA-p$(LA)_{20}$-OH, vinyl group was at 6.44ppm and 5.87ppm, the area of 5.25-5.15ppm belong to the -CH- of the repeating unit of LA. First of all, the two

peaks of the terminal double bond were integrated separately and set them to 1 and ensured that they were in a 1:1 relationship. Then, the peak of repeating unit of LA was integrated. The integration of this area represents the number of hydrogens of the Methine group in LA. This value can represent the actual degree of polymerization [153].

Polymer name	Theoretical DP	Actual DP
HEMA-P$(LA)_{10}$-OH	10	10
HEMA-P$(LA)_{20}$-OH	20	19
HEA-P$(LA)_{10}$-OH	10	8
HEA-P$(LA)_{20}$-OH	20	19

Table 3.1-1 theoretical DP and actual DP with HE(M)A-p$(LA)_n$-OH (n=10, 20)

Macromonomer	**Mn (^{1}H-NMR)**	**Mn (GPC)**	**Đ**
HEMA-p$(LA)_{10}$	1570	3800	1.33
HEMA-p$(LA)_{20}$	3010	4200	1.25
HEA-p$(LA)_{10}$	1556	3700	1.35
HEA-p$(LA)_{20}$	2996	4500	1.27

Table 3.1-2 molecule weight from calculation of NMR and GPC

From Table 3.1-1 and 3.1-2, the actual degree of polymerizations were very close to the theoretical ones, this showed that DBU is a good catalyst for ROP of LA. With DBU the degree of polymerisation could be controlled, as well as providing a high conversion after only 20min of reaction. Also, relatively low dispersion can be obtained (Đ<1.4).

From the Table 3.1-2, there were different values between tested by GPC and calculated by NMR. it can be explained that the Mn tested via GPC was an average molecular weight based on calibrant polymer, while for NMR, the Mn was calculated by the integration of repeating unit based on the sample [154].

3.2 Synthesis and characterization of HE(M)A-p(LA)$_n$-COOH (n=10, 20)

As there is a terminal hydroxyl group in the dye structure, and esterification is a simple solution for attaching the terminal hydroxyl group. Therefore, in this section, the synthesis of HE(M)A-(LA)n-OH and succinic anhydride is a shrewd way to obtain end-group carboxylic acids. Initially, the synthesis of HE(M)A-p(LA)$_n$-OH and succinic anhydride failed. For example, based on the method mentioned in 3.1, if a product of a theoretical degree of polymerization of 20, (HEMA-p(LA)$_{20}$-OH) was aimed to obtain, then its integration should be 40 via the ^{1}H NMR spectrum. However, it showed that the integration was almost the double (78 units). It was likely due to the self-polymerization initiated by the end-group double bond leaded to chain growth. In fact, here is a terminal carbon-carbon double bond in the HEMA and HEA, which is a typical π electronic system. This type of structure is easy to be oxidised or triggers a free radical reaction.

Normally, there is a low concentration of hydroquinone in the HEMA or HEA to inhibit the activity of terminal double bond. However, it can be removed through precipitation. Therefore, to avoid this inconvenient, a one-pot reaction was used.

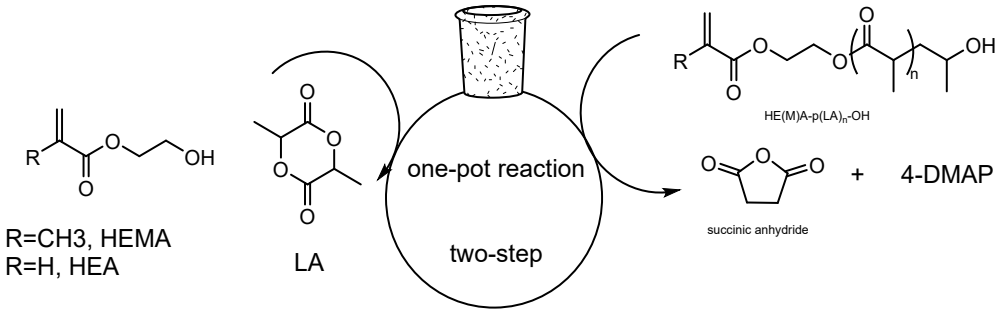

Scheme 3.2-1 the synthesis of HE(M)A-p(LA)$_n$-COOH (n=10, 20) in one-pot reaction

According to scheme 3.2-1, HE(M)A, DBU and LA were added to a vial to synthesize HE(M)A-p(LA)$_n$-OH, after the termination of reaction, succinic anhydride and 4-DMAP were added (one-pot) to start the next reaction to obtain HE(M)A-p(LA)$_n$-COOH. The advantage of a one-pot reaction is that there is still a low concentration of hydroquinone in the reaction system which maintains stability.

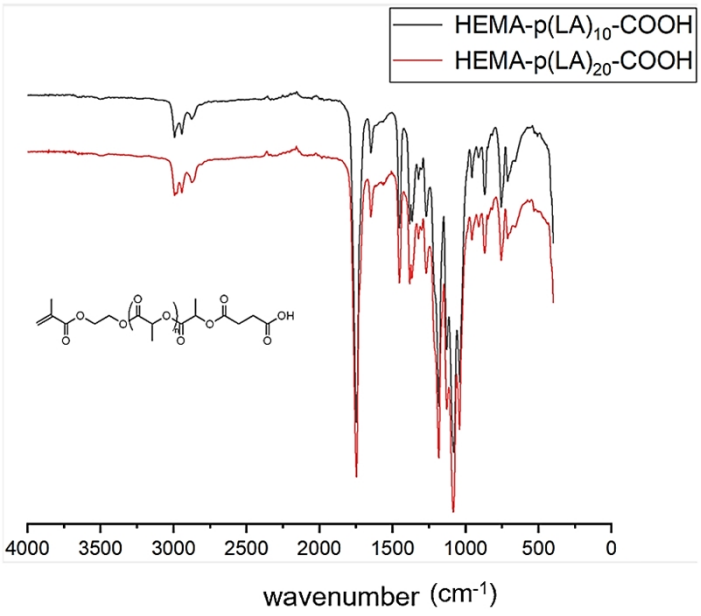

Figure 3.2-1 the FT-IR spectrum of HEMA-p(LA)$_n$-COOH (n=10, 20)

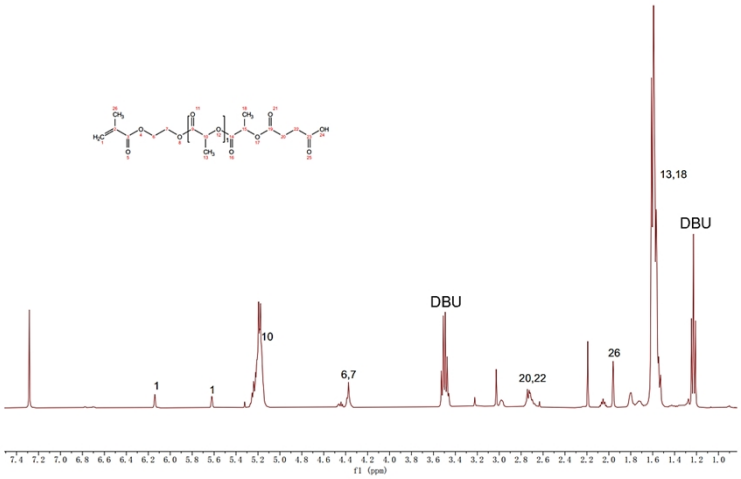

Figure 3.2-2 ^{1}H NMR spectrum of HEMA-p(LA)$_{10}$-COOH via one-pot reaction

From Figure 3.2-1, FT-IR spectrum shows that C=O stretching was at 1760 cm^{-1}; C=C stretching was at 1650 cm^{-1}; C-O stretching was at 1275-1200 cm^{-1}. They were the main group of HEMA-p(LA)$_n$-COOH.

From Figure 3.2-2, ^{1}H NMR data shows that the end-group double bond was in 6.14ppm and 5.52pm; the repeating unit of LA was at 5.20ppm; two methylenes of HEMA was at 4.40ppm; two methylenes of succinic anhydride was at 2.73ppm; methyl of HEMA was at 1.97ppm; two methyl of LA was at 1.58ppm. Besides, residual DBU also showed in ^{1}H-NMR spectrum.

In summary, the main groups of the polymer can be confirmed via FT-IR spectrum, such as vinyl, carbonyl, hydroxyl. Each hydrogen can be assigned via ^{1}H NMR spectrum. The success of the reaction can be proven by the analysis of FT-IR and ^{1}H NMR.

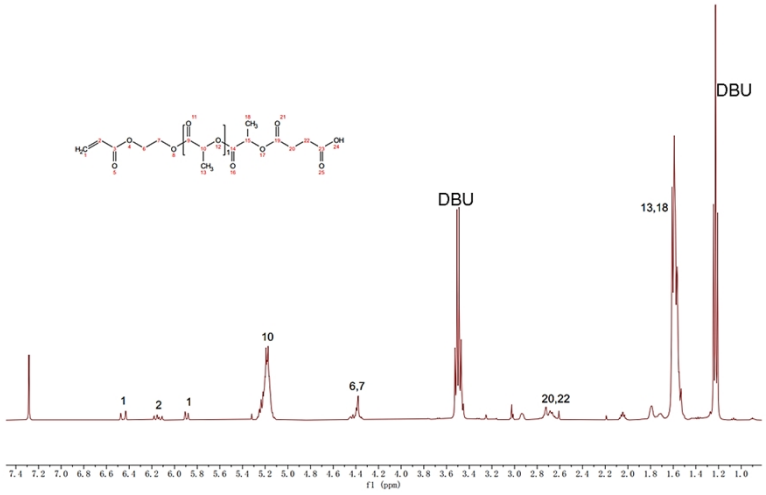

Figure 3.2-3 ^{1}H NMR spectrum of HEA-p$(LA)_{10}$-COOH via one-pot reaction

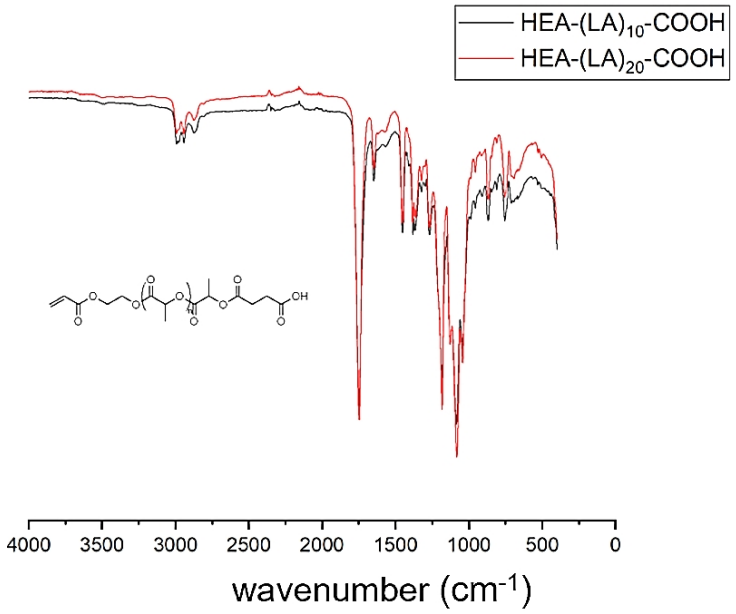

Figure 3.2-4 the FT-IR spectrum of HEA-p$(LA)_n$-COOH (n=10, 20)

In the Figure 3.2-3, FT-IR spectrum shows that C=O stretching was at 1760 cm^{-1}; C=C stretching was at 1650 cm^{-1}; C-O stretching was at 1275-1200 cm^{-1}. They were the main group of HEA-p$(LA)_n$-COOH.

In the Figure 3.2-4, ^{1}H NMR sprctrum shows that the double bond end-group was at around 6.48ppm and 5.87ppm; α-H of vinyl was at 6.15ppm; the repeating unit of LA

was at 5.20ppm; two methylenes of HEA were at 4.40ppm; two methylenes of succinic anhydride were at 2.69ppm; two methynes of LA were at 1.58ppm.

In the ^{1}H NMR of Figure 3.2-1 or 3.2.2, the peak at 2.73ppm represents the two methylenes of succinic anhydride. One is connected to the carbonyl group (-CO**CH_2**-) and one is connected to the carboxylic acid (-**CH_2**-COOH).

In summary, main the groups can be confirmed via FT-IR spectrum, such as vinyl, carbonyl, hydroxyl. Each hydrogen can be assigned via ^{1}H NMR spectrum. The success of the reaction can be proved by the analysis of FT-IR and ^{1}H NMR.

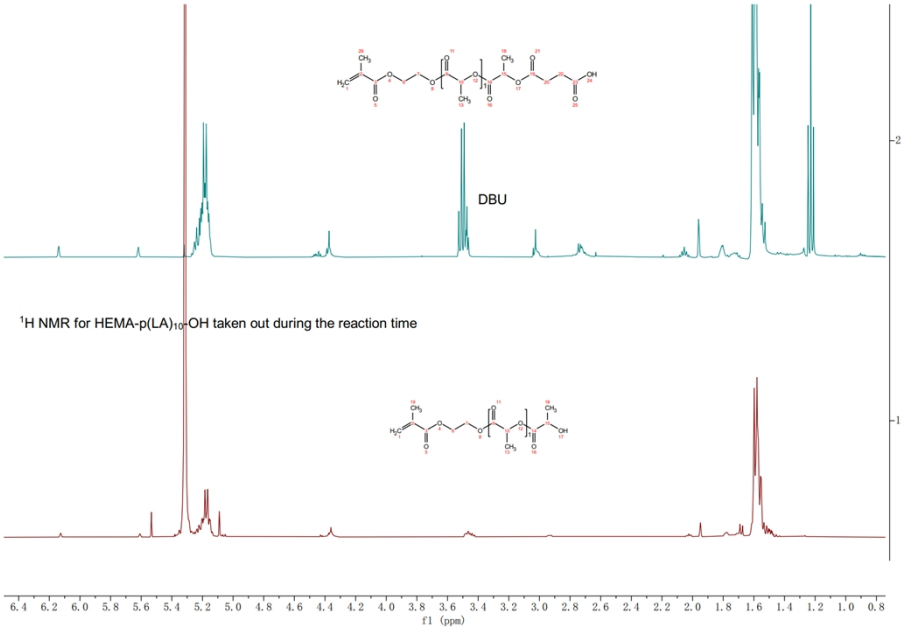

Figure 3.2-5 ^{1}H NMR data of one-pot reaction for two products

The first step of the one-pot reaction was the synthesis of HEMA-p(LA)$_n$-OH, the second step was the synthesis of HEMA-p(LA)$_n$-COOH, after the termination of the reaction, a sample was taken. The ^{1}H NMR data (fig. 3.2-3) shows that the shape of the peaks of double bond were normal, the ratio of integration of the double bond was 1:1, and the degree of polymerization did not increase (seen via the integration of the repeat unit of LA), it means that the one-pot reaction was effective.

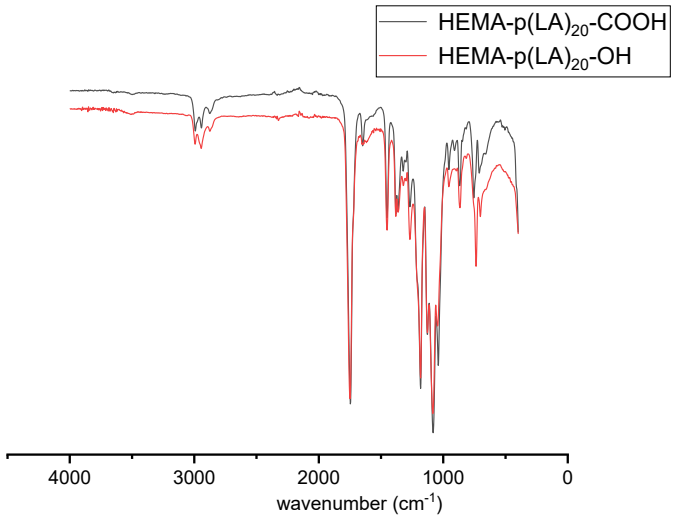

Figure 3.2-6 the comparison of FT-IR spectrum between HEMA-p(LA)$_{10}$-OH and HEMA-p(LA)$_{10}$-COOH

From the Figure 3.2-6, these two FT-IR data shows that were similar, because the structure of HEMA-p(LA)$_n$-OH and HEMA-p(LA)$_n$-COOH are similar.

There is a carboxylic fingerprint area is at about 950 cm^{-1}.

Due to the similar structure, ^{1}H NMR spectrum of HE(M)A-(LA)20-COOH were put in appendix section to be not analyse them further.

3.3 Synthesis of Dispersed Red I or Dispersed Yellow and HE(M)A-p(LA)$_n$-COO-Red (Yellow)

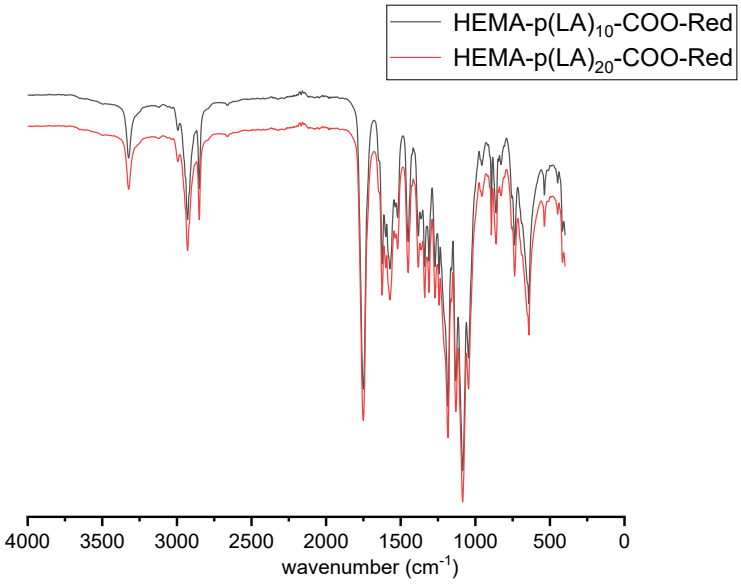

Figure 3.3-1 FT-IR spectrum of HEMA-p(LA)$_n$-COO-Red (n=10, 20)

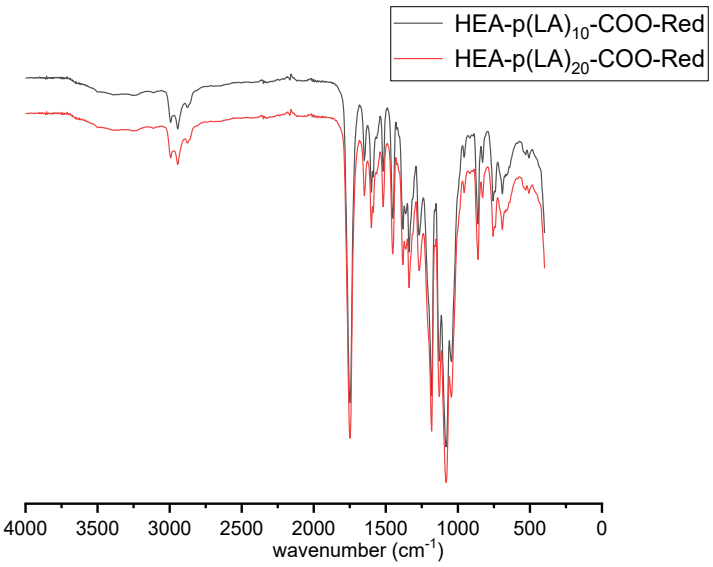

Figure 3.3-2 FT-IR spectrum of HEA-p(LA)$_n$-COO-Red (n=10, 20)

From the Figures 3.3-1 and 3.3-2, N-H stretching was at 3300 cm^{-1}; =C-H stretching of arene was in 3080-3010 cm^{-1}; C=C of arene stretching was in 1600-1450 cm^{-1}; N=N stretching was in 1410-1400 cm^{-1}; C-H (arene) bending was in 880-860 cm^{-1}, which were the main groups of red compound.

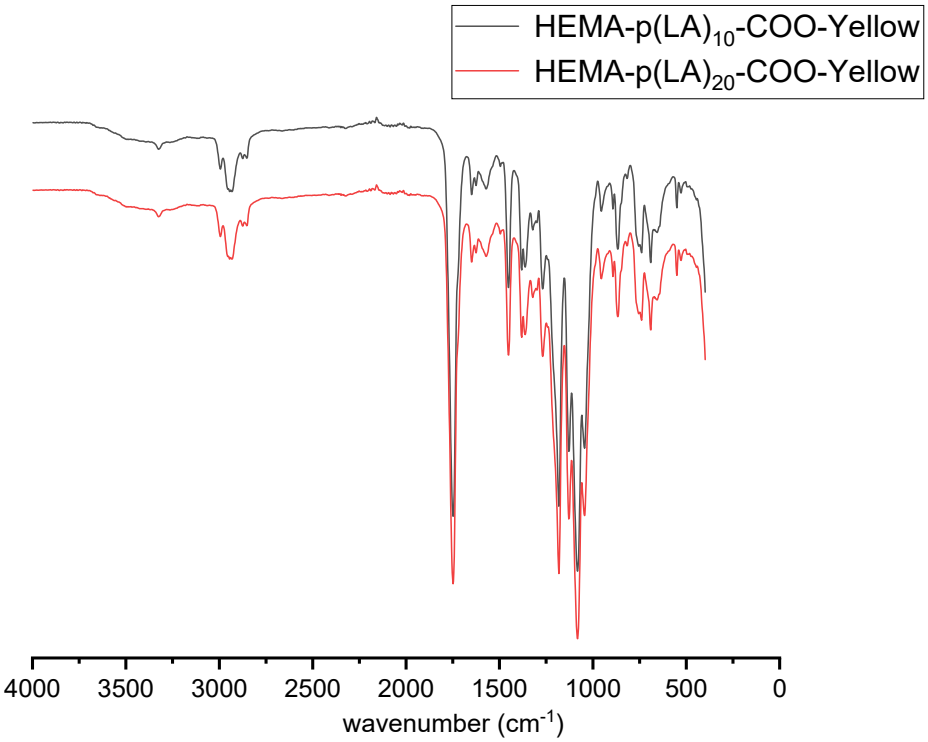

Figure 3.3-3 FT-IR spectrum of HEMA-p(LA)$_n$-COO-Yellow (n=10, 20)

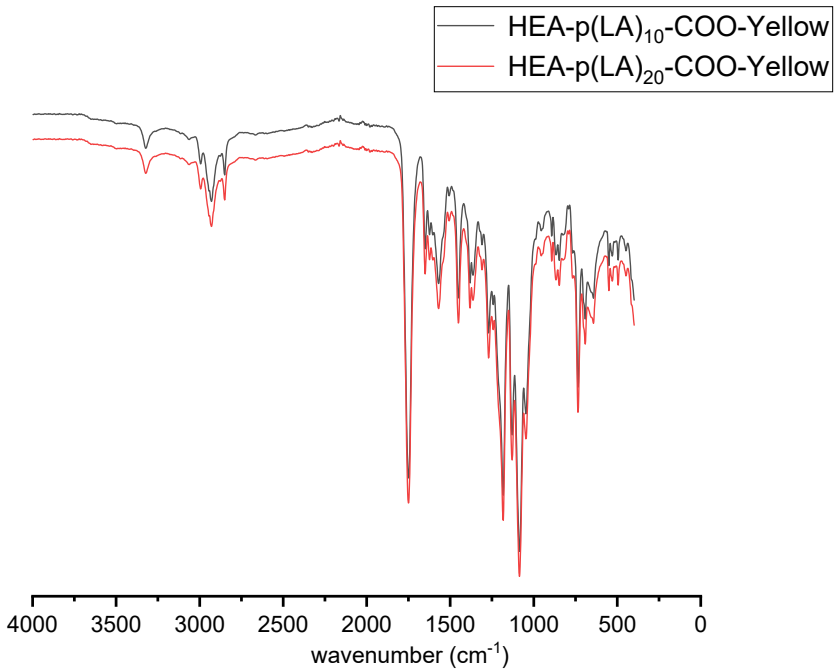

Figure 3.3-4 FT-IR spectrum of HEA-p(LA)$_n$-COO-Yellow (n=10, 20)

From Figure 3.3-3 and 3.3-4, =C-H stretching of arene was in 3080-3010 cm^{-1}; C=C of arene stretching was in 1600-1450 cm^{-1}; N=N stretching was in 1410-1400 cm^{-1}; C-H of arene bending was in 880-860 cm^{-1}, which were the main groups of yellow compound.

In the Figure 3.3-4, a peak at 3300 cm^{-1} can be supposed that N-H stretching due to combination of N and H_2O to form N=N-H bond.

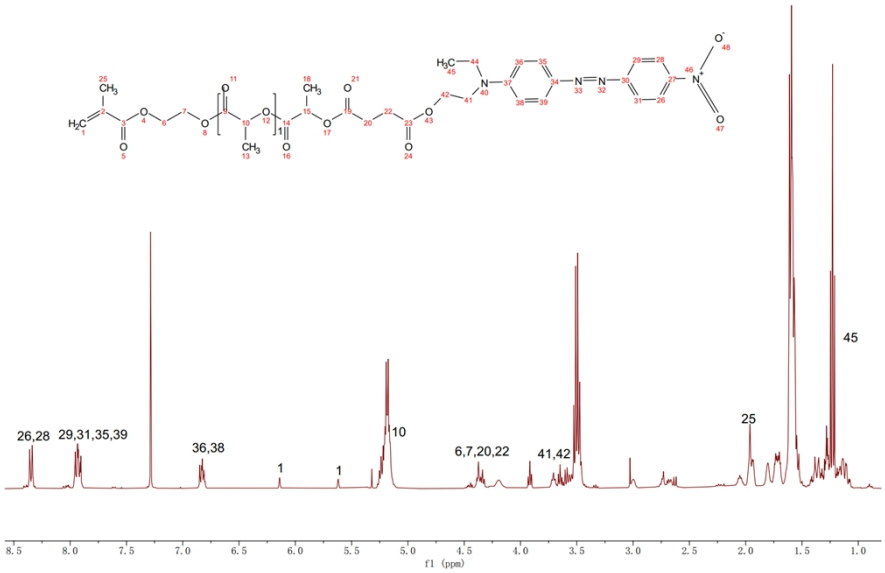

Figure 3.3-5 the ^{1}H-NMR spectrum of HEMA-p(LA)$_{10}$-COO-Red

Reaction of HEMA-p(LA)$_{10}$-COOH and Dispersed Red 1, DCC and 4-DMAP as catalysts

In the Figure 3.3-5, two phenyl were in 8.85ppm, 7.93ppm, 6.83ppm; end-group double was in 6.13ppm and 5.61ppm; the repeating unit of LA was in 5.20ppm; two methylene of HEMA and two methylene of succinic anhydride were in 4.38ppm; two methylene of dispersion red I was in 3.68ppm; methyl of HEMA was in 1.98ppm; two methyl of LA was in 1.53ppm; methyl of dispersion red I was in 1.23ppm.

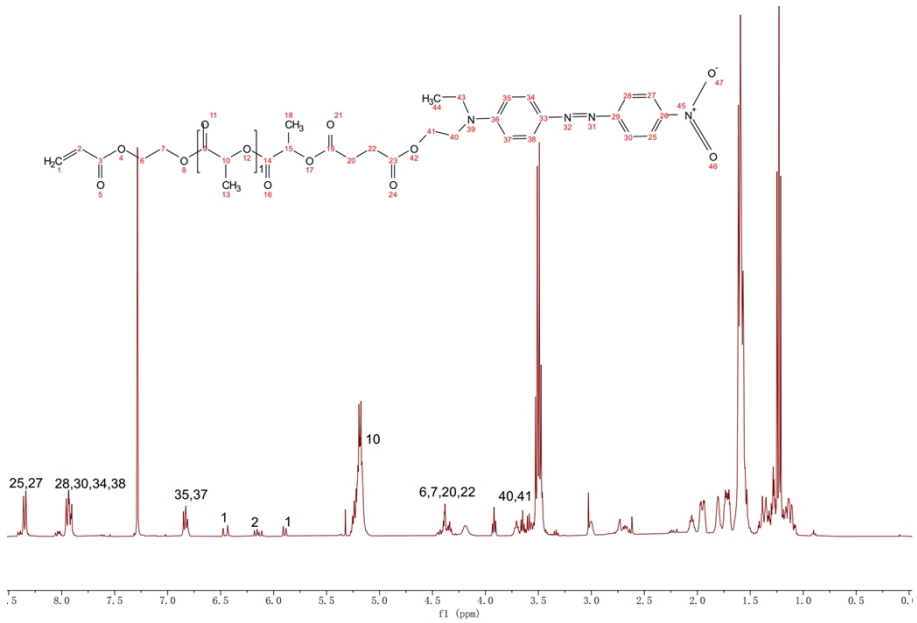

Figure 3.3-6 the ^{1}H-NMR spectrum of HEA-p(LA)$_{10}$-COO-Red

Reaction of HEA-p(LA)$_{10}$-COOH of Dispersed Red 1, DCC and 4-DMAP as catalysts

In the Figure 3.3-6, two phenyl were in 8.33ppm, 7,95ppm, 6.85ppm; end-group double bond was in 6.47ppm and 5.89ppm; α-H of vinyl was in 6.15ppm; the repeating unit of LA was in 5.18ppm; two methylene of HEA and two methylene of succinic anhydride were in 4.38ppm; two methylene of dispersion red I was in 3.68ppm; methyl of LA was in 1.52ppm; methyl of dispersion red I was in 1.21.

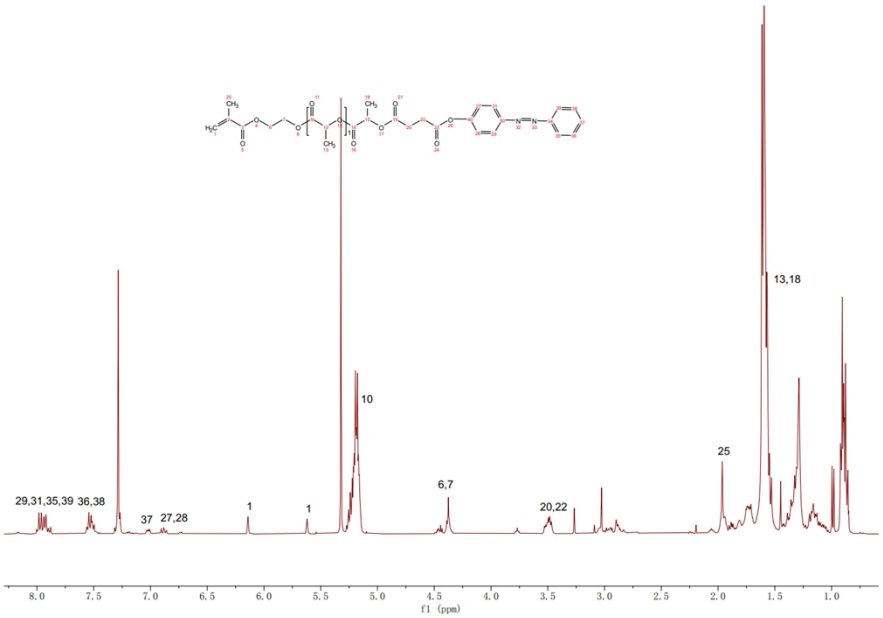

Figure 3.3-7 the ^{1}H-NMR spectrum of HEMA-p(LA)$_{10}$-COO-Yellow

Reaction of HEMA-p(LA)$_{10}$-COOH and Dispersed Yellow, DCC and 4-DMAP as catalysts

In the Figure 3.3-7, two phenyl were in 7.96ppm, 7.7ppm, 7.01ppm, 6.88ppm; end-group double bond was in 6.14ppm, 5.62ppm; the repeating unit of LA was at 5.18ppm; two methylene of HEMA was at 4.38ppm; two methylene of succinic anhydride was at 3.49ppm; methyl of HEMA was at 2.0ppm; two methyl of LA was at 1.52ppm.

The ^{1}H NMR spectrum and FT-IR spectrum can prove that the esterification has sucessfully connected with the red or yellow compound and HE(M)A-(LA)$_{10/20}$-COOH. Steglich esterification reaction is to use DCC as a coupling reagent and 4-DMAP as the catalyst to promote the esterification reaction (figure 3.3-8) [155].

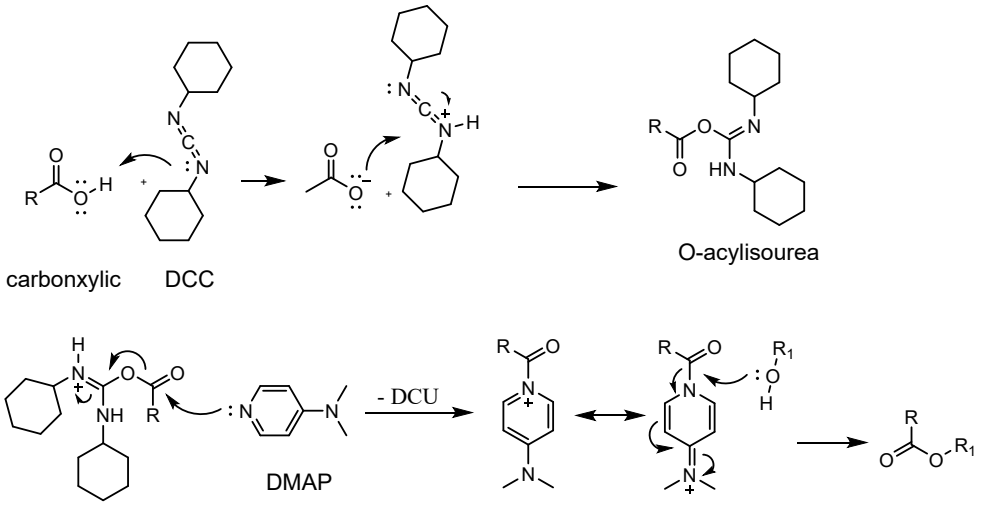

Figure 3.3-8 the mechanism of Steglich esterification reaction

Hydroquinone (trace amount) was added to maintain the stability of end-group double bond. DCU as a by-product can be created during reaction. It cannot be dissolved by most common solvents, but as the reaction time progresses, white solid can be seen to be precipitated. Syringe filter was used to filter DCU. Hexane and Et_2O were used for precipitation, but traces of DCU can also be separated out. This may affect the analysis of the spectrum.

According to all ^1H NMR and FT-IR data, the products of red and yellow monomer can be confirmed. Also, after purification, color products can be reserved stably in hexane or Et_2O without fading.

Due to the similar structure, ^1H NMR and FT-IR of HEMA-$(LA)_{20}$-COO-Red were put in appendix section.

3.3.1 Degradation of dye macromonomers

A series of degradation tests were set up to observe the process of degradation of the dye monomers. It has been demonstrated that esters are cleavable in acidic and basic conditions, so 1M NaOH and H_2SO_4 were prepared. Red and yellow monomers were put in vials with aqueous solutions of 1M NaOH or H_2SO_4. Each vial was left at ambient temperature. When the color compound was cleaved, the color change of the solution can be observed. Samples were taken to test by GPC and ^1H NMR.

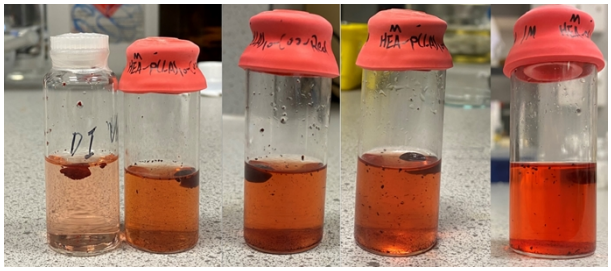

Figure 3.3.1-1 degradation test of HEMA-p$(LA)_{20}$-COO-Red in 1M NaOH aqueous and deionized water. From left to right: deionized water (20h), 1M NaOH 20h, 24h, 40h, 48h, respectively.

In the Figure 3.3.1-1, as time progresses, the color of the solution gradually deepened, which indicated that the red part was cleaved.

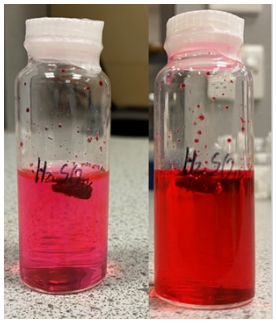

Figure 3.3.1-2 degradation test of HEMA-p$(LA)_{20}$-COO-Red in 1M H_2SO_4 aqueous. on the left the sample which was put into an acidic solution (t=0), right was after 20h (t=20h).

From Figure 3.3.1-2, after putting the sample into the vial, the aqueous medium immediately turned red. It shows that red monomer demonstrated a high sensitivity in acidic conditions or red monomer has certain solubility in acidic solutions. As time progresses, the color of the solution gradually deepened, but after 20h, the color change of the solution stopped, at least the naked eye could not distinguish the degree of color change.

Base/acid	Original Mn	Mn of after degradation	Mn of after degradation
1M NaOH	4.8×10^3	t=48h, 6.97×10^2	t=96h, 6.4×10^2
1M H_2SO_4	4.8×10^3	t=48h, 3.63×10^3	t=96h, 3.5×10^3

Table 3.3.1-1 comparison of the change of Mn in base and acid aqueous

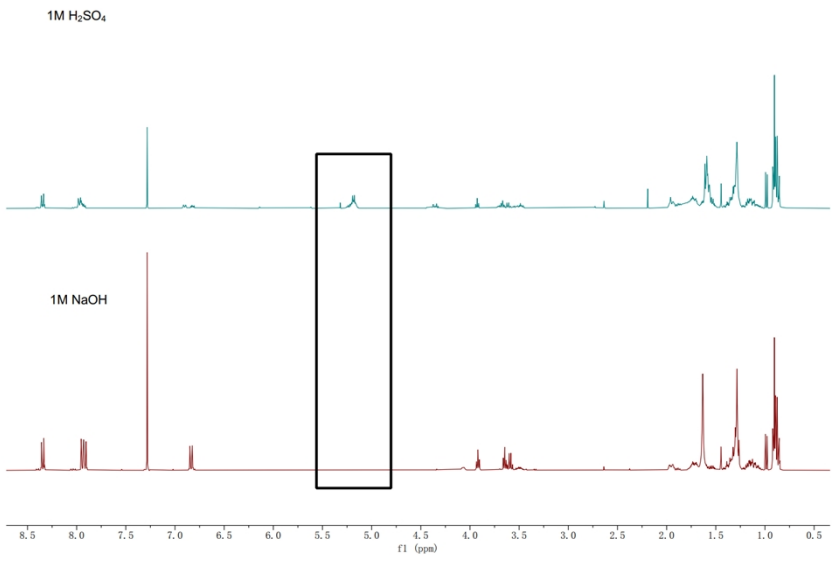

Figure 3.3.1-3 comparison of ^1H NMR of HEMA-p$(LA)_{20}$-COO-Red

After 48h, in basic solutions, Mn decreases to a great extent (Table 3.3.1-1). From Figure 3.3.1-3, δ 5.2 (m, 1H, CH) which belongs to the repeat unit of LA, disappears in 1M NaOH after 48h suggesting complete degradation. However, in 1M H_2SO_4 after 48h, there was still the peak of the repeat unit of LA, but the integration was 33 instead of 40, hinting at a certain degree of degradation.

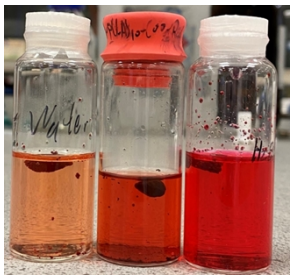

Figure 3.3.1-4 comparison of red monomer in deionized water (left), 1M NaOH (middle), 1M H_2SO_4 (right)

For the red monomer, the degradation process in basic conditions was faster than in acidic conditions. The red monomer demonstrated a high responsiveness in basic conditions, while the part of red group can be partially dissolved in acidic conditions as well (fig. 3.3.1-4).

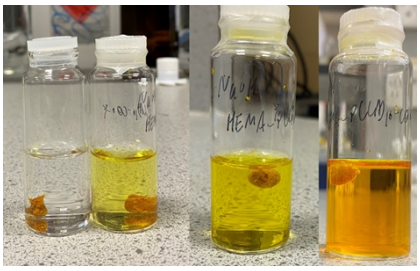

Figure 3.3.1-5 degradation test of HEMA-p$(LA)_{20}$-COO-Yellow in deionized water and 1M NaOH. From left to right: deionized water (20h), 1M NaOH 2h, 4h, 20h, respectively

From the Figure 3.3.1-5, the color was fading as the time went on, the color change of the solution was getting darker. It means that HEMA-p$(LA)_{20}$-COO-Yellow was degrading.

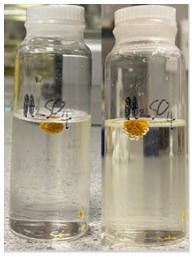

Figure 3.3.1-6 degradation test in 1M H_2SO_4 aqueous, on the left the sample is seen after 3h, on the right after 24h.

From the Figure 3.3.1-6, the color change of aqueous was not obvious, it seems that yellow compound was not cleaved in the H_2SO_4 aqueous environment, the yellow monomer demonstrated a low sensitivity towards acidic conditions.

Base/acid	Original Mn	Mn of after degradation	Mn of after degradation
1M NaOH	4.68×10^3	t=20h, 3.55×10^3	t=48h, 3.07×10^3
1M H_2SO_4	4.68×10^3	t=20h, 3.77×10^3	t=48h, 3.62×10^3

Table 3.3.1-2 comparison of the change of Mn in basic and acidic conditions

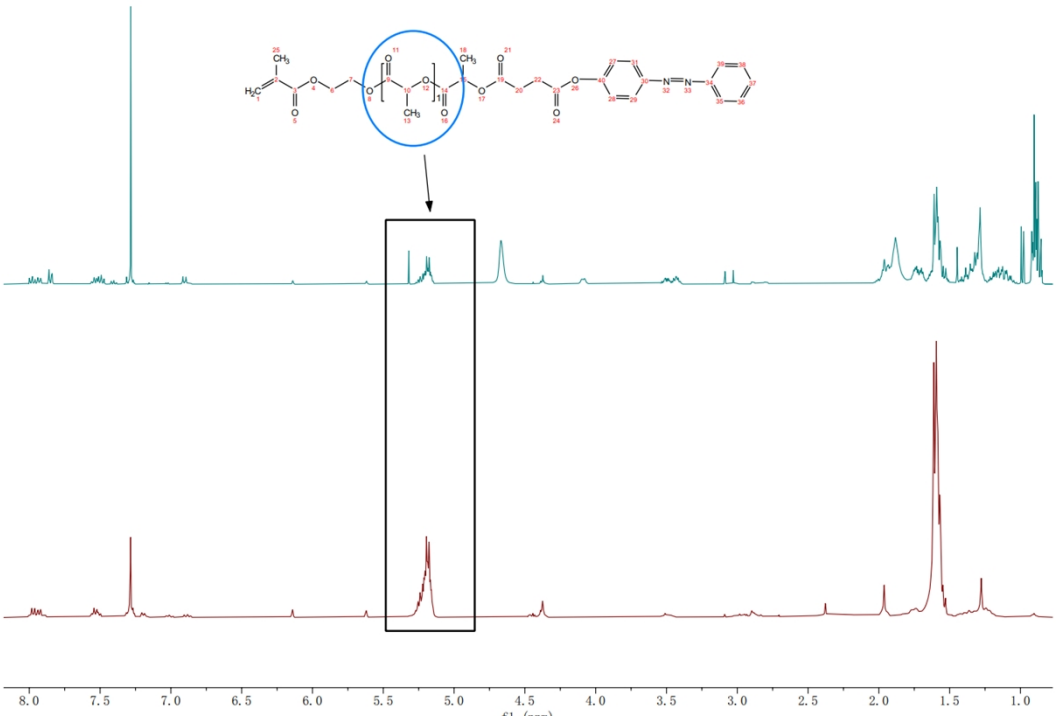

Figure 3.3.1-7 comparison of ^1H NMR of HEMA-p$(LA)_{20}$-COO-Yellow in basic and acidic conditions after 48h

The Table 3.3.1-2 shows that the degradation process of the yellow monomer in basic conditions was faster than in acidic conditions. From the Figure 3.3.1-7, after 48h, the integration of repeat unit of LA in basic conditions was 31 instead of 37, so the degree of polymerization decreased by 6 units, while in acidic conditions, the integration was 34, so the degree of polymerization decreased by 3 units.

In summary, both the red and yellow macromonomers demonstrated high sensitivity in basic conditions. In the basic aqueous system, the yellow moiety cleaved faster than the red moiety, so the fading rate of yellow monomer was faster than red monomer but based on the analysis of ^{1}H NMR and GCP, the degradation process of red monomer in basic aqueous was faster than yellow monomer.

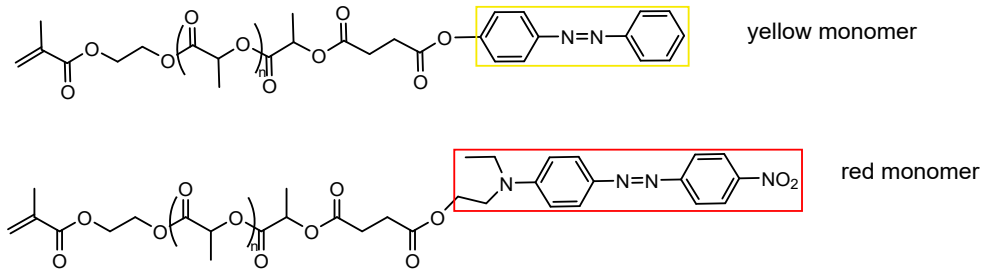

Figure 3.3.1-8 structure of yellow and red monomer

From the Figure 3.3.1-8, there is an obvious difference of structure between red and yellow monomer that there is a nitro group (-NO_2) in the red monomer. Normally, nitro groups can form hydrogen bonds with water molecules in aqueous solutions, enhancing the hydrophilic nature of the compound. In other words, the interaction between the red monomer and the water molecules is stronger, so the red monomer degrades more quickly in basic aqueous solutions.

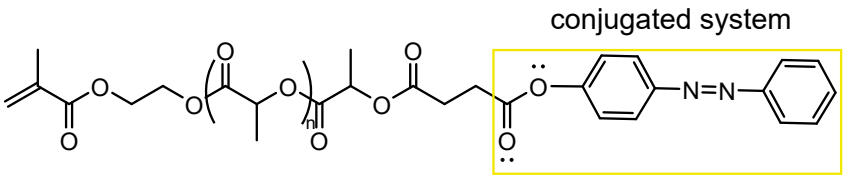

Figure 3.3.1-9 structure of yellow monomer

From the Figure 3.3.1-9, there is a conjugated part in the yellow monomer, it means that this structure enhances the stability of the carbocation on the carbonyl group, so it

is easier to initiate a nucleophilic reaction. However, due to the lone pair of the oxygen atom on the carbonyl group participates in the conjugation, its ability to bind to hydrogen ions is weakened, so the fading rate of yellow monomer in acidic aqueous is slower than red monomer.

In Summary, the red monomer demonstrated a higher sensitivity towards acidic aqueous solutions than the yellow monomer. The degradation process of the red and yellow monomers in basic aqueous solutions was faster than in acid conditions. Both the red and yellow monomers have been obtained successfully, and the degradation process was promising under acidic and basic conditions. Besides, different sensitivity of the red and yellow monomers in basic or acidic condition is an inspiration that according to different situations, they can be applied in specific circumstances respectively. For example, if a faster degradation process was expected in basic condition, both red and yellow monomer can be used, but red monomer was a better choice. however, if a faster degradation process was expected in acidic condition, red monomer was a primary choice.

3.4 FRP copolymerization of dye monomer and MMA

PMMA has been shown to be a suitable material to be used as an “ink” for SLS printing [156]. In this part of my project, we focused on the functionalization of PMMA by copolymerizing our colored monomers with MMA.

Free radical polymerizations, which are thermally initiated were adopted as the model method of polymerization of MMA and our functionalized monomers. AIBN was selected as a thermal initiator.

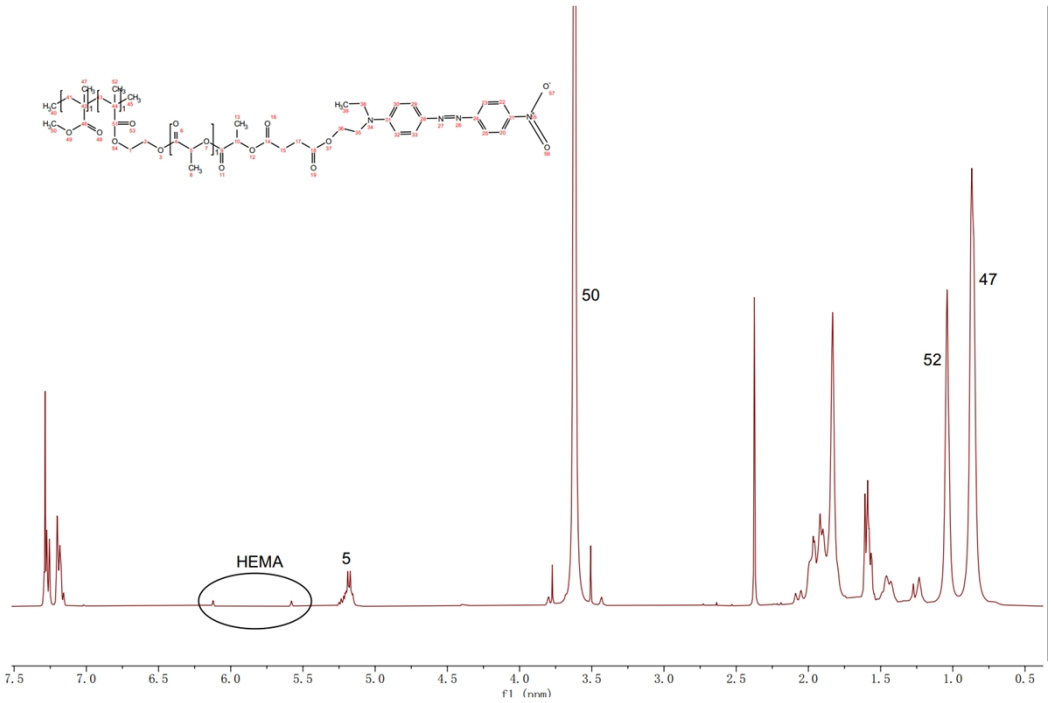

Figure 3.4-1 ^{1}H-NMR spectrum of poly-(MMA-co-HEMA-p(LA)$_{10}$-COO-Red)

After FRP polymerization and precipitation in methanol, the presence of some residual unreacted monomer can be observed in the ^{1}H-NMR spectrum (fig.3.4-1). δ 6.12 (s, 1H) and 5.61 (s, 1H) belong to the double bond of MMA, 3.7 (s, 3H) belongs to the methoxy (-OCH_3) of MMA. δ 1.13 (s, 3H, CH_3), 0.88 (s, 3H, CH_3) belong to the methyl of PHEMA and PMMA after polymerization respectively. Conversion can be calculated via the integration of methoxy of MMA in ^{1}H-NMR data of before purification.

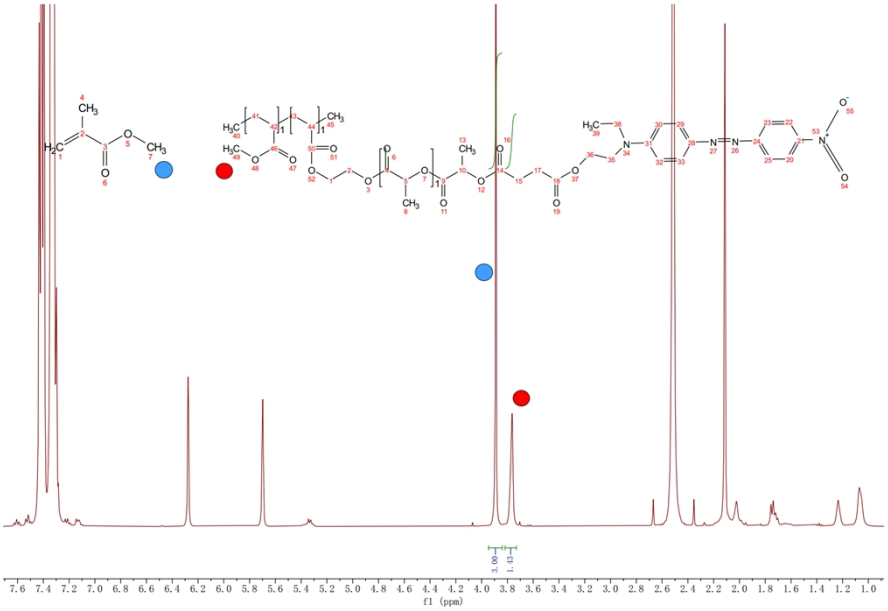

Figure 3.4-2 ^{1}H NMR spectrum of poly(MMA-co-HEMA-$(LA)_{20}$-COO-Red) for before purification.

From the Figure 3.4-2, δ 3.88ppm (blue) can be assigned to the -O**C**$\mathbf{H_3}$ of MMA, the integration of 3.88ppm was set to 3, it can represent the total amount of monomer of MMA before polymerization. δ 3.76ppm (red) can be assigned to the -O**C**$\mathbf{H_3}$ of PMMA, the integration of 3.76ppm can represent the amount of copolymer after polymerization. Therefore, based on this method, the conversion of the polymerization is $\frac{1.43}{3+1.43} = 32\%$.

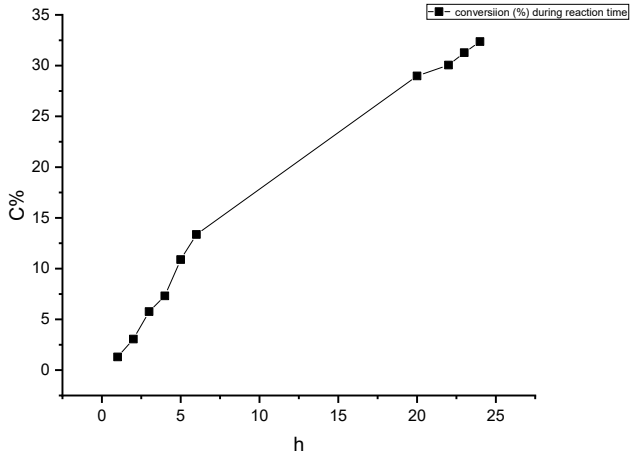

Figure 3.4-3 Kinetics of the synthesis of a copolymer of HEMA-p$(LA)_{20}$-COO-Red (10%) and MMA (90%) The calculation method is the same as mentioned above

The conversion of this polymerization is low. From the Figure 3.4-3, the initial conversion rate has grown fast, however, as the polymerization progressed, the conversion gradually decreased. Hypothetically, HEMA-p$(LA)_{20}$-COO-Red is a long

side chain, so during the reaction time, as the main chain increases, the density of side chain of copolymer was increasing, the side chain began to entangle, and as the main chain grew, the entanglement phenomenon increased. Besides, there was also an entanglement between side chain and monomer. The entanglement between the side chains can reduce the penetration of the solvent, thereby reducing the solubility of the solvent to the copolymer, and further causing the reaction to be hindered. This situation inhibited the progress of polymerization.

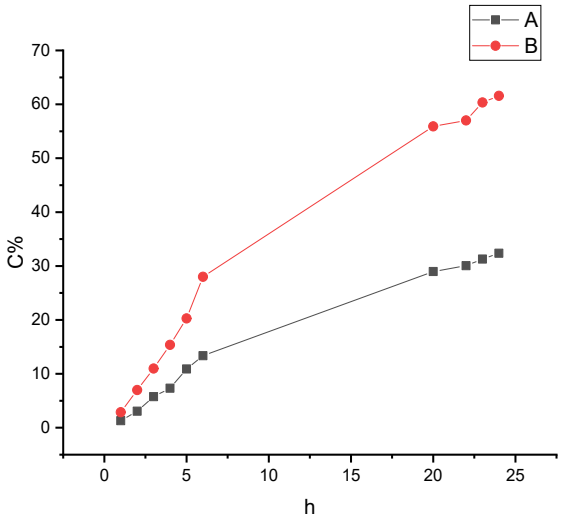

Figure 3.4-4 comparison of conversion of two polymerizations with different monomers. A is a polymerization of HEMA-p$(LA)_{20}$-COO-Red as a monomer. B is a polymerization of HEMA-p$(LA)_{10}$-COO-Red as a monomer.

From figure 3.4-4, the conversion of HEMA-p$(LA)_{10}$-COO-Red as a co-monomer was higher than conversion of HEMA-p$(LA)_{20}$-COO-Red as a co-monomer. For HEMA-p$(LA)_{10}$-COO-Red, the repeating unit of LA is 10, so the length of side chain of B is shorter than A (fig. 3.4-4), therefore, the side chain has a lower degree of entanglement. Also, methanol was used as an antisolvent in the precipitation step, while the dye monomer can be dissolved in methanol, so normally, copolymer and monomer can be separated out via washes with methanol. However, after purification, a signification amount of dye monomer remained in the product. It demonstrates that even though

methanol has washed away most of the monomers, some monomers were still wrapped and precipitated by the product, so the conversion of dye monomer is low.

To increase the conversion of polymerization, a diluted system was used, the weight percentage of toluene and total amount of monomer was changed to 70% and 30%, the weight percentage of AIBN used in the polymerizations was 1% of the HEMA-p$(LA)_{20}$-COO-Red (Yellow) monomer. The dilution system alleviated the entanglement of the side chain.

Glass transition temperature (Tg) is an indispensable parameter for SLS. The Tg of PMMA is about 100^{o}C [157].

Tg was measured by DSC, excessive high Tg (>200^{o}C) means that higher laser energy is needed to melt it, resulting in a waste of laser energy, excessive low Tg (<80^{o}C) means that it takes longer to cool down after printing.

Sample	Tg (^{o}C)
MMA (90%), red (10%)	106
MMA (85%), red (15%)	104
MMA (80%), red (20%)	102
MMA (90%), yellow (10%)	105
MMA (85%), yellow (15%)	103
MMA (80%), yellow (20%)	100

Table 3.4-1 Tg's of copolymers

Based on the DSC data (Table 3.4-1), the Tg of copolymer and Tg of PMMA were close, it means that these kinds of copolymers may be suitable for SLS.

Tg usually is affected by many factors, such as the properties of co-monomers, the properties of polymers and the length of side chain [158]. From the Table 3.4-1, as the ratio of color monomers in the copolymer increased, the Tg of the copolymer decreased. It has been reported that for the copolymer of MMA and HEMA (poly-[MMA-co-HEMA]), Tg was decreased as the amount of HEMA in the co-polymer was increased [159]. Also, side chain length and density can also impact Tg.

A series of copolymers of MMA and red or yellow monomer have been obtained, due to the similar structure, we did not analyze their ^{1}H NMR and FT-IR further, data was put in the appendix section.

3.4.1 Degradation test of copolymer of MMA and dye monomer

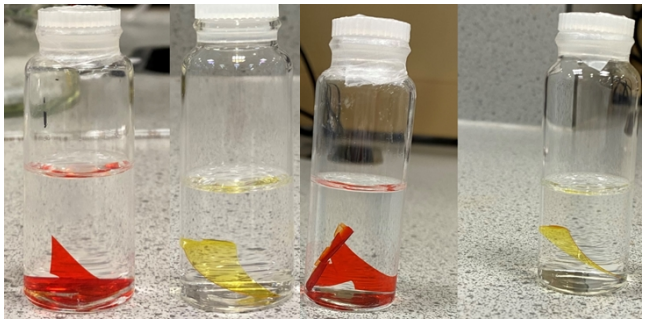

Figure 3.4.1-1 degradation test in 1M NaOH after 1 month (left) and 3 months (right)

Figure 3.4.1-1 demonstrated the result of degradation test after 1 and 3 months. The left figure shows that there was no change of colour in the aqueous media. The surface of the film also showed no signs of fading after 1 month. Similarly, the figures on the right shows that there was no change in colour in any of the aqueous media even though after 3 months.

After casting into film, the surface size of the film becomes smaller, so the exchange rate between hydroxyl groups and the film was too low for the degradation process to occur, since the aqueous phase could not permeate into the film. Therefore, the degradation process of film should take an extremely long time to happen.

According to the previous research result, films are not a suitable material to be used for performing degradation tests, so the original copolymer was directly used to carry out a model degradation test.

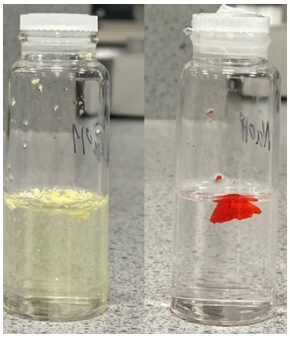

Figure 3.4.1-2 degradation test in 1M NaOH after 3 months

Figure 3.4.1-2 was taken 3 months after setting up the degradation test. From this figure, there was a little bit of change of colour for yellow copolymer, but there was no change of colour for red copolymer.

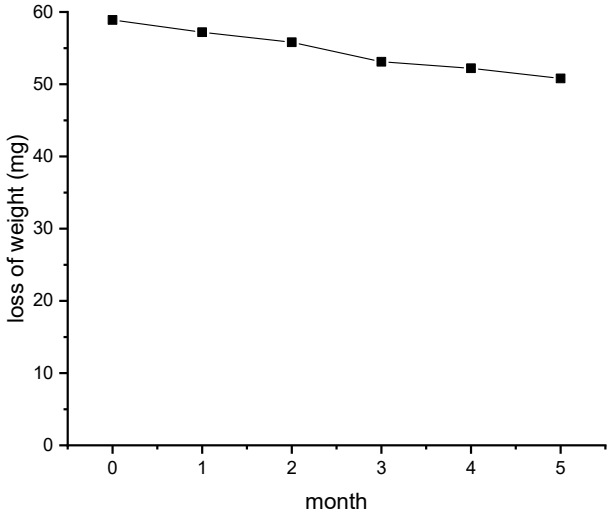

Figure 3.4.1-4 analysis of loss of weight of red copolymer (film)

Based on the figure 3.4.1-4, the original weight of red copolymer film was 58.9mg, the weight of film was weighed each month. After 5 months, the film was 50.8mg, degradation ratio was 13.8%.

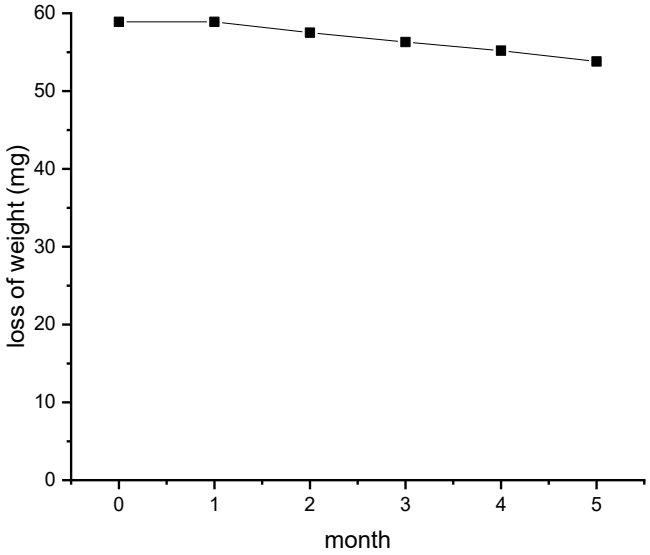

Figure 3.4.1-5 analysis of loss of weight of yellow copolymer (film)

Based on Figure 3.4.1-5, the original weight of yellow copolymer film was 58.9mg, the weight of film was weighed each month. After 5 months, the film was 53.8mg, degradation ratio was 8.7%.

Even though there was no obvious change in colour of the solution that can be observed, according to the loss of weight, a slow degradation process was taking place.

material	Original Mn	Mn of after 3 months	Degradation rate
Red copolymer	1.07×10^5	7.73×10^4	27.75%
Yellow copolymer	6.55×10^4	5.87×10^4	10.38%

Table 3.4.1-1 comparison of the change of Mn with red and yellow copolymer

From Table 3.4.1-1, even though the change of colour in the solution was not obvious, the Mn of red and yellow copolymer decreased a little. The degradation rate of the red copolymer was faster than yellow copolymer in basic conditions.

It supposes that a polymer obtained by copolymerization of two hydrophobic monomers, the side chain cannot stretch in the aqueous solution, and the surface pore diameter of the copolymer is small, so the aqueous solution cannot penetrate it. These factors limit the exchange capacity between hydroxide and hydrogen and the degradable moiety. In addition, it is possible that the degraded portions were poorly soluble in the aqueous media with little or no visual effect on the final solution colour.

3.5 FRP copolymerization of TEGMA and red monomer

TEGMA is a hydrophilic molecule with several appealing properties, such as self-assembling in water or alcohol solution, biocompatibility, etc. TEGMA has been used as co-monomer to produce different materials for inkjet printing [160]. Based on this, in this part of the project, a copolymer of TEGMA (wt% 90%) and HEMA-p$(LA)_{20}$-COO-Red (wt% 10%) was synthesized to obtain a kind of coloured copolymer with pH-responsiveness for potential applications in inkjet printing.

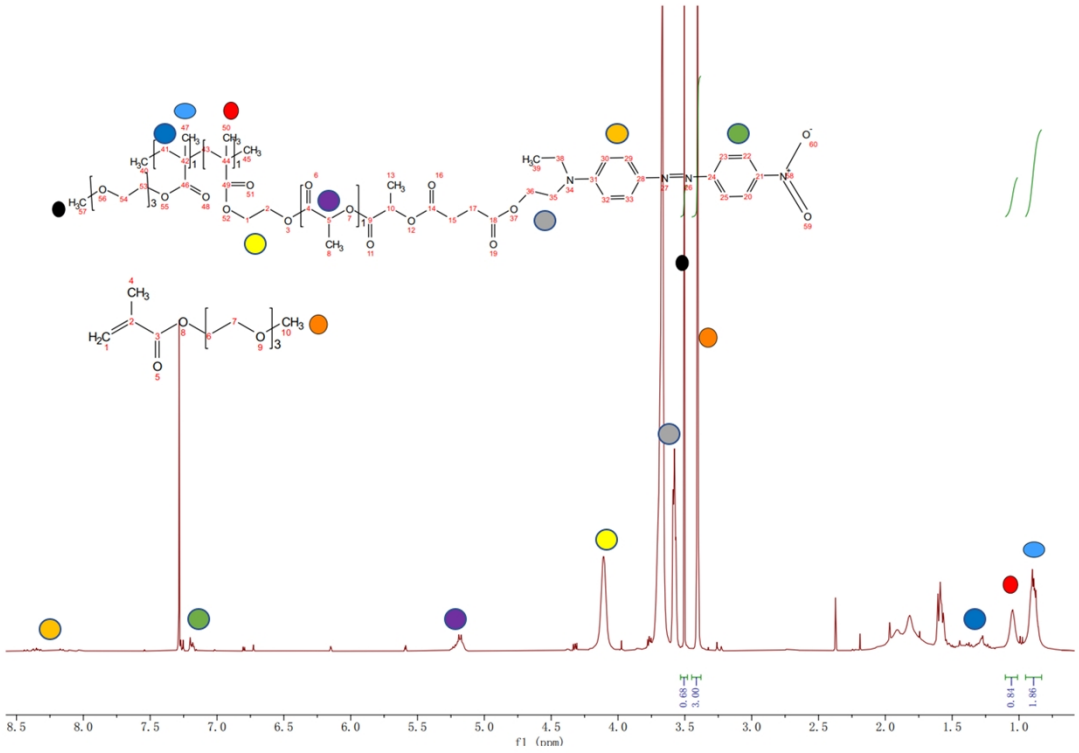

Figure 3.5-1 ^{1}H NMR spectrum of poly(TEGMA-co-HEMA-p(LA)$_{20}$-COO-Red)

In the Figure 3.5-1, the composition of TEGMA and red monomer can be calculated by the integration of their α-methyl, as these peaks will only appear after polymerization. Based on this, the composition of TEGMA was $\frac{1.86}{1.86+0.84} = 69\%$, the composition of red monomer was $\frac{0.84}{1.86+0.84} = 0.31\%$ (table 3.5-1).

Theoretical composition	Actual composition	Mn (GPC)	Đ
TEGMA (90%), red monomer (10%)	TEGMA (69%), red monomer (31%)	4.8×10^4	1.45

Table 3.5-1 analysis of composition (calculated by ^{1}H NMR) and Mn (GPC)

Form the Figure 3.5-1, end-group double bond can be observed, it means that some monomer remained in the product. The copolymer can be dissolved in methanol, so hexane was used for purification via precipitation. However, the dye monomer did not show high solubility in hexane. Therefore, copolymer and unreacted monomer can be precipitated at the same time.

The conversion of TEGMA can be calculated by ^{1}H NMR data before purification.

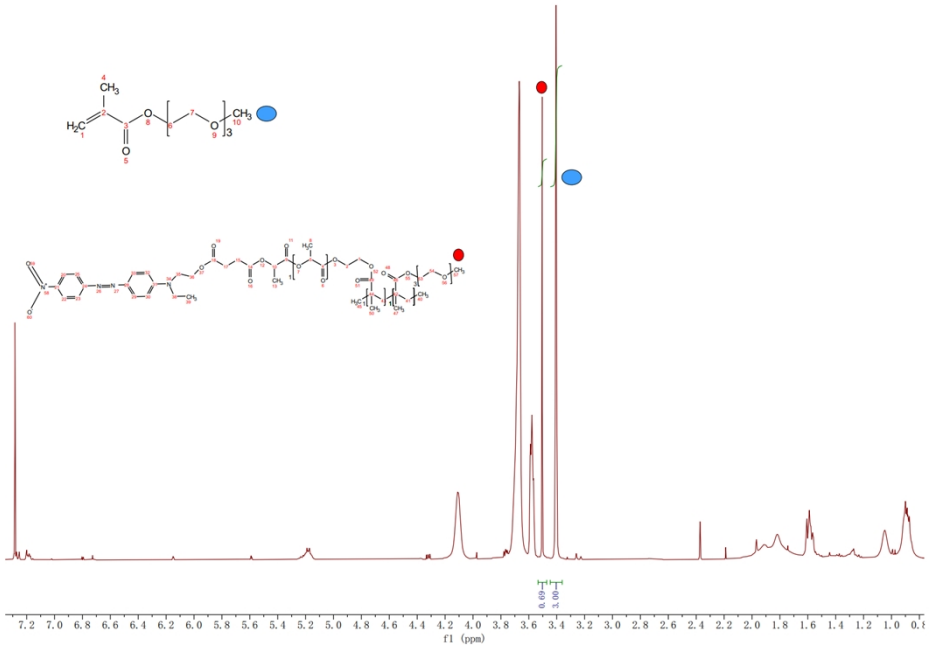

Figure 3.5-2 ^{1}H NMR spectrum before purification

From the Figure 3.5-2, δ 3.4ppm (blue) belongs to the peak of end-group methoxy of TEGMA monomer, 3.5ppm (red) belongs to same group after polymerization. The integration at 3.4ppm was set to 3, which can represent the total amount of monomer, then, the amount of polymer produced can be represented via the integration of 3.5ppm. Based on this, the conversion of polymerization was $\frac{0.69}{0.69+3} = 18\%$.

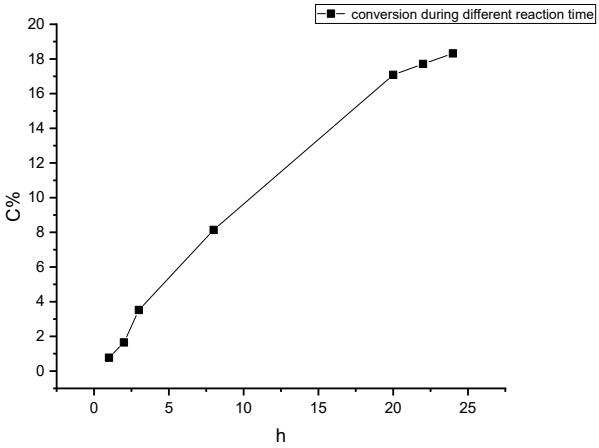

Figure 3.5-3 conversion of TEGMA during different time

In Figure 3.5-3, as the reaction progresses, the conversion was getting lower and lower. With the increase of the chain length, the degree of entanglement of the side chains may be enhanced, this situation can inhibit the increase of Mn. Due to the molecular weight and copolymer composition were affected by the growth of the main chain, the actual copolymer composition and the theoretical one was greatly different (tab. 3.5-1), which has a negative impact on the tailored preparation of the copolymer [161].

3.5.1 Degradation test of the copolymer of TEGMA and dye macromonomer

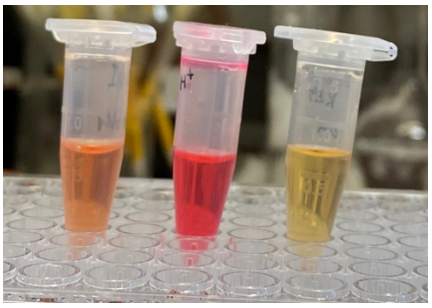

Figure 3.5.1-1 degradation test of copolymer of TEGMA and red monomer. From left to right was in deionized water, 1M H_2SO_4, 1M NaOH

Figure 3.5.1-1 was taken 24h after the degradation test was set up. Due to TEGMA hydrophilicity, these copolymers can be dissolved in a little amount of water (this can be observed via the color change of water). In a 1M H_2SO_4 solution, the sample can be dissolved completely. Hydrogen bond between the hydrophilic moiety TEGMA and the hydrogen in the acidic conditions can be formed, and there was also a hydrogen bond between the end-group nitro of red monomer and the hydrogen. This can increase the solubility of the copolymer in acidic aqueous environments. Therefore, in acidic conditions, the copolymer dissolves really fast (fig 3.5.1-1). The final copolymer can also dissolve in basic conditions, but the color of aqueous looked like yellow. So, the copolymer can be dissolved in basic and acidic conditions.

The use of non-toxic and volatile solvents is one of the research topics of inkjet printing, such as the use of water as a solvent [162,163]. As mentioned above, the copolymer of

TEGMA and red monomer can be dissolved in ethanol and water. It means that the use of a hydrophilic structure as a co-monomer provides an idea for preparing stimuli-responsiveness that can use non-toxic solvents.

3.6 Photopolymerization of HEMA (or TEGMA, PEGMA) and HEA-p$(LA)_{20}$-COO-Red (or Yellow)

To synthesize some colored amphiphilic materials with pH-responsiveness for digital light processing, photopolymerization of HEMA (or TEGMA and PEGMA and HEA-p$(LA)_{20}$-COO-Red) were undertaken in order to mimic the curing conditions after ink dispensing.

Modifications to HEA, HEMA, TEGMA and PEGMA which are then applied to DLP have been reported [164,165,166]. Compared to HEMA, there is no α methyl in HEA, which makes this molecule more suitable for photopolymerization. 2,2-Dimethoxy-2-phenylacetophenone (DMPA) was used as a photo initiator. DMAP has a maximum absorption wavelength of 337 nm and is suitable for the polymerization of unsaturated polyesters and acrylates with high photo initiating activity [167].

A series of photopolymerizations were set up in a well plate (fig. 3.6-1). Some advantages of using well plates were that: 1) a series of reactions can be set up at the same time; 2) well plate was easily to put in the photo reactor; 3) all reactions can be performed under the same exact conditions. The red or yellow monomer and DMAP were dissolved in pure HEMA (or TEGMA, PEGMA) without the addition of any solvents. When HEMA and TEGMA were used as co-monomer, the products were hard gel-like materials, while if PEGMA was as a co-monomer, the product was a soft gel-like material.

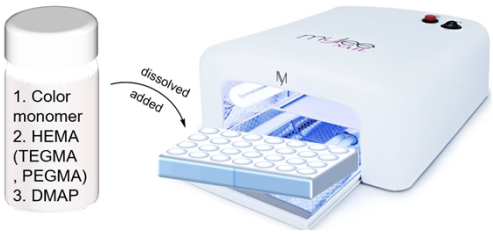

Figure 3.6-1 an illustration of photopolymerization

Copolymers of PEGMA as a monomer can be dissolved in THF but cannot dissolved in acetone or $CHCl_3$. However, copolymers of TEGMA and HEMA used as monomers cannot be dissolved in any kind of organic solvent. Due to the photopolymerization taking place in the bulk phase, the molecular weight is high, and the side chain of copolymer is long, this can inhibit solvent permeation into the copolymer if there is an entanglement of side chain. It means that all copolymers cannot be tested by ^1H NMR and GPC.

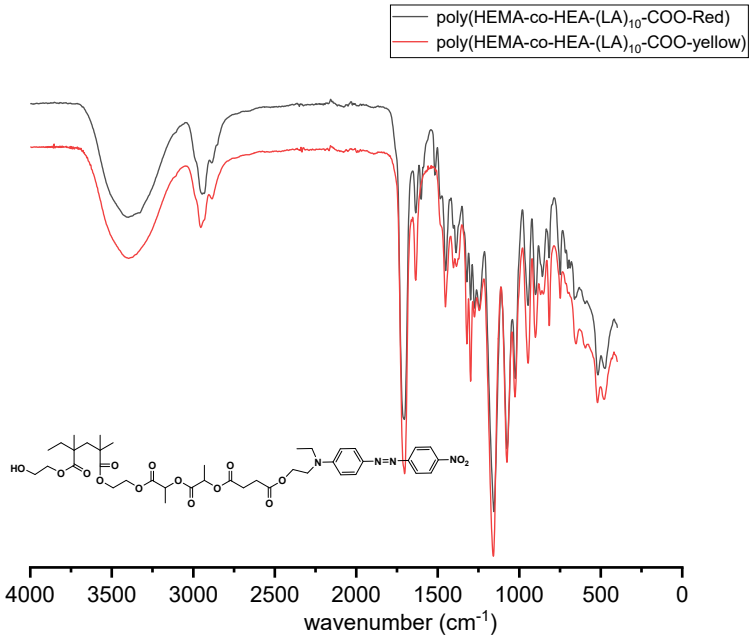

Figure 3.6-2 FT-IR spectrum of poly[HEMA-co-HEA-p$(LA)_{20}$-COO-Red (and yellow)]

Some specific groups can be observed in the Figure 3.6-2: O-H stretching was at 3500 cm^{-1}; C-H (alkane) stretching was at 3000 cm^{-1}; C=O stretching was at 1750 cm^{-1}; C=C (arene) stretching was at 1600-1400 cm^{-1}; N=N stretching was at 1410-1400 cm^{-1}; C-O stretching was at 1250-1200 cm^{-1}; C-H (arene) bending was at 880-680 cm^{-1}.

From the Figure 3.6-2, it shows that there was no peak for C-H stretching and C=C stretching of the alkene. It means that the two monomers have converted to polymer completely, so polymerization via photo-initiated in this section is an efficient method.

Sample	Mn (GPC)	Đ
Poly(PEGMA-co-HEA-p$(LA)_{20}$-COO-Red)	1.13×10^5	2.54
Poly(PEGMA-co-HEA-p$(LA)_{20}$-COO-Yellow)	1.87×10^5	2.87

Table 3.6-1 analysis of Mn

A specific amount of copolymer was taken and put in a vial with THF. The vial was shaken for 48h. The solvent was collected and filtered to perform GPC tests. However, only a small Mn part can be dissolved in THF, the rest can absorb THF and swell.
Most copolymers cannot be dissolved in THF. From the Table 3.6-1, the Mn of two copolymer were large, and the dispersion of them were wide.

Sample	Mn	Đ
poly[TEGMA-co-HEA-p$(LA)_{10}$-COO-Red] (25%)	2.01×10^4	4.4
poly[TEGMA-co-HEA-p$(LA)_{10}$-COO-Red] (50%)	1.74×10^4	5.3
poly[TEGMA-co-HEA-p$(LA)_{10}$-COO-Yellow] (25%)	2.15×10^4	5.85
poly[TEGMA-co-HEA-p$(LA)_{10}$-COO-Yellow] (50%)	3.64×10^4	3.74

Table 3.6-2 analysis of Mn

From the Table 3.6-2, Mn of copolymer of TEGMA as co-monomer were smaller than the copolymer of HEMA as co-monomer. It may be explained that TEGMA as a side chain was longer than HEMA, and entanglement of the side chain can affect the increase of Mn.
Based on the analysis of FT-IR, GPC and the appearance of these copolymers, DLP of hydrophilic monomers and hydrophobic monomers may be a promising way to prepare gel-like materials. However, due to the molecular weight of all copolymers were too large and the dispersion were too wide, their solubility in organic solvents were very poor, which will limit their application in inkjet printing. The control of Mn and dispersion will be an essential work in the future.
Due to the similar structure of these three copolymers, their FT-IR spectra were similar too. Therefore, we did not analyze the FT-IR spectrum of poly[TEGMA-co-HEA-$(LA)_{10}$-COO-Red (and Yellow)] and poly[PEGMA-co-HEA-$(LA)_{10}$-COO-Red (and Yellow)] further, and put them in the appendix section.

3.6.1 Degradation test of photo polymers

To prove that these set of copolymers can undergo degradation, a piece of each material was taken and added in a vial containing 1M NaOH or 1M H_2SO_4.

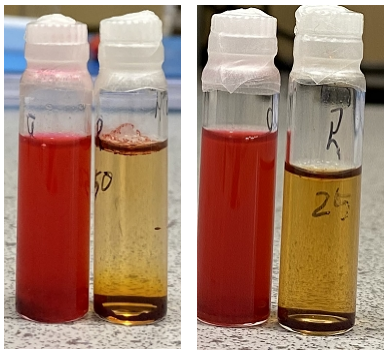

Figure 3.6.1-1 degradation test of poly[TEGMA-co-HEA-p(LA)10-COO-Red (or Yellow)]. Left photo is 50% (wt%) in 1M NaOH (left) and 1M H_2SO_4 (right); right photo is 25% (wt%) 1M NaOH (left) and 1M H_2SO_4 (right)

Figure 3.6.1-1 was taken 24h after the degradation test was set up. From this figure, the color of the acidic solution was much darker than that of the basic solution. Due to the hydrogen bonding between the hydrophilic side chain (TEGMA) and the hydrogen, it has high sensitivity in acidic solutions.

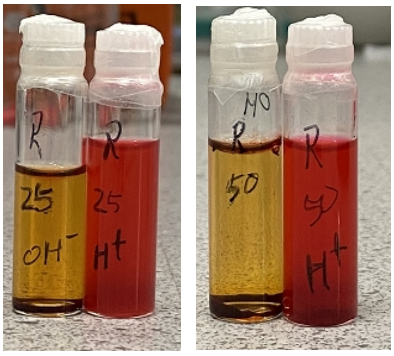

Figure 3.6.1-2 degradation of poly[TEGMA-co-HEA-p(LA)10-COO-Red]. Left photo is 25% (wt%) in 1M NaOH (left) and 1M H_2SO_4 (right); right photo is 50% (wt%) 1M NaOH (left) and 1M H_2SO_4 (right)

Figure 3.6.1-2 was taken after 48h since degradation test was set up, there was not a big difference between Figure 3.6.1-1 and Figure 3.6.1-2. It means that both degradation and dissolution of this copolymer in acidic conditions have reached saturation.

Poly[TEGMA-co-HEA-p(LA)10-COO-Red] was highly sensitivite towards acidic conditions, and it can also respond to basic conditions. After 24 hours, the degradation process was close to saturation.

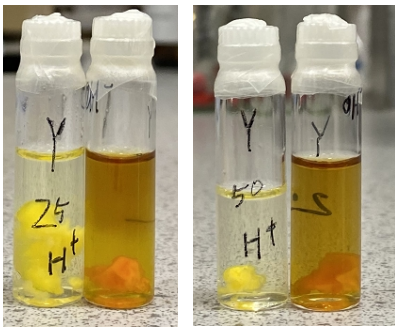

Figure 3.6.1-3 degradation of poly[TEGMA-co-HEA-p(LA)10-COO-Yellow]. Left photo is 25% (wt%) in 1M H_2SO_4 (left) and 1M NaOH (right); right photo is 50% (wt%) 1M H_2SO_4 (left) and 1M NaOH (right)

Figure 3.6.1-3 was taken 24h after the degradation test was set up. From this figure, the colour of NaOH aqueous has been changed to yellow, while it is not a obvious change in a H_2SO_4solution. This means that the degradation process of the yellow copolymer was faster in basic conditions than in acidic conditions.

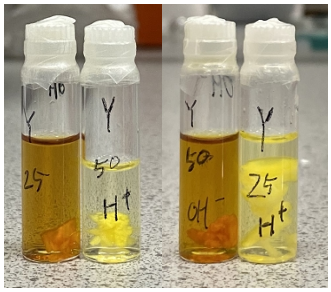

Figure 3.6.1-4 degradation test of poly[TEGMA-co-HEA-p(LA)10-COO-Yellow] after 48h

Figure 3.6.1-4 was taken after 48h after degradation test was set up. There was not big difference between 24h and 48h.

In summary, judging by the color change of the solution, the degradation rate of yellow polymer in basic conditions was faster than that in acidic conditions, or in other words, it has higher sensitivity towards basic conditions. Also, based on the degree of color change of the solutions, after 24 hours, the degradation process was close to saturation.

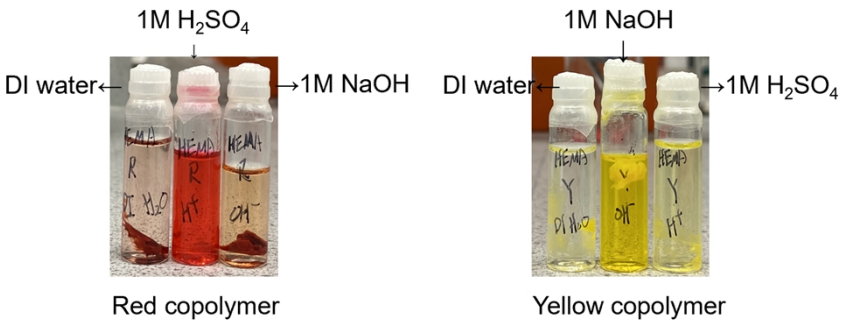

Figure 3.6.1-5 degradation test of poly[HEMA-co-HEA-p$(LA)_{10}$-COO-Red (and Yellow)] in 1M H_2SO_4 (left) and 1M NaOH (right) Right photo from left to right was poly[HEMA-co-HEA-p$(LA)_{10}$-COO-Red] in deinionized water, 1M H_2SO_4, 1M NaOH. Left photo from left to right was poly[HEMA-co-HEA-p$(LA)_{10}$-COO-Yellow] in deionized water, 1M NaOH, 1M H_2SO_4.

Figure 3.6.1-5 was taken 24h after the degradation test was set up. From this figure, the red material shows remarkable color change in acidic conditions, while the yellow material has the largest color change in basic conditions.

In summary, similar to the results previously mentioned, the hydrogen bond formed by the hydrophilic side chain and hydrogen promoted the solubility of the polymer in acidic conditions, and at the same time promoted the penetration of the solution into the polymer, thereby speeding up the exchange rate of the degraded moiety and the hydrogen. Based on the color change of the aqueous, the degradation rate of the yellow polymer in basic colutions was faster than that in acid solutions. Secondly, since its color in aqueous and acidic aqueous solutions was similar, it seems that it was more stable in acidic aqueous solutions.

In this section, the red and yellow copolymers were tested for degradation in basic and acidic aqueous solutions, respectively, and the results were basically the same. Due to the hydrogen bond between the hydrogen and hydrophilic side chain, the red polymers had solubility in acidic conditions, and the degradation rate was faster than in basic conditions. For the yellow copolymers, the degradation rates were faster in basic aqueous solutions than in acidic aqueous solutions via the judging of color change of the solutions. it shows that red copolymers were highly sensitive towards acidic aqueous solutions, but also can respond in basic aqueous. However, the yellow

copolymers can respond to basic conditions aqueous, but have low responsiveness towardsacidic conditions.

Based on these results, these gel-like materials can be applied in different conditions with specific pH value, so the rate of fading can be observed. For example, if a faster degradation process is expected under acidic circumstance, red material will be used, otherwise, yellow materials will be used. However, if a degradation process is expected to be faster under basic circumstance, yellow material is a primary choice. Alos, it provides the idea that photopolymerization with hydrophilic structures as a co-monomer obtain gel-like materials with stimuli-responsiveness for DLP.

4. Conclusion

In this project, a series of new chemicals have been obtained. 1) synthesis of colored monomers with pH-responsiveness. The ring-opening reaction started with HEMA (or HEA) and LA as the starting reactants and ended with the esterification reaction, a series of red or yellow monomers have been obtained. ^{1}H NMR and FT-IR data confirmed the structures. Degradation processes showed that red monomer was highly sensitive towards basic conditions and responded to acidic conditions as well. However, the yellow monomer was sensitive towards basic conditions but had a lower sensitivity towards acidic conditions than the red monomer.; 2) synthesis of colored copolymers of MMA as a co-monomer with pH-responsiveness. Different copolymers were obtained, and DSC data shows that they were suitable for SLS. However, the degradation process was slow; 3) synthesis of copolymer of HEMA (or TEGMA, PEGMA) as a co-monomer with pH-responsiveness via photopolymerization. Gel-like materials were suitable for inkjet printing and DLP. Degradation processes showed that all red materials were highly sensitive to acidic conditions and responded well to basic conditions as well. All yellow materials were highly sensitive to basic conditions but had low sensitivity towards acidic conditions.

All in all, all copolymers were promising materials for SLS or inkjet printing. They not only solve the problem of the single color of printing materials, but also provide ideas for preparing stimuli-responsive materials. If a faster rate of degradation process will be expected, gel-like material for inkjet printing is a prefer choice, while if a slower rate of degradation process will be expected, hard materials for SLS should be considered. Besides, stimuli-responsive material with a cleavable moiety of color as indicator to make the degradation process to be more convenient to be observed.

5. Future work

Even though many kinds of novel materials for 3D printing have been obtained, due to time constraints, 3D printing tests could not be arranged. Therefore, the future work is that 1) SLS of colored copolymer of MMA as a co-monomer and degradation test of printed objects; 2) inkjet print and DLP of gel-like copolymer and degradation test of printed objects. 3) exploration of potential application of novel degradable materials.

6. Appendix

In this section, some figures were demonstrated. Due to some structures were similar, so the ^{1}H NMR or FT-IR spectrum were also similar, which did not be expected to analyze further.

6.1 ^{1}H NMR spectrum of HEMA-p(LA)$_n$-OH and HEA-p(LA)$_n$-OH (n=10,20)

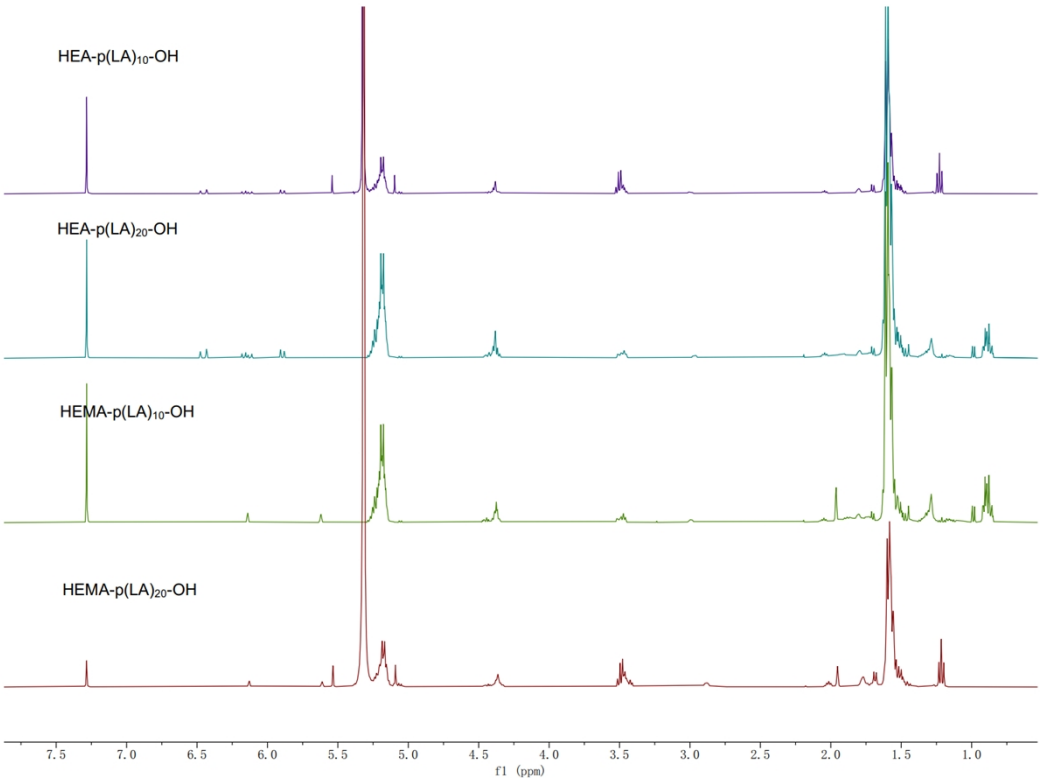

Figure 6.1-1 ^{1}H NMR spectrum of HEMA-p(LA)$_n$-OH and HEA-p(LA)$_n$-OH (n=10,20)

All ^{1}H NMR spectrum of structures that had been obtained.

6.2 ^{1}H NMR spectrum of HEMA-p(LA)$_{20}$-COOH and HEA-p(LA)$_{20}$-COOH via one-pot reaction

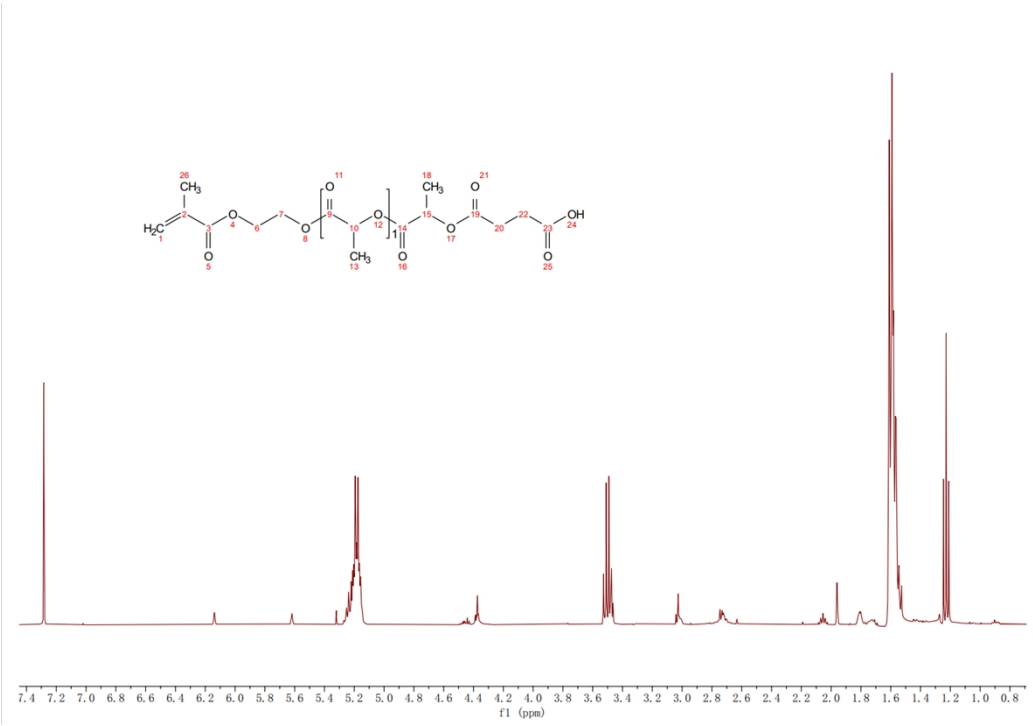

Figure 6.2-1 ^{1}H NMR spectrum of HEMA-(LA)$_{20}$-COOH

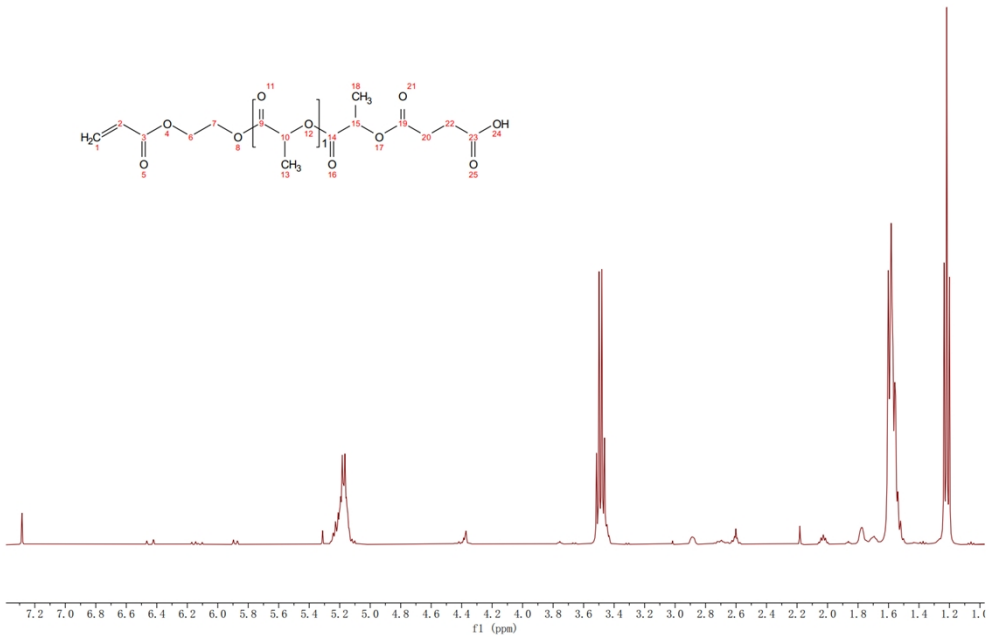

Figure 6.2-2 ^{1}H NMR spectrum of HEA-(LA)$_{20}$-COOH

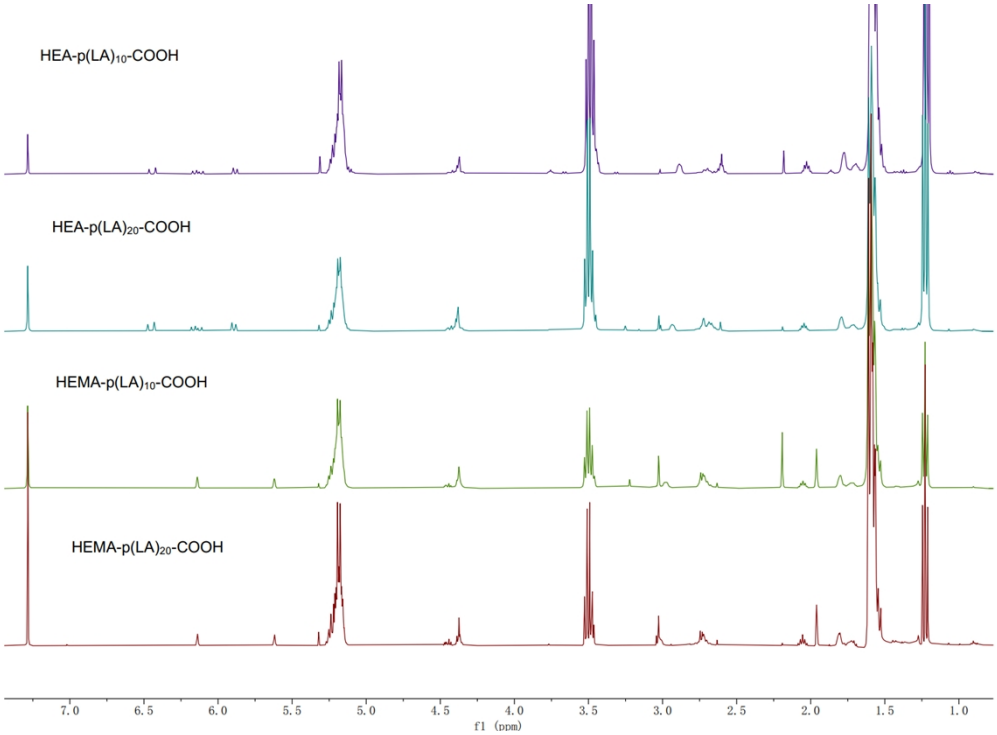

Figure 6.2-1 ^{1}H-NMR spectrum of HEMA-p(LA)$_n$-COOH and HEA-p(LA)$_n$-COOH (n=10, 20) via one-pot reaction

All ^{1}H NMR spectrum of structures that had been obtained.

6.3 ^{1}H-NMR spectrum of HEMA-p(LA)$_{20}$-COO-Red (or Yellow)

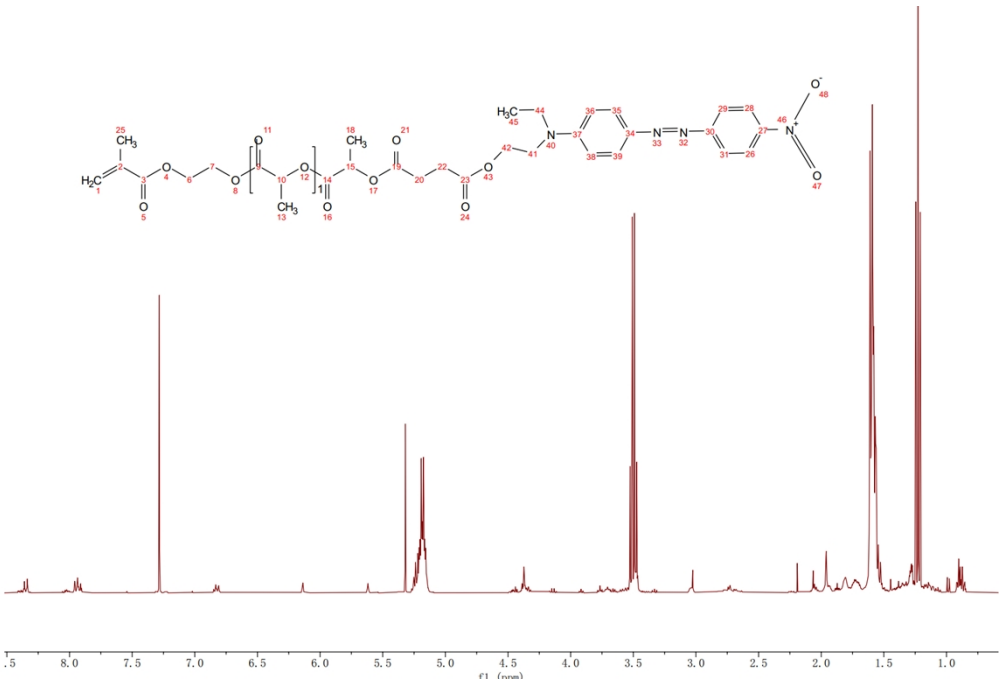

Figure 6.3-1 ^{1}H-NMR spectrum of HEMA-p(LA)$_{20}$-COO-Red

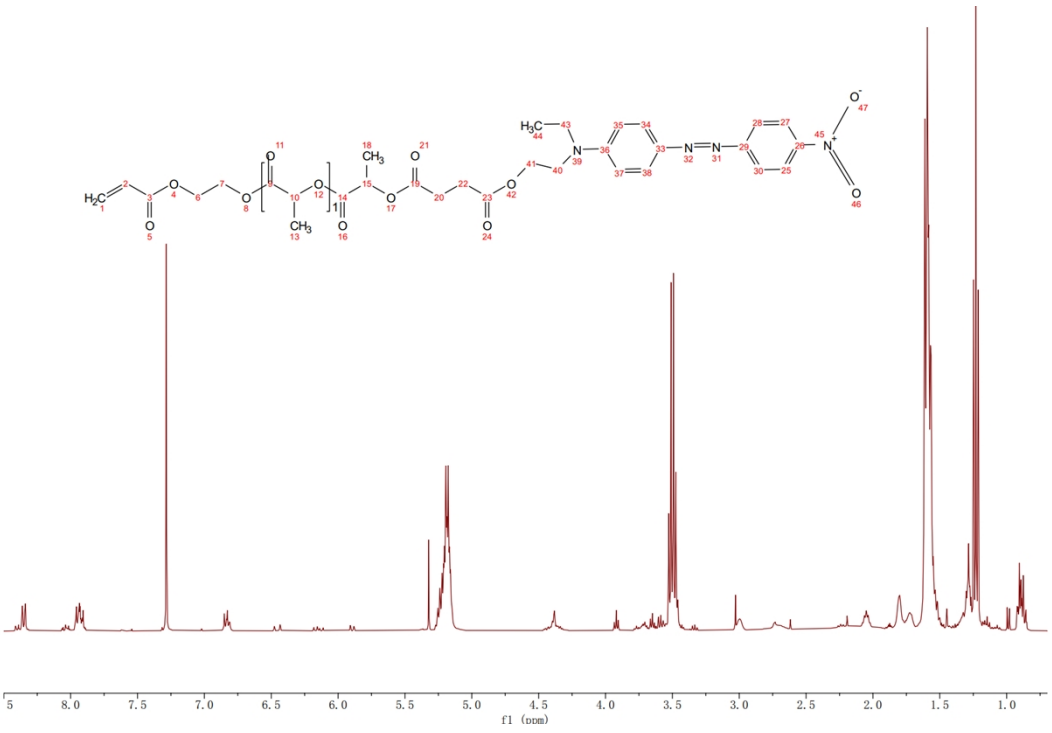

Figure 6.3-2^{1}H-NMR spectrum of HEA-p(LA)$_{20}$-COO-Red

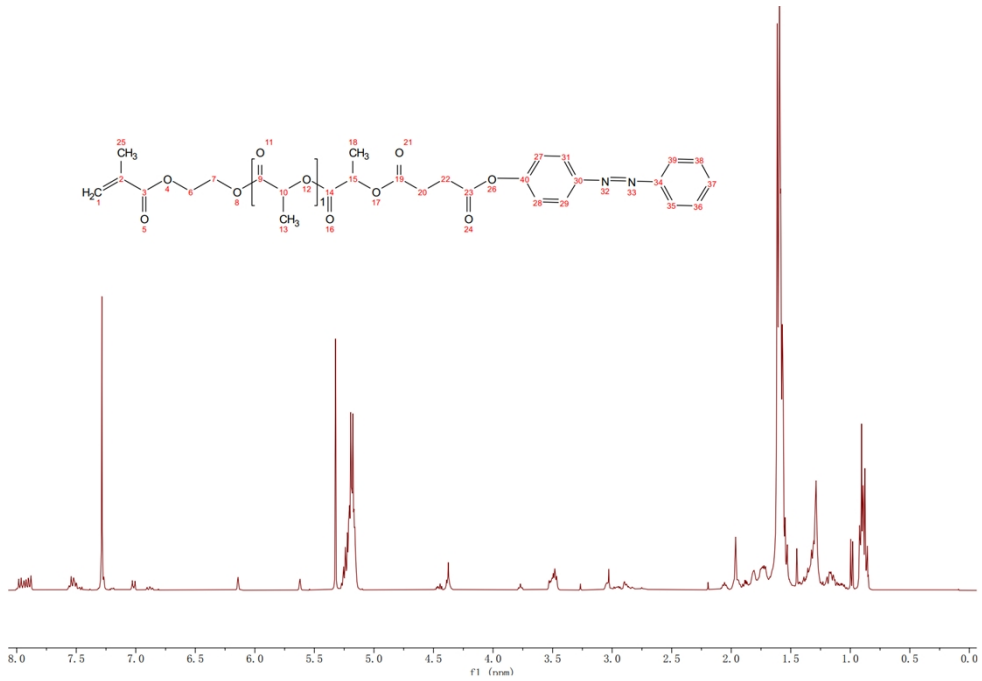

Figure 6.3-3 ^{1}H-NMR spectrum of and HEMA-p(LA)$_{20}$-COO-Yellow

6.4 1H NMR spectrum of all copolymers of MMA and dye monomer

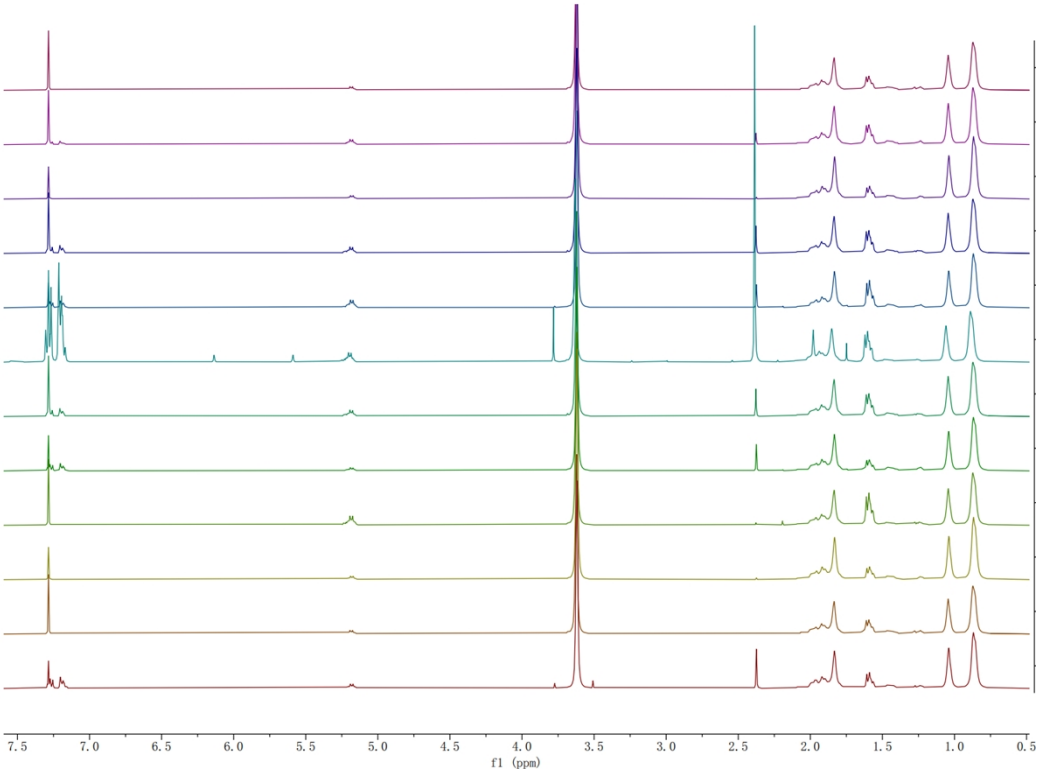

Figure 6.4-1 ^{1}H NMR spectrum of all copolymers of MMA and dye monomer

	Theoretical composition (%)	Actual composition (%)	Conversion (%)	Mn	Đ
MAA	90%	81.3%	61%	1.21×10^5	1.45
Red (DP of LA is 10)	10%	18.7%	54%		
MAA	85%	85%	62%	3.87×10^4	1.07
Red (DP of LA is 10)	15%	15%	52%		
MAA	80%	66%	63%	1.03×10^5	1.25
Red (DP of LA is 10)	20%	34%	52%		
MAA	90%	85%	61%	7.18×10^4	1.83
Yellow (DP of LA is 10)	10%	15%	53%		
MAA	85%	75%	62%	4.22×10^4	1.87
Yellow (DP of LA is 10)	15%	25%	54%		
MAA	80%	70%	63%	3.28×10^5	1.07
Yellow (DP of LA is 10)	20%	30%	50%		
MAA	90%	81.3%	61%	1.07×10^5	1.71
Red (DP of LA is 20)	10%	18.7%	52%		
MAA	85%	80%	63%	5.71×10^4	1.35
Red (DP of LA is 20)	15%	20%	50%		
MAA	80%	77%	62%	1.08×10^5	1.32
Red (DP of LA is 20)	20%	23%	53%		
MAA	90%	88%	65%	6.55×10^4	1.55
Yellow (DP of LA is 20)	10%	12%	56%		
MAA	85%	80%	63%	6.13×10^4	1.21
Yellow (DP of LA is 20)	15%	20%	55%		
MAA	80%	77%	65%	4.95×10^4	1.48
Yellow (DP of LA is 20)	20%	23%	58%		

Table 3.4-1 analysis of all copolymers

6.5 FT-IR spectrum of copolymer via photopolymerization

6.5.1 poly[PEGMA-co-HEA-$(LA)_{10}$-COO-Red (and Yellow)]

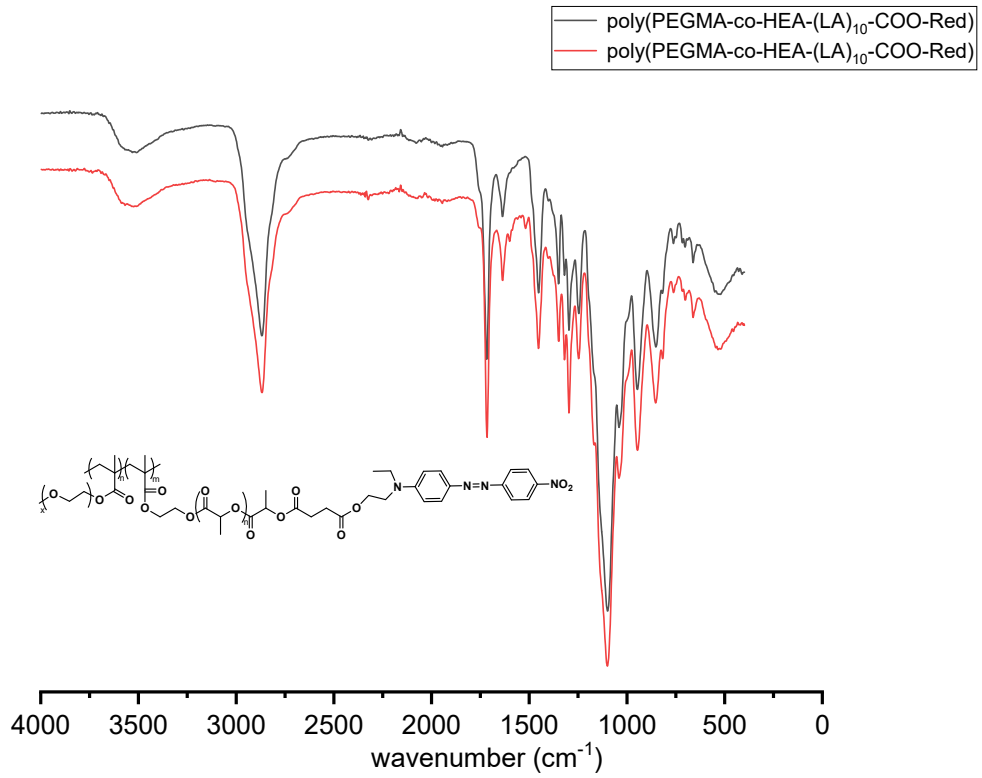

Figure 6.5.1-1 FT-IR spectrum of poly[PEGMA-co-HEA-$(LA)_{10}$-COO-Red (and Yellow)]

some specific group can be observed in the Figure 6.5.1-1: O-H stretching was at 3520 cm^{-1}; C-H (alkane) stretching was at 2980 cm^{-1}; C=O stretching was at 1750 cm^{-1}; C=C (alkene) stretching was at 1680 cm^{-1}; C=C (arene) stretching was at 1600-1400 cm^{-1}; N=N stretching was at 1420 cm^{-1}; C-O stretching was at 1250-1200 cm^{-1}; C-H (arene) bending was at 880-680 cm^{-1}.

6.5.2 poly[TEGMA-co-HEA-$(LA)_{10}$-COO-Red (and Yellow)]

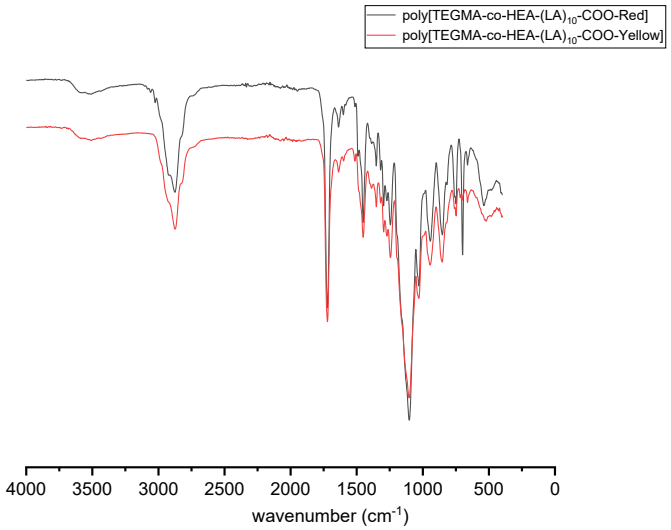

Figure 6.5.2-1 FT-IR spectrum of poly[TEGMA-co-HEA-$(LA)_{10}$-COO-Red (and Yellow)]

(TEGMA wt% 50%)

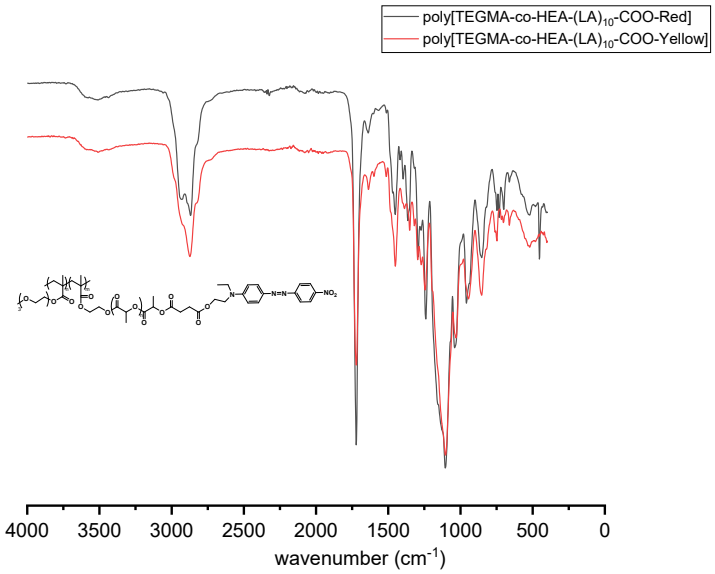

Figure 6.5.2-2 FT-IR spectrum of poly[TEGMA-co-HEA-$(LA)_{10}$-COO-Red (and Yellow)]

(TEGMA wt% 25%)

Some specific group can be observed in the figure 3.6-3 and 3.6-4: O-H stretching was at 3520 cm^{-1}; C-H (alkane) stretching was at 2980 cm^{-1}; C=O stretching was at 1750 cm^{-1}; C=C (alkene) stretching was at 1680 cm^{-1}; C=C (arene) stretching was at 1600-1400 cm^{-1}; N=N stretching was at 1420 cm^{-1}; C-O stretching was at 1250-1200 cm^{-1}; C-H (arene) bending was at 880-680 cm^{-1}.

7. Reference

[1] V. Rajan, B. Sniderman, & P. Baum, “3D opportunity for life: Additive manufacturing takes humanitarian action,” Delight Insight, Vol. 1 No. 19, pp. 1-8, 2016.

[2] Berman B. 3-D printing: the new industrial revolution. Bus Horiz 2012;55(2):155–62.

[3] Bhushan B, Caspers M. An overview of additive manufacturing (3D printing) for microfabrication. Microsyst Technol 2017;23(4):1117–24.

[4] S. C. Joshi, & A. A. Sheikh, “3D-printing in aerospace and its long-term sustainability,” Virtual and Physical Prototyping, Vol. 10, No.4, pp. 175-185, 2015.

[5] Huang R, Riddle M, Graziano D, Warren J, Das S, Nimbalkar S, Cresko J, Masanet E (2016) Energy and emissions saving potential of additive manufacturing: the case of lightweight aircraft components. J Clean Prod 135:1559–1570

[6] V. Sreehitha, “Impact of 3D printing in automotive industry,” International Jurnal of Mechanical and Production Engineering, Vol.5, No.2, pp. 91-94, 2017.

[7] D. Pai, “3D-Printing skin is real: Here’s what you need to know,” Allure News. 2017. [Online]. Available: https://www.allure.com/story/3dprinting-skin. [Accessed 2019].

[8] J. Norman, R.D. Madurawe, C. M. V. Moore, M. A. Khan, & A. Khairuzzaman, “A new chapter in pharmaceutical manufacturing: 3Dprinted drug products,” Advance Drug Delivery Review, Vol.108, pp. 39-50, 2018.

[9] Fina, F., Gaisford, S., Basit, A.W., 2018a. Powder bed fusion: the working process, current applications and opportunities, in: Basit, A.W., Gaisford, S. (Eds.), 3D Printing of Pharmaceuticals, 1 ed. Springer International Publishing, pp. 81-105. 10.1007/9783-319-90755-0.

[10] Beaman, J.J., Deckard, C.R., Selective laser sintering with assisted powder handling US 4938816 A. 1990.

[11] Choudha, S., Tiwari, S.K. and Pande, S. (2012), “A Review of different selection procedures for additive manufacturing techniques”, Proceeding of 17th Annual

Conference of Gwalior Academy of Mathematical Sciences and National Symposium on Computational Mathematics & Information Technology, JUET, Guna.

[12] i Giacomo, G.d.A., Cury, P.R., da Silva, A.M., da Silva, J.V., Ajzen, S.A., 2016. A selective laser sintering prototype guide used to fabricate immediate interim fixed complete arch prostheses in flapless dental implant surgery: Technique description and clinical results. J. Prosthetic Dentistry 116, 874–879.

[13] George, M., Aroom, K.R., Hawes, H.G., Gill, B.S., Love, J., 2017. 3D printed surgical instruments: the design and fabrication process. World J. Surg. 41, 314–319.

[14] Hettesheimer, T., Hirzel, S., Roß, H.B., 2018. Energy savings through additive manufacturing: an analysis of selective laser sintering for automotive and aircraft components. Energy Effi. 11, 1227–1245.

[15] Jiba, Z., Focke, W.W., Kalombo, L., Madito, M.J., 2019. Coating processes towards selective laser sintering of energetic material composites. Defence Technol.

[16] Revilla-León, M., Özcan, M., 2017. Additive manufacturing technologies used for 3D metal printing in dentistry. Curr. Oral Health Reports 4, 201–208.

[17] Theodorakos, I., Zacharatos, F., Geremia, R., Karnakis, D., Zergioti, I., 2015. Selective laser sintering of Ag nanoparticles ink for applications in flexible electronics. Appl. Surf. Sci. 336, 157–162.

[18] Goodridge, R., Ziegelmeier, S., 2017. 7 – Powder bed fusion of polymers, in: Brandt, M.

(Ed.), Laser Additive Manufacturing. Woodhead Publishing, pp. 181-204.

[19] Kruth, J.P., Mercelis, P., Van Vaerenbergh, J., Froyen, L., Rombouts, M., 2003a. Advances in selective laser sintering. In: Proceedings of the 1st International Conference on Advanced Research in Virtual and Rapid Prototyping, pp. 59–70.

[20] Akande, S.O., Dalgarno, K.W., Munguia, J., Pallari, J., 2016. Assessment of tests for use in process and quality control systems for selective laser sintering of polyamide powders. J. Mater. Process. Technol. 229, 549–561.

[21] Ma, F., Zhang, H., Hon, K.K.B., Gong, Q., 2018. An optimization approach of selective laser sintering considering energy consumption and material cost. J. Cleaner Prod. 199, 529–537.

[22] Tiwari, S.K., Pande, S., Agrawal, S., Bobade, S.M., 2015. Selection of selective laser sintering materials for different applications. Rapid Prototyp. J. 21, 630–648.
[23] Childs, T.H.C., Hauser, C., Taylor, C.M, Tontovi, A.E., 2000, Simulation and experimental verification of crystalline polymer and direct metal selective laser sintering, Proc. SFF Symp., Austin: 100-109.
[24] Tontowi, A.E. Childs, T.H.C., 2001, Density prediction of crystalline polymer sintered parts at various powder bed temperatures, Rapid Prototyping J., 7/3: 180184.
[25] Wendel, B., Dallner, C., Schmachtenberg, E., 2007, New developments in selective laser sintering of polymers, Proc. LANE, Erlangen: 323-331.
[26] Tiwari, S.K. and Pande, S. (2012), "Review of material properties and selection for selective laser sintering process", Proceeding of International Conference in Design and Manufacturing (InnDeM-2012), IIITDM, Jabalpur.
[27] Gibson, I., Rosen, W.D. and Stucker, B. (2010), Additive Manufacturing Technologies: Rapid Prototyping to Direct Digital Manufacturing, Springer Publishers, UK.
[28] Gibson, I. and Shi, D. (1997), "Material properties and fabrication parameters in selective laser sintering process", Rapid Prototyping Journal, Vol. 3 No. 4, pp. 129-136.
[29] J. P. Kruth, G.N. Levy et al., Consolidation phenomena in laser and powder-bed based layerd manufacturing CIRP Annals Manufacturing Technology, 56(2), 2007, 730-759
[30] M. Schmid, A. Amado, G.N. Levy, iCoPP - A New Polyolefin for Additive Manufacturing (SLS), Proceedings of the International Conference on Additive Manufacturing, Session 7, Loughborough, U.K., 2011
[31] D. Drummer, Development of a characterization approach for the sintering behavior of new thermoplastics for selective laser sintering, Physics Procedia (5), 2010, 533 – 542
[32] G.W. Ehrenstein, G. Riedel, P. Trawiel, Thermal Analysis of Plastics, ISBN-10: 3-446-22673-7, 2004
[33] Kruth, J.P., Wang, X., Laoui, T. and Froyen, L. (2003), "Laser and materials in selective laser sintering", Assembly Automation, Vol. 23 No. 4, pp. 357-371.

[34] Tolochko, N.K., Laoui, T., Khlopkov, Y.V., Mozzharov, S.E., Titov, V.I. and Ignative, M.B. (2000), "Absorption of powder materials suitable for laser sintering", Rapid Prototyping Journal, Vol. 6 No. 3, pp. 155-160.

[35] Fred, L.A., Lohrengel, A., Neubert, V., Camila, F.H., Czelusniak, T., 2014. Selective laser sintering of Mo-CuNi composite to be used as EDM electrode. Rapid Prototyp. J. 20, 59–68.

[36] Williams, J.M., Adewunmi, A., Schek, R.M., Flanagan, C.L., Krebsbach, P.H., Feinberg, S.E., Hollister, S.J., Das, S., 2005. Bone tissue engineering using polycaprolactone scaffolds fabricated via selective laser sintering. Biomaterials 26, 4817–4827.

[37] Schulze, D., 2008. Powders and Bulk Solids: Behavior, Characterization, Storage and Flow. Springer, Berlin Heidelberg New York.

[38] Leong, K.F., Chua, C.K., Gui, W.S., Verani, 2006. Building porous biopolymeric microstructures for controlled drug delivery devices using selective laser sintering. Int. J. Adv. Manuf. Technol. 31, 483–489.

[39] Kruth, J.P., Wang, X., Froyen, L., 2003b. Lasers and materials in selective laser sintering. Assembly Automation 23, 357–371.

[40] J.-P. Kruth., G. Levy., F. Klocke., T.H.C. Childs, 2007. Consolidation phenomena in laser and powder-bed based layered manufacturing. ScienceDirect. 56(2), 730-759.

[41] Lewis G. Properties of antibiotic-loaded acrylic bone cements for use in cemented arthroplasties. J Biomed Mater Res Part B: Appl Biomater 2009; 89B: 558–574.

[42] Puska M, Kokkari A, Na¨rhi T, et al. Mechanical properties of oligomermodified acrylic bone cement. Biomaterials 2003; 24: 417–425.

[43] Popis¸ ter F, Popescu D and Hurgoiu D. A new method for using reverse engineering in case of ceramic tiles. Qual Access Success 2012; 13: 409–412.

[44] Ahato I. Reverse engineering the ceramic art of algae. Science 1999; 286: 1059–1061.

[45] Freeman MAR, Bradley GW and Ravell PA. Observation upon the interface between bone and polymethylmethacrylate cement. J Bone Joint Surg 1982; 64B: 489–493.

[46] Espalin D, Arcaute K, Rodriguez D, et al. Rapid Prototyping J 2010; 16: 164.

[47] Hao L, Savalani MM, Zhang Y, et al. Selective laser sintering of hydroxyapatite reinforced polyethylene composites for bioactive implants and tissue scaffold development. Proc IMechE, Part H: J Engineering in Medicine 2006; 220: 521.

[48] Bressan, L.P., Adamo, C.B., Quero, R.F., de Jesus, D.P. and da Silva, J.A., 2019. A simple procedure to produce FDM-based 3D-printed microfluidic devices with an integrated PMMA optical window. *Analytical methods*, *11*(8), pp.1014-1020.

[49] Rajkumar Velu, Sarat Singamneni. Evaluation of the influences of process parameters while selective laser sintering PMMA powders. Journal of mechanical engineering science 229; 4: 603-613.

[50] Kafle, A., Luis, E., Silwal, R., Pan, H.M., Shrestha, P.L. and Bastola, A.K., 2021. 3D/4D Printing of polymers: Fused deposition modelling (FDM), selective laser sintering (SLS), and stereolithography (SLA). *Polymers*, *13*(18), p.3101.

[51] Tekin E, Smith PJ, Schubert US. Inkjet printing as a deposition and patterning tool for polymers and inorganic particles. Soft Matter. 2008;4(4):703-13.

[52] Pesach D, Marmur A. Marangoni effects in the spreading of liquid mixtures on a solid. Langmuir. 1987 Jul;3(4):519-24.

[53] Lim, J.A., Lee, W.H., Lee, H.S., Lee, J.H., Park, Y.D. and Cho, K., 2008. Self-organization of ink-jet-printed triisopropylsilylethynyl pentacene via evaporation-induced flows in a drying droplet. *Advanced functional materials*, *18*(2), pp.229-234.

[54] Wang, Y., Bokor, J. and Lee, A., 2004, May. Maskless lithography using drop-on-demand inkjet printing method. In *Emerging Lithographic Technologies VIII* (Vol. 5374, pp. 628-636). International Society for Optics and Photonics.

[55] Sirringhaus, H. and Shimoda, T., 2003. Inkjet printing of functional materials. *MRS bulletin*, *28*(11), pp.802-806.

[56] Zhang, J. and Xiao, P., 2018. 3D printing of photopolymers. *Polymer Chemistry*, *9*(13), pp.1530-1540.

[57] Bagheri, A. and Jin, J., 2019. Photopolymerization in 3D printing. *ACS Applied Polymer Materials*, *1*(4), pp.593-611.

[58] Zhu, W., Qu, X., Zhu, J., Ma, X., Patel, S., Liu, J., Wang, P., Lai, C.S.E., Gou, M., Xu, Y. and Zhang, K., 2017. Direct 3D bioprinting of prevascularized tissue constructs with complex microarchitecture. *Biomaterials*, *124*, pp.106-115.

[59] Hamidi, M., Azadi, A. and Rafiei, P., 2008. Hydrogel nanoparticles in drug delivery. *Advanced drug delivery reviews*, *60*(15), pp.1638-1649.

[60] Huang, T.Q., Qu, X., Liu, J. and Chen, S., 2014. 3D printing of biomimetic microstructures for cancer cell migration. *Biomedical microdevices*, *16*(1), pp.127-132.

[61] Pan, L., Yu, G., Zhai, D., Lee, H.R., Zhao, W., Liu, N., Wang, H., Tee, B.C.K., Shi, Y., Cui, Y. and Bao, Z., 2012. Hierarchical nanostructured conducting polymer hydrogel with high electrochemical activity. *Proceedings of the National Academy of Sciences*, *109*(24), pp.9287-9292.

[62] Jungst, T., Smolan, W., Schacht, K., Scheibel, T. and Groll, J., 2016. Strategies and molecular design criteria for 3D printable hydrogels. *Chemical reviews*, *116*(3), pp.1496-1539.

[63] Nakagawa, Y., Ohta, S., Nakamura, M. and Ito, T., 2017. 3D inkjet printing of star block copolymer hydrogels cross-linked using various metallic ions. *RSC advances*, *7*(88), pp.55571-55576.

[64] Simaite, A., Mesnilgrente, F., Tondu, B., Souères, P. and Bergaud, C., 2016. Towards inkjet printable conducting polymer artificial muscles. *Sensors and Actuators B: Chemical*, *229*, pp.425-433.

[65] Shim, G.H., Han, M.G., Sharp-Norton, J.C., Creager, S.E. and Foulger, S.H., 2008. Inkjet-printed electrochromic devices utilizing polyaniline–silica and poly (3, 4-ethylenedioxythiophene)–silica colloidal composite particles. *Journal of Materials Chemistry*, *18*(5), pp.594-601.

[66] Hiemenz, P.C. and Lodge, T.P., 2007. *Polymer chemistry*. CRC press.

[67] Stevens, M.P., 1990. *Polymer chemistry* (Vol. 2). New York: Oxford university press.

[68] Odian, G., 2004. *Principles of polymerization*. John Wiley & Sons.

[69] Matyjaszewski, K. and Davis, T.P., 2003. *Handbook of radical polymerization*. John Wiley & Sons.

[70] Balke, S.T. and Hamielec, A.E., 1973. Bulk polymerization of methyl methacrylate. *Journal of applied Polymer science*, *17*(3), pp.905-949.

[71] Scott, R.A. and Peppas, N.A., 1997. Kinetic study of acrylic acid solution polymerization. *AIChE Journal*, *43*(1), pp.135-144.

[72] Yuan, H.G., Kalfas, G. and Ray, W.H., 1991. Suspension polymerization. *Journal of Macromolecular Science, Part C: Polymer Reviews*, *31*(2-3), pp.215-299.

[73] Chern, C.S., 2006. Emulsion polymerization mechanisms and kinetics. *Progress in polymer science*, *31*(5), pp.443-486.

[74] Kawaguchi, S. and Ito, K., 2005. Dispersion polymerization. *Polymer particles*, pp.299-328.

[75] Yoshida, E., 2010. Photo-living radical polymerization of methyl methacrylate using alkoxyamine as an initiator. *Colloid and Polymer Science*, *288*(1), pp.7-13.

[76] Liu, J., Zhang, Y., Zhou, R. and Gao, L., 2017. Volatile alcohol-responsive visual sensors based on p (HEMA-co-MA)-infiltrated SiO 2 inverse opal photonic crystals. *Journal of Materials Chemistry C*, *5*(24), pp.6071-6078.

[77] Kaminoyama, M., Watanabe, M., Nishi, K., Kamiwano, M., 1999. Numerical simulation of local heat transfer coefficients in stirred vessel with impeller for highly viscous fluids. Journal of Chemical Engineering of Japan 32, 23–30.

[78] Gedde, U.L.F., 1995. *Polymer physics*. Springer Science & Business Media.

[79] Dinu, M.V., Spulber, M., Renggli, K., Wu, D., Monnier, C.A., Petri-Fink, A. and Bruns, N., 2015. Filling Polymersomes with Polymers by Peroxidase-Catalyzed Atom Transfer Radical Polymerization. *Macromolecular rapid communications*, *36*(6), pp.507-514.

[80] Marian, C.M., 2012. Spin–orbit coupling and intersystem crossing in molecules. *Wiley Interdisciplinary Reviews: Computational Molecular Science*, *2*(2), pp.187-203.

[81] Kakiuchi, F., Kan, S., Igi, K., Chatani, N. and Murai, S., 2003. A Ruthenium-Catalyzed Reaction of Aromatic Ketones with Arylboronates: A New Method for the Arylation of Aromatic Compounds via C− H Bond Cleavage. *Journal of the American Chemical Society*, *125*(7), pp.1698-1699.

[82] Wang, W., Guo, Y. and Otaigbe, J.U., 2008. Synthesis and characterization of novel biodegradable and biocompatible poly (ester-urethane) thin films prepared by homogeneous solution polymerization. *Polymer*, *49*(20), pp.4393-4398.

[83] Romack, T.J., Maury, E.E. and DeSimone, J.M., 1995. Precipitation polymerization of acrylic acid in supercritical carbon dioxide. *Macromolecules*, *28*(4), pp.912-915.

[84] Yagci, Y., Jockusch, S. and Turro, N.J., 2010. Photoinitiated polymerization: advances, challenges, and opportunities. *Macromolecules*, *43*(15), pp.6245-6260.

[85] Xiao, P., Zhang, J., Dumur, F., Tehfe, M.A., Morlet-Savary, F., Graff, B., Gigmes, D., Fouassier, J.P. and Lalevee, J., 2015. Visible light sensitive photoinitiating systems: Recent progress in cationic and radical photopolymerization reactions under soft conditions. *Progress in Polymer Science*, *41*, pp.32-66.

[86] Tasdelen, M.A. and Yagci, Y., 2011. Photochemical methods for the preparation of complex linear and cross-linked macromolecular structures. *Australian Journal of Chemistry*, *64*(8), pp.982-991.

[87] Qin, S.H., Qin, D.Q. and Qiu, K.Y., 2001. A novel photo atom transfer radical polymerization of methyl methacrylate. *New Journal of Chemistry*, *25*(7), pp.893-895.

[88] Ramakers, G., Krivcov, A., Trouillet, V., Welle, A., Möbius, H. and Junkers, T., 2017. Organocatalyzed Photo-Atom Transfer Radical Polymerization of Methacrylic Acid in Continuous Flow and Surface Grafting. *Macromolecular rapid communications*, *38*(21), p.1700423.

[89] Quan, Q., Gong, H. and Chen, M., 2018. Preparation of semifluorinated poly (meth) acrylates by improved photo-controlled radical polymerization without the use of a fluorinated RAFT agent: facilitating surface fabrication with fluorinated materials. *Polymer Chemistry*, *9*(30), pp.4161-4171.

[90] Wei, Y., Zeng, Q., Bai, S., Wang, M. and Wang, L., 2017. Nanosized difunctional photo responsive magnetic imprinting polymer for electrochemically monitored light-driven paracetamol extraction. *ACS applied materials & interfaces*, *9*(50), pp.44114-44123.

[91] Gurnani, P. and Perrier, S., 2020. Controlled radical polymerization in dispersed systems for biological applications. *Progress in Polymer Science*, *102*, p.101209.

[92] Karabulut, H.R.F., Mert, B., Altinkok, C., Karatavuk, A.O., Acik, G. and Turkyilmaz, M., 2021. Synthesis of new bio-based hydrogels derived from bile acids by free-radical photo-polymerization. *Polymers for Advanced Technologies*, *32*(1), pp.220-227.

[93] Bagheri, A., Engel, K.E., Bainbridge, C.W.A., Xu, J., Boyer, C. and Jin, J., 2020. 3D printing of polymeric materials based on photo-RAFT polymerization. *Polymer Chemistry*, *11*(3), pp.641-647.

[94] Dubois, P., Coulembier, O. and Raquez, J.M. eds., 2009. *Handbook of ring-opening polymerization*. John Wiley & Sons.

[95] Nair, L.S. and Laurencin, C.T., 2007. Biodegradable polymers as biomaterials. *Progress in polymer science*, *32*(8-9), pp.762-798.

[96] Humberstone, A.J. and Charman, W.N., 1997. Lipid-based vehicles for the oral delivery of poorly water soluble drugs. *Advanced drug delivery reviews*, *25*(1), pp.103-128.

[97] Yoon, S.J., Kim, S.H., Ha, H.J., Ko, Y.K., So, J.W., Kim, M.S., Yang, Y.I., Khang, G., Rhee, J.M. and Lee, H.B., 2008. Reduction of inflammatory reaction of poly (D, L-lactic-C o-glycolic acid) using demineralized bone particles. *Tissue Engineering Part A*, *14*(4), pp.539-547.

[98] Acemoglu, M., 2004. Chemistry of polymer biodegradation and implications on parenteral drug delivery. *International journal of pharmaceutics*, *277*(1-2), pp.133-139.

[99] Zhang, Z., Kuijer, R., Bulstra, S.K., Grijpma, D.W. and Feijen, J., 2006. The in vivo and in vitro degradation behavior of poly (trimethylene carbonate). *Biomaterials*, *27*(9), pp.1741-1748.

[100] Artham, T. and Doble, M., 2008. Biodegradation of aliphatic and aromatic polycarbonates. *Macromolecular bioscience*, *8*(1), pp.14-24.

[101] Dadsetan, M., Christenson, E.M., Unger, F., Ausborn, M., Kissel, T., Hiltner, A. and Anderson, J.M., 2003. In vivo biocompatibility and biodegradation of poly (ethylene carbonate). *Journal of controlled release*, *93*(3), pp.259-270.

[102] Feng, J., Zhuo, R.X. and Zhang, X.Z., 2012. Construction of functional aliphatic polycarbonates for biomedical applications. *Progress in polymer science*, *37*(2), pp.211-236.

[103] Jérôme, C. and Lecomte, P., 2008. Recent advances in the synthesis of aliphatic polyesters by ring-opening polymerization. *Advanced drug delivery reviews*, *60*(9), pp.1056-1076.

[104] Ajellal, N., Carpentier, J.F., Guillaume, C., Guillaume, S.M., Helou, M., Poirier, V., Sarazin, Y. and Trifonov, A., 2010. Metal-catalyzed immortal ring-opening polymerization of lactones, lactides and cyclic carbonates. *Dalton Transactions*, *39*(36), pp.8363-8376.

[105] Xu, J., Song, J., Pispas, S. and Zhang, G., 2014. Metal-free controlled ring-opening polymerization of ε-caprolactone in bulk using tris (pentafluorophenyl) borane as a catalyst. *Polymer Chemistry*, *5*(16), pp.4726-4733.

[106] Kobayashi, S., Uyama, H. and Kimura, S., 2001. Enzymatic polymerization. *Chemical Reviews*, *101*(12), pp.3793-3818.

[107] Takwa, M., Xiao, Y., Simpson, N., Malmström, E., Hult, K., Koning, C.E., Heise, A. and Martinelle, M., 2008. Lipase catalyzed HEMA initiated ring-opening polymerization: In situ formation of mixed polyester methacrylates by transesterification. *Biomacromolecules*, *9*(2), pp.704-710.

[108] Duda, A., Kowalski, A., Penczek, S., Uyama, H. and Kobayashi, S., 2002. Kinetics of the ring-opening polymerization of 6-, 7-, 9-, 12-, 13-, 16-, and 17-membered lactones. Comparison of chemical and enzymatic polymerizations. *Macromolecules*, *35*(11), pp.4266-4270.

[109] Uyama, H., Takeya, K. and Kobayashi, S., 1995. Enzymatic ring-opening polymerization of lactones to polyesters by lipase catalyst: unusually high reactivity of macrolides. *Bulletin of the Chemical Society of Japan*, *68*(1), pp.56-61.

[110] Albertsson, A.C. and Srivastava, R.K., 2008. Recent developments in enzyme-catalyzed ring-opening polymerization. *Advanced drug delivery reviews*, *60*(9), pp.1077-1093.

[111] Takwa, M., Larsen, M.W., Hult, K. and Martinelle, M., 2011. Rational redesign of Candida antarctica lipase B for the ring opening polymerization of D, D-lactide. *Chemical Communications*, *47*(26), pp.7392-7394.

[112] Takwa, M., Xiao, Y., Simpson, N., Malmström, E., Hult, K., Koning, C.E., Heise, A. and Martinelle, M., 2008. Lipase catalyzed HEMA initiated ring-opening

polymerization: In situ formation of mixed polyester methacrylates by transesterification. *Biomacromolecules*, *9*(2), pp.704-710.

[113] Shen, J., Nguyen, T.T., Goh, Y.P., Ye, W., Fu, X., Xu, J. and Tan, C.H., 2006. Chiral bicyclic guanidine-catalyzed enantioselective reactions of anthrones. *Journal of the American Chemical Society*, *128*(42), pp.13692-13693.

[114] Simoni, D., Rossi, M., Rondanin, R., Mazzali, A., Baruchello, R., Malagutti, C., Roberti, M. and Invidiata, F.P., 2000. Strong bicyclic guanidine base-promoted Wittig and Horner− Wadsworth− Emmons reactions. *Organic letters*, *2*(24), pp.3765-3768.

[115] Simoni, D., Rondanin, R., Morini, M., Baruchello, R. and Invidiata, F.P., 2000. 1, 5, 7-Triazabicyclo [4.4. 0] dec-1-ene (TBD), 7-methyl-TBD (MTBD) and the polymer-supported TBD (P-TBD): Three efficient catalysts for the nitroaldol (Henry) reaction and for the addition of dialkyl phosphites to unsaturated systems. *Tetrahedron Letters*, *41*(10), pp.1607-1610.

[116] Schuchardt, U., Vargas, R.M. and Gelbard, G., 1995. Alkylguanidines as catalysts for the transesterification of rapeseed oil. *Journal of Molecular Catalysis A: Chemical*, *99*(2), pp.65-70.

[117] Pratt, R.C., Lohmeijer, B.G., Long, D.A., Waymouth, R.M. and Hedrick, J.L., 2006. Triazabicyclodecene: a simple bifunctional organocatalyst for acyl transfer and ring-opening polymerization of cyclic esters. *Journal of the American Chemical Society*, *128*(14), pp.4556-4557.

[118] Lohmeijer, B.G., Pratt, R.C., Leibfarth, F., Logan, J.W., Long, D.A., Dove, A.P., Nederberg, F., Choi, J., Wade, C., Waymouth, R.M. and Hedrick, J.L., 2006. Guanidine and amidine organocatalysts for ring-opening polymerization of cyclic esters. *Macromolecules*, *39*(25), pp.8574-8583.

[119] Nederberg, F., Connor, E.F., Möller, M., Glauser, T. and Hedrick, J.L., 2001. New paradigms for organic catalysts: the first organocatalytic living polymerization. *Angewandte Chemie International Edition*, *40*(14), pp.2712-2715.

[120] Kamber, N.E., Jeong, W., Waymouth, R.M., Pratt, R.C., Lohmeijer, B.G. and Hedrick, J.L., 2007. Organocatalytic ring-opening polymerization. *Chemical reviews*, *107*(12), pp.5813-5840.

[121] Slomkowski, S., Gadzinowski, M., Sosnowski, S., Radomska-Galant, I., Pucci, A., De Vita, C. and Ciardelli, F., 2006. Nanoparticles from polylactide and polyether block copolymers: Formation, properties, encapsulation, and release of pyrene—Fluorescent model of hydrophobic drug. *Journal of nanoscience and nanotechnology*, *6*(9-10), pp.3242-3251.

[122] Lou, X., Detrembleur, C. and Jérôme, R., 2003. Novel aliphatic polyesters based on functional cyclic (di) esters. *Macromolecular rapid communications*, *24*(2), pp.161-172.

[123] Szwarc, M., Levy, M. and Milkovich, R., 1956. Polymerization initiated by electron transfer to monomer. A new method of formation of block polymers1. *Journal of the American Chemical Society*, *78*(11), pp.2656-2657.

[124] Webster, O.W., 1991. Living polymerization methods. *Science*, *251*(4996), pp.887-893.

[125] Owens III, D.E. and Peppas, N.A., 2006. Opsonization, biodistribution, and pharmacokinetics of polymeric nanoparticles. *International journal of pharmaceutics*, *307*(1), pp.93-102.

[126] Montheard, J.P., Chatzopoulos, M. and Chappard, D., 1992. 2-hydroxyethyl methacrylate (HEMA): chemical properties and applications in biomedical fields. *Journal of Macromolecular Science, Part C: Polymer Reviews*, *32*(1), pp.1-34.

[127] Weaver, J.V.M., Bannister, I., Robinson, K.L., Bories-Azeau, X., Armes, S.P., Smallridge, M. and McKenna, P., 2004. Stimulus-responsive water-soluble polymers based on 2-hydroxyethyl methacrylate. *Macromolecules*, *37*(7), pp.2395-2403.

[128] Mun, G.A., Khutoryanskiy, V.V., Akhmetkalieva, G.T. *et al.* Interpolymer complexes of poly(acrylic acid) with poly(2-hydroxyethyl acrylate) in aqueous solutions. *Colloid Polym Sci* **283,** 174–181 (2004).

[129] Mun, G.A., Nurkeeva, Z.S., Beissegul, A.B., Dubolazov, A.V., Urkimbaeva, P.I., Park, K. and Khutoryanskiy, V.V., 2007. Temperature-responsive water-soluble copolymers based on 2-hydroxyethyl acrylate and butyl acrylate. *Macromolecular Chemistry and Physics*, *208*(9), pp.979-987.

[130] Eguiburu, J.L., Jose, M., Berridi, F. and San Roma, J., 1995. Functionalization of poly (L-lactide) macromonomers by ring-opening polymerization of L-lactide initiated with hydroxyethyl methacrylate-aluminium alkoxides. *Polymer*, *36*(1), pp.173-179.

[131] Xiao, Y., Takwa, M., Hult, K., Koning, C.E., Heise, A. and Martinelle, M., 2009. Systematic Comparison of HEA and HEMA as Initiators in Enzymatic Ring-Opening Polymerizations. *Macromolecular bioscience*, *9*(7), pp.713-720.

[132] Yang, H.J., Chai, C.Q., Zuo, Y.K., Huang, J.F., Song, Y.Y., Jiang, L., Huang, W.Y., Jiang, Q.M., Xue, X.Q. and Jiang, B.B., 2020. Hybrid copolymerization via the combination of proton transfer and ring-opening polymerization. *Chinese Journal of Polymer Science*, *38*(3), pp.231-239.

[133] Leja, K. and Lewandowicz, G., 2010. Polymer biodegradation and biodegradable polymers-a review. *Polish Journal of Environmental Studies*, *19*(2).

[134] Zhang, Q., Ko, N.R. and Oh, J.K., 2012. Recent advances in stimuli-responsive degradable block copolymer micelles: synthesis and controlled drug delivery applications. *Chemical communications*, *48*(61), pp.7542-7552.

[135] Bawa, K.K. and Oh, J.K., 2017. Stimulus-responsive degradable polylactide-based block copolymer nanoassemblies for controlled/enhanced drug delivery. *Molecular pharmaceutics*, *14*(8), pp.2460-2474.

[136] Kricheldorf, H.R., 2009. Syntheses of biodegradable and biocompatible polymers by means of bismuth catalysts. *Chemical reviews*, *109*(11), pp.5579-5594.

[137] Mutlu, H., Geiselhart, C.M. and Barner-Kowollik, C., 2018. Untapped potential for debonding on demand: the wonderful world of azo-compounds. *Materials Horizons*, *5*(2), pp.162-183.

[138] Paramonov, S.E., Bachelder, E.M., Beaudette, T.T., Standley, S.M., Lee, C.C., Dashe, J. and Fréchet, J.M., 2008. Fully acid-degradable biocompatible polyacetal microparticles for drug delivery. *Bioconjugate Chemistry*, *19*(4), pp.911-919.

[139] Tachibana, Y., Baba, T. and Kasuya, K.I., 2017. Environmental biodegradation control of polymers by cleavage of disulfide bonds. *Polymer Degradation and Stability*, *137*, pp.67-74.

[140] Xia, J., Li, T., Lu, C. and Xu, H., 2018. Selenium-containing polymers: perspectives toward diverse applications in both adaptive and biomedical materials. *Macromolecules*, *51*(19), pp.7435-7455.

[141] Yardley, R.E., Kenaree, A.R. and Gillies, E.R., 2019. Triggering depolymerization: Progress and opportunities for self-immolative polymers. *Macromolecules*, *52*(17), pp.6342-6360.

[142] Ayer, M.A., Schrettl, S., Balog, S., Simon, Y.C. and Weder, C., 2017. Light-responsive azo-containing organogels. *Soft matter*, *13*(22), pp.4017-4023.

[143] Diesendruck, C.E., Peterson, G.I., Kulik, H.J., Kaitz, J.A., Mar, B.D., May, P.A., White, S.R., Martínez, T.J., Boydston, A.J. and Moore, J.S., 2014. Mechanically triggered heterolytic unzipping of a low-ceiling-temperature polymer. *Nature chemistry*, *6*(7), pp.623-628.

[144] Song, C.C., Du, F.S. and Li, Z.C., 2014. Oxidation-responsive polymers for biomedical applications. *Journal of Materials Chemistry B*, *2*(22), pp.3413-3426.

[145] Li, Y., Maciel, D., Rodrigues, J., Shi, X. and Tomas, H., 2015. Biodegradable polymer nanogels for drug/nucleic acid delivery. *Chemical reviews*, *115*(16), pp.8564-8608.

[146] Cai, Z., Wan, Y., Becker, M.L., Long, Y.Z. and Dean, D., 2019. Poly (propylene fumarate)-based materials: Synthesis, functionalization, properties, device fabrication and biomedical applications. *Biomaterials*, *208*, pp.45-71.

[147] Kai, D., Zhang, K., Jiang, L., Wong, H.Z., Li, Z., Zhang, Z. and Loh, X.J., 2017. Sustainable and antioxidant lignin–polyester copolymers and nanofibers for potential healthcare applications. *ACS Sustainable Chemistry & Engineering*, *5*(7), pp.6016-6025.

[148] Hill, M.R., Kubo, T., Goodrich, S.L., Figg, C.A. and Sumerlin, B.S., 2018. Alternating radical ring-opening polymerization of cyclic ketene acetals: access to tunable and functional polyester copolymers. *Macromolecules*, *51*(14), pp.5079-5084.

[149] Koh, J., 2011. Dyeing with disperse dyes. *Textile dyeing*, *10*, pp.195-220.

[150] Chen Rongqi, 2007. Development of modern reactive dyes and disperse dyes (Doctoral dissertation).

[151] Li, B., Shen, J., Liang, R., Ji, W. and Kan, C., 2012. Synthesis and characterization of covalently colored polymer latex based on new polymerizable anthraquinone dyes. *Colloid and Polymer Science*, *290*(18), pp.1893-1900.

[152] Bourell, D.L., Watt, T.J., Leigh, D.K. and Fulcher, B., 2014. Performance limitations in polymer laser sintering. *Physics Procedia*, *56*, pp.147-156.

[153] Bandara, H.D. and Burdette, S.C., 2012. Photoisomerization in different classes of azobenzene. *Chemical Society Reviews*, *41*(5), pp.1809-1825.

[154] Jiang, H.Y., Kelch, S. and Lendlein, A., 2006. Polymers move in response to light. *Advanced Materials*, *18*(11), pp.1471-1475.

[150] Li, Y., He, Y., Tong, X. and Wang, X., 2005. Photoinduced deformation of amphiphilic azo polymer colloidal spheres. *Journal of the American Chemical Society*, *127*(8), pp.2402-2403.

[151] Zhang, Y., Cheng, Z., Chen, X., Zhang, W., Wu, J., Zhu, J. and Zhu, X., 2007. Synthesis and photoresponsive behaviors of well-defined azobenzene-containing polymers via RAFT polymerization. *Macromolecules*, *40*(14), pp.4809-4817.

[152] Hafiz, H.R. and Nakanishi, F., 2003. Photoresponsive liquid crystal display driven by new photochromic azobenzene-based Langmuir–Blodgett films. *Nanotechnology*, *14*(6), p.649.

[153] Izunobi, J.U. and Higginbotham, C.L., 2011. Polymer molecular weight analysis by 1H NMR spectroscopy. *Journal of Chemical Education*, *88*(8), pp.1098-1104.

[154] Izunobi, J.U. and Higginbotham, C.L., 2011. Polymer molecular weight analysis by 1H NMR spectroscopy. *Journal of Chemical Education*, *88*(8), pp.1098-1104.

[155] Neises, B. and Steglich, W., 1978. Simple method for the esterification of carboxylic acids. *Angewandte Chemie International Edition in English*, *17*(7), pp.522-524.

[156] Velu, R. and Singamneni, S., 2015. Evaluation of the influences of process parameters while selective laser sintering PMMA powders. *Proceedings of the Institution of Mechanical Engineers, Part C: Journal of Mechanical Engineering Science*, *229*(4), pp.603-613.

[157] Kuo, S.W., Kao, H.C. and Chang, F.C., 2003. Thermal behavior and specific interaction in high glass transition temperature PMMA copolymer. *Polymer*, *44*(22), pp.6873-6882.

[158] Bhat, A., Smith, B., Dinu, C.Z. and Guiseppi-Elie, A., 2019. Molecular engineering of poly (HEMA-co-PEGMA)-based hydrogels: Role of minor AEMA and DMAEMA inclusion. *Materials Science and Engineering: C*, *98*, pp.89-100.

[159] Vargün, E., Sankir, M., Aran, B., Sankir, N.D. and Usanmaz, A., 2010. Synthesis and characterization of 2-hydroxyethyl methacrylate (HEMA) and methyl methacrylate (MMA) copolymer used as biomaterial. *Journal of Macromolecular Science®, Part A: Pure and Applied Chemistry*, *47*(3), pp.235-240.

[160] Vallieres, C., Hook, A.L., He, Y., Crucitti, V.C., Figueredo, G., Davies, C.R., Burroughs, L., Winkler, D.A., Wildman, R.D., Irvine, D.J. and Alexander, M.R., 2020. Discovery of (meth) acrylate polymers that resist colonization by fungi associated with pathogenesis and biodeterioration. *Science advances*, *6*(23), p.eaba6574.

[161] Emaldi, I., Hamzehlou, S., Sanchez-Dolado, J. and Leiza, J.R., 2017. Kinetics of the Aqueous-Phase Copolymerization of MAA and PEGMA Macromonomer: Influence of Monomer Concentration and Side Chain Length of PEGMA. *Processes*, *5*(2), p.19.

[162] McManus, D., Vranic, S., Withers, F., Sanchez-Romaguera, V., Macucci, M., Yang, H., Sorrentino, R., Parvez, K., Son, S.K., Iannaccone, G. and Kostarelos, K., 2017. Water-based and biocompatible 2D crystal inks for all-inkjet-printed heterostructures. *Nature nanotechnology*, *12*(4), pp.343-350.

[163] Cader, H.K., Rance, G.A., Alexander, M.R., Gonçalves, A.D., Roberts, C.J., Tuck, C.J. and Wildman, R.D., 2019. Water-based 3D inkjet printing of an oral pharmaceutical dosage form. *International journal of pharmaceutics*, *564*, pp.359-368.

[164] Chen, H., Lee, S.Y. and Lin, Y.M., 2020. Synthesis and formulation of PCL-based urethane acrylates for DLP 3D printers. *Polymers*, *12*(7), p.1500.

[165] Li, J., Wang, L., Dai, L., Zhong, L., Liu, B., Ren, J. and Xu, Y., 2018. Synthesis and characterization of reinforced acrylate photosensitive resin by 2-hydroxyethyl methacrylate-functionalized graphene nanosheets for 3D printing. *Journal of Materials Science*, *53*(3), pp.1874-1886.

[166] Cosola, A., Sangermano, M., Terenziani, D., Conti, R., Messori, M., Grützmacher, H., Pirri, C.F. and Chiappone, A., 2021. DLP 3D–printing of shape memory polymers stabilized by thermoreversible hydrogen bonding interactions. *Applied Materials Today*, *23*, p.101060.

[167] Mucci, V. and Vallo, C., 2012. Efficiency of 2, 2 ‐ dimethoxy ‐ 2 ‐ phenylacetophenone for the photopolymerization of methacrylate monomers in thick sections. *Journal of Applied Polymer Science*, *123*(1), pp.418-425.